NATIONAL AERONAUTICS AND SPACE ADMINISTRATION

Technical Report 32-1092

The Superior Conjunction of Mariner IV

R. M. Goldstein, et al.

N67-25998

(PAGES)

(NASA OR TMX OR AD NUMBER)

(THRU)

(CODE)

(CATEGORY)

JET PROPULSION LABORATORY
CALIFORNIA INSTITUTE OF TECHNOLOGY
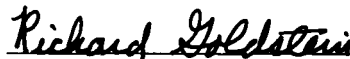PASADENA, CALIFORNIA

April 1, 1967

Technical Report 32-1092

The Superior Conjunction of Mariner IV

R. M. Goldstein, et al.

Approved by:

Richard Goldstein

R. M. Goldstein, Manager
Communications Systems Research Section

TECHNICAL REPORT 32-1092

Contents

Tables

Tables (contd)

Figures

Figures (contd)

Figures (contd)

The Superior Conjunction of *Mariner IV*

I. Experiment and System Description

The remarkable lifetime of the *Mariner IV* radio system, still operating 10 mo after the designed end of its mission, has provided us with a rare opportunity to probe the solar corona with an S-band radio signal.

Mariner IV's orbit carried the spacecraft behind and slightly above the Sun, so that on March 26 the radio signals passed within 0.6 deg of the solar surface.

Reception of the signals at this time was made unusually difficult for three reasons: (1) *Mariner IV* was over 200,000,000 mi from Earth; (2) the high-gain antenna was no longer pointed at Earth, so that the spacecraft had been commanded to transmit from the omnidirectional antenna; and (3) the Sun is a powerful source of radio interference — if the receiving antenna were to be pointed directly at the Sun, the system noise level would increase over a hundred fold.

The received signal power, at the time of encounter with Mars, was −156 dbm at the 85-ft antennas of the standard tracking stations. By the time of superior conjunction, and with the aid of the new 210-ft antenna, the power had decreased to only −170 dbm.

Because of this weak signal and greatly increased noise, it was not possible to observe the signal in the normal manner. Instead, we used an adaptation of the techniques we have developed to study extremely weak planetary radar reflections. The basis of this technique is spectral analysis of the signal. That is, the power spectrum of the received waveform was measured.

A signal, spectrally pure as possible when transmitted to the spacecraft, arrived spectrally impure at the spacecraft receiver, because it passed through the solar corona. The transponder of *Mariner IV* maintained phase-lock with the signal and retransmitted it towards Earth. Of course, the transponder interacted with the signal and, perhaps, modified its spectrum. The return trip through the corona again increased the spectral width of the signal.

The returning signal was too weak to track with phase-lock methods, so the receiver was automatically tuned

under ephemeris control. The ephemerides were calculated in advance from the known orbits of *Mariner IV* and the Earth. Automatic tuning served to remove the doppler shift from the signal so that it was centered in the passband of the receiver.

The power spectrum of the signal was obtained by the autocorrelation approach. The autocorrelation function of the signal was measured with a small special-purpose computer, and the fourier transform was performed on a general purpose machine, yielding the power spectrum. The spectrograms, which constitute all the data of this experiment, were displayed on an x-y plotter by the computer.

Figure 1 is a block diagram of the system, considerably simplified. The transmitter was located at the Venus station of the Goldstone tracking facility. The receiver was at the Mars station, over 14 mi away. Since the spectrograms represent the information of the experiment, each of the components which might influence them have been identified.

All of the reference frequencies of the system were derived from a primary rubidium frequency standard located at the Venus station. An output from this standard was transmitted to the other station via a microwave link, where it was used to phase-lock the remote standard.
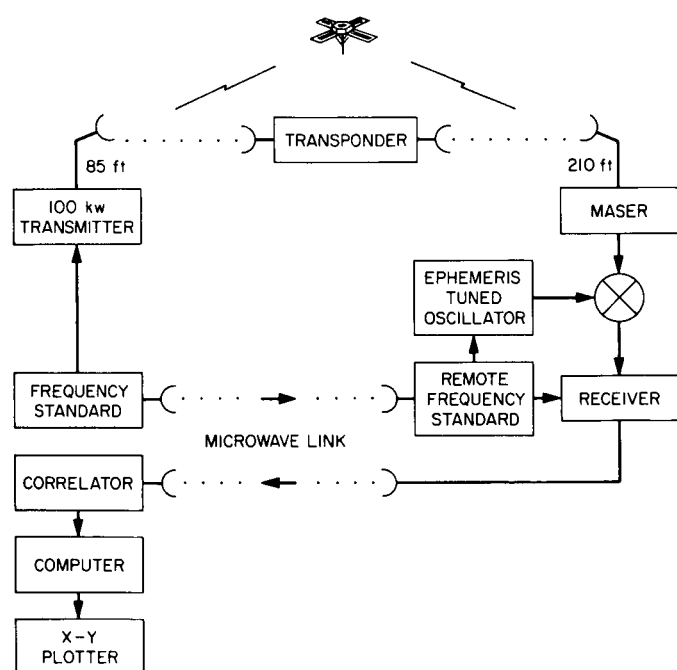
Fig. 1. Block diagram of the experimental system

A test link was also provided, which included a transponder similar to that on board *Mariner IV*. The transponder provided the same frequency multiplication as *Mariner IV* of 240/221. The test link was used to test the condition and stability of the entire system, except for certain parts of the ephemeris tuned oscillator, a necessary exception. Because the transponder had no velocity, it produced no frequency shift.

The next chapter contains a description of these critical components, so that their influence on the received spectrograms may be understood.

II. Critical Components

A. *Mariner IV* Uplink Exciter and Transmitter

The *Mariner IV* uplink transmission system for the Sun occultation experiment consisted of a tunable, phase-locked voltage controlled oscillator (VCO) whose output frequency was harmonically multiplied to a nominal output frequency of 2115.7 MHz, amplified by a driver stage to a 3-w power level and then further amplified by a klystron amplifier to the 100-kw (+80 dbm) power level at the input to the antenna feed system. A block diagram of the system is shown in Fig. 2, and a picture of the amplifier klystron is shown in Fig. 3.

Fig. 2 shows that the absolute frequency of the uplink transmission system is controlled by the 1-MHz input signal to the exciter from the central frequency synthesizer. This 1-MHz input signal is derived from an atomic resonance standard of the rubidium buffer gas cell type and thus is based upon Al rather than UT2 time intervals, with a corresponding high degree of absolute accuracy.

The power output of the uplink system is nominally 100 kw (+80 dbm), supplied by a multicavity amplifier klystron. Operational monitoring of both forward and back power is done by means of carefully calibrated directional couplers feeding commercial microwave power meters of the double thermistor bridge type. Before and after each day's track, the transmitter was operated into a fluid calorimeter, consisting of a suitably cooled RF water load, instrumented to measure accurately input and output water temperatures, and water flow rate in gallons. The transmitter output power was raised until a nominal 100 kw was measured on the microwave power meter. The power being delivered to the water load was then computed and compared with the indicated power. Usual agreement between the two instruments was ±2 kw.
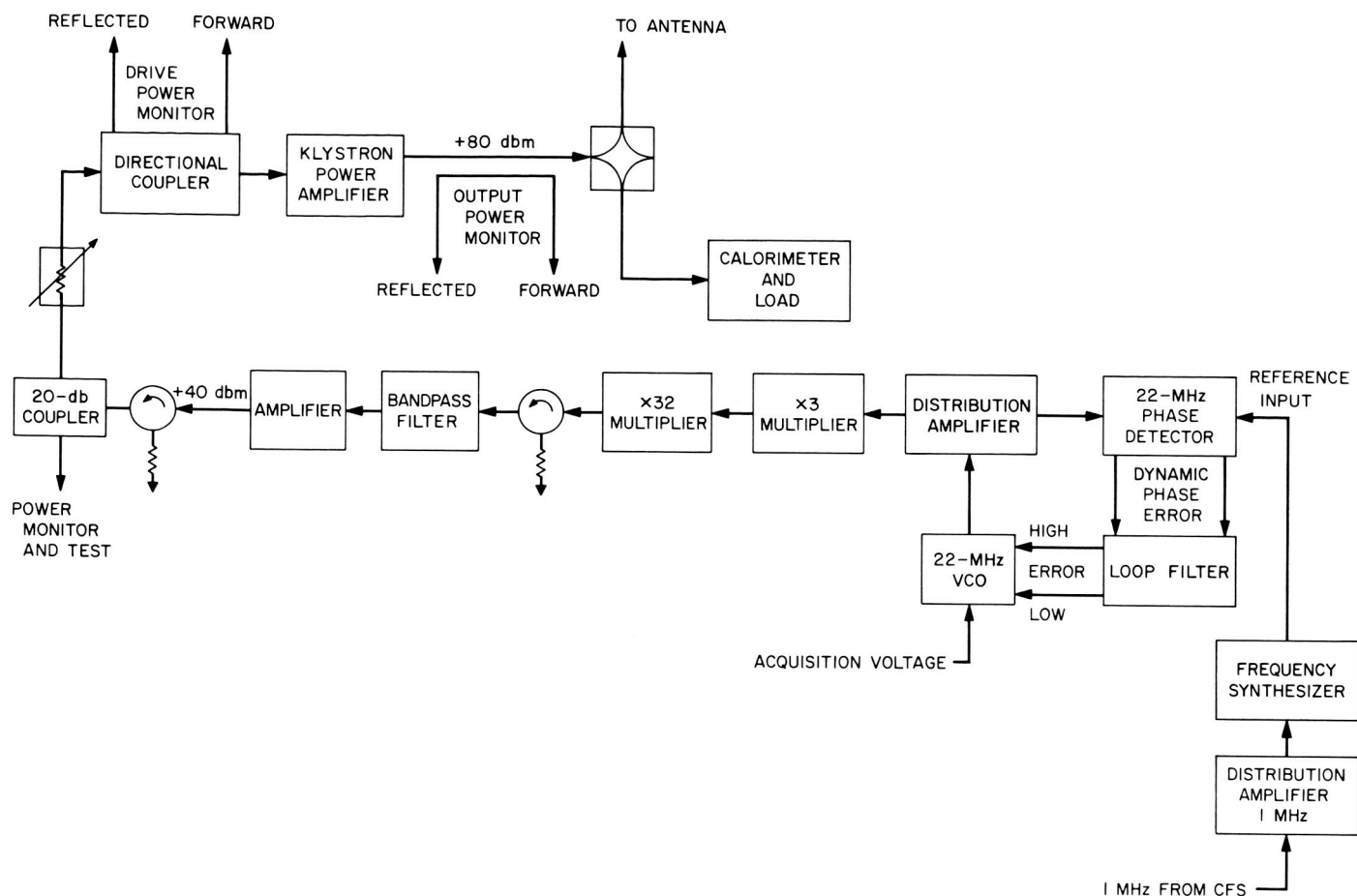
Fig. 2. *Mariner IV* uplink exciter and transmitter

Fig. 3. *Mariner IV* Sun occultation uplink transmitter with covers removed
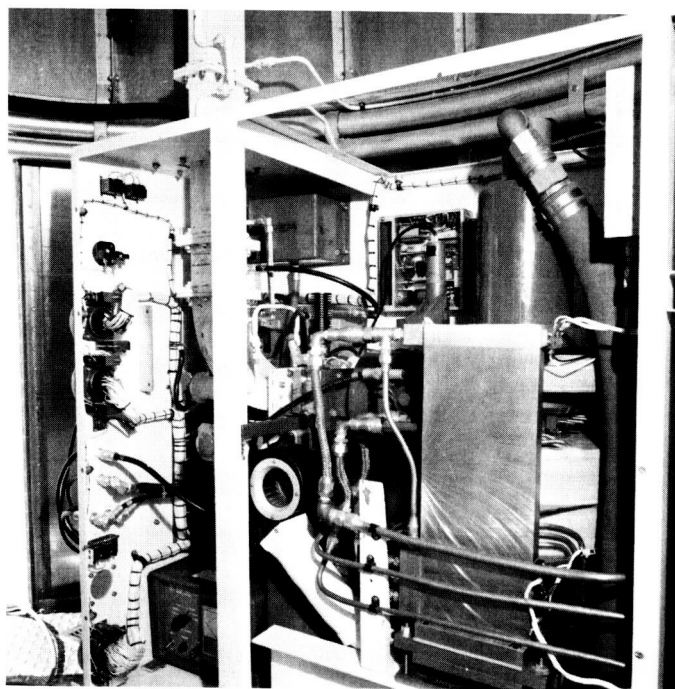
A detailed discussion of the errors associated with the water calorimeter may be found in SPS 37-31, Vol III, pp. 33, 34, but nominal accuracy is within ±3%.

Possibly the most important transmitter parameter is output frequency (phase) stability, which is primarily determined by the short term stability of the 1-MHz reference frequency, the loop noise bandwidth of the phase locked loop, the phase noise contributed by the multiplier chain and "phase pushing" in the amplifier klystron as a result of short term variations in beam voltage. Of these possible sources of phase instability, the major contributor is the phase locked loop which controls the VCO frequency. Typical loop phase jitter is illustrated in Fig. 4, a chart recording of the dynamic phase error (DPE) taken with a chart recorder at 20 mm/sec chart speed. The recorder gain was adjusted to provide a convenient absolute phase scale, and occasional peaks of approximately 0.25 deg are seen. However, the rms value of the phase jitter is probably of more concern, and this was obtained by sampling DPE with an analog to digital (A/D) converter at a rate somewhat in excess of the Nyquist rate and then feeding the A/D converter output into a digital computer programmed to compute
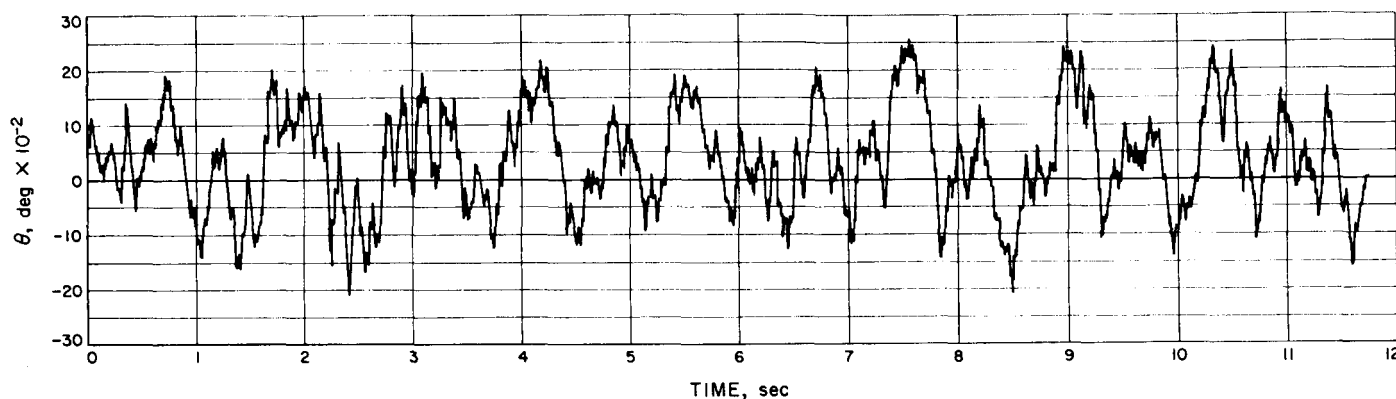
Fig. 4. Ground transmitter VCO phase jitter
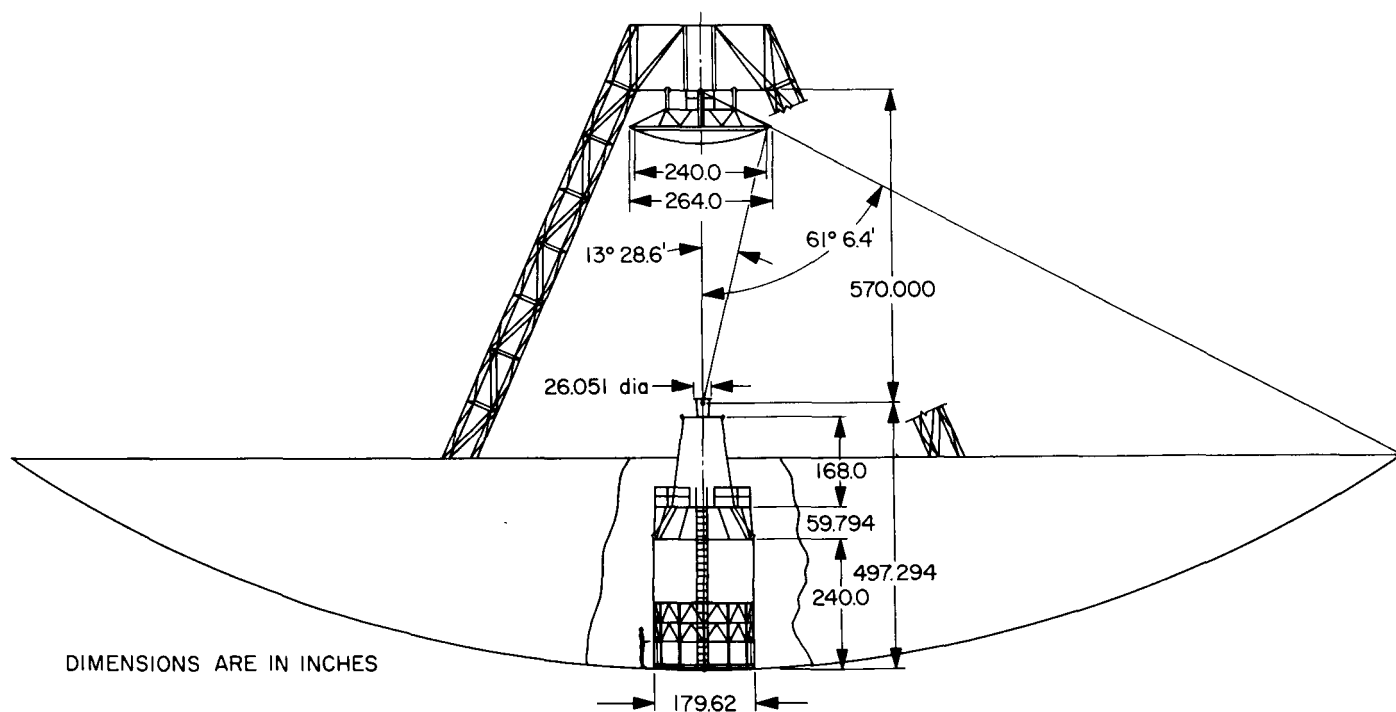
Fig. 5. AAS multifrequency feed system configuration

rms values. For a 10-min sample period, the computed value of the rms phase jitter is 0.105 deg at the VCO output. Assuming that the other contributions to phase instability are negligible, the phase jitter at the final output frequency is found by multiplying the phase jitter at the VCO output by the number of times the frequency is multiplied, in this case 96 times. This yields an rms phase jitter at 2115.7 MHz of 10.08 deg.

B. Antenna Feed

The 210-ft antenna feed used during the *Mariner IV* superior conjunction consists of the S-band Cassegrain microwave optics configuration, similar to that used during the 1962 Venus radar experiment (Ref. 1) and subsequently used throughout the deep space instrumentation facility (DSIF) on all 85-ft reflectors. Focal lengths and subreflector diameters have been scaled by 2.500, yielding a 50-wavelength hyperboloid at S-band. Figure 5 shows the configuration with the multifrequency feedcone installed.

A block diagram of the multifrequency feedcone used is shown in Fig. 6. This feedcone is designed to provide two RF paths from the feedhorn to the maser. One path, not used during the solar occultation experiment, will allow future diplexed operations with a receive system temperature of approximately 40°K. The second path, used during the experiment, provides a listening capability with a receive system temperature of 27°K.
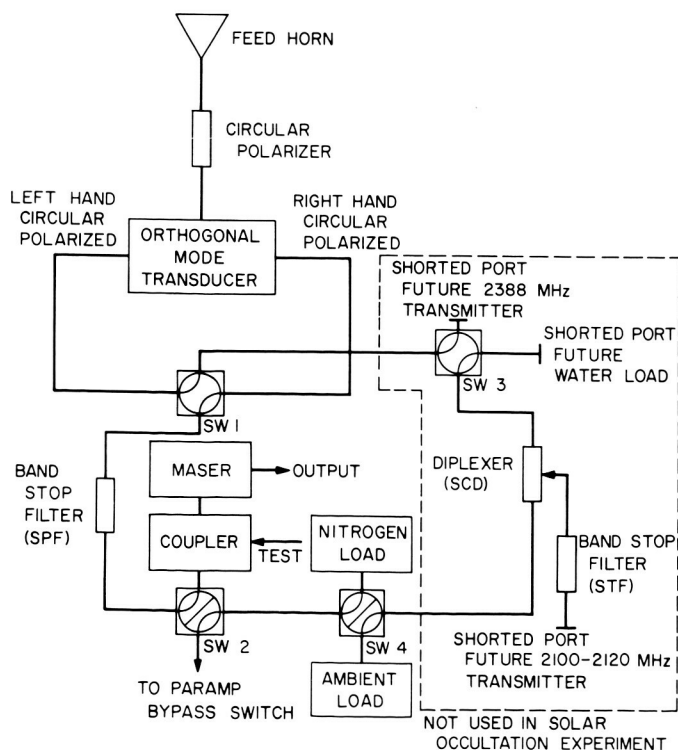
The multifrequency feedcone uses a broadband dual mode horn (Ref. 2 and 3) and a recently developed broadband circular polarizer and orthogonal mode transducer (Ref. 4). Figure 7 shows the broadband feed prior to installation within the feedcone. Figure 8 shows 2295-MHz radiation pattern performance of the full scale broadband horn while Fig. 9 shows 2295-MHz scattered pattern performance of a ¼th scale model of the advanced antenna system (AAS) hyperboloid and beamshaping flange.

For the 2290 to 2300-MHz right hand circular polarization (RCP) receive mode, measured feed ellipticity is 0.10-db with the transducer LCP arm perfectly terminated. Referring to Fig. 6, the operating ellipticity is a function of SW2 position. A worse case exists when SW2 terminates the LCP arm in a short circuit; under these conditions the effective discrimination performance for a one way propagation polarimeter is 24.6 to 26.6 db, depending upon path length, for a perfect spacecraft antenna ellipticity.

Aperture efficiency and the associated gain of the 210-ft reflector using the multifrequency feedcone at 2295 MHz have been calculated (Ref. 5) and initially verified by comparison of radio source temperatures and comparisons of the *Mariner IV* and *Pioneer VI* spacecraft signal levels with the standard DSIF 85-ft systems. Recently, the *Surveyor I* spacecraft was employed in a direct gain test of the 210-ft reflector (Ref. 6). The method of calculation begins with experimentally determined full scale primary feed radiation patterns (Fig. 8). These patterns are input to the JPL developed paraboloidal antenna efficiency program (Ref. 7) and are also input to the JPL developed surface scattering computer program (Ref. 8). The

Fig. 6. Multifrequency feedcone *Mariner IV* superior conjunction configuration
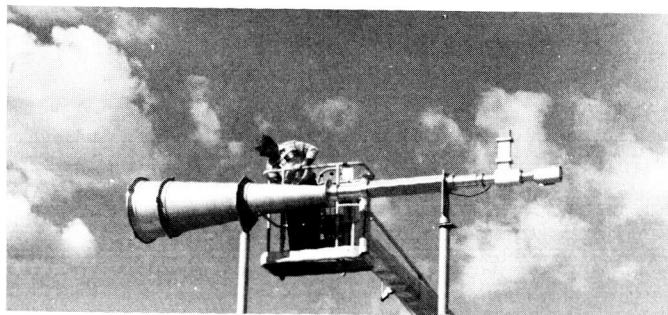
Fig. 7. Broadband feed for multifrequency feedcone
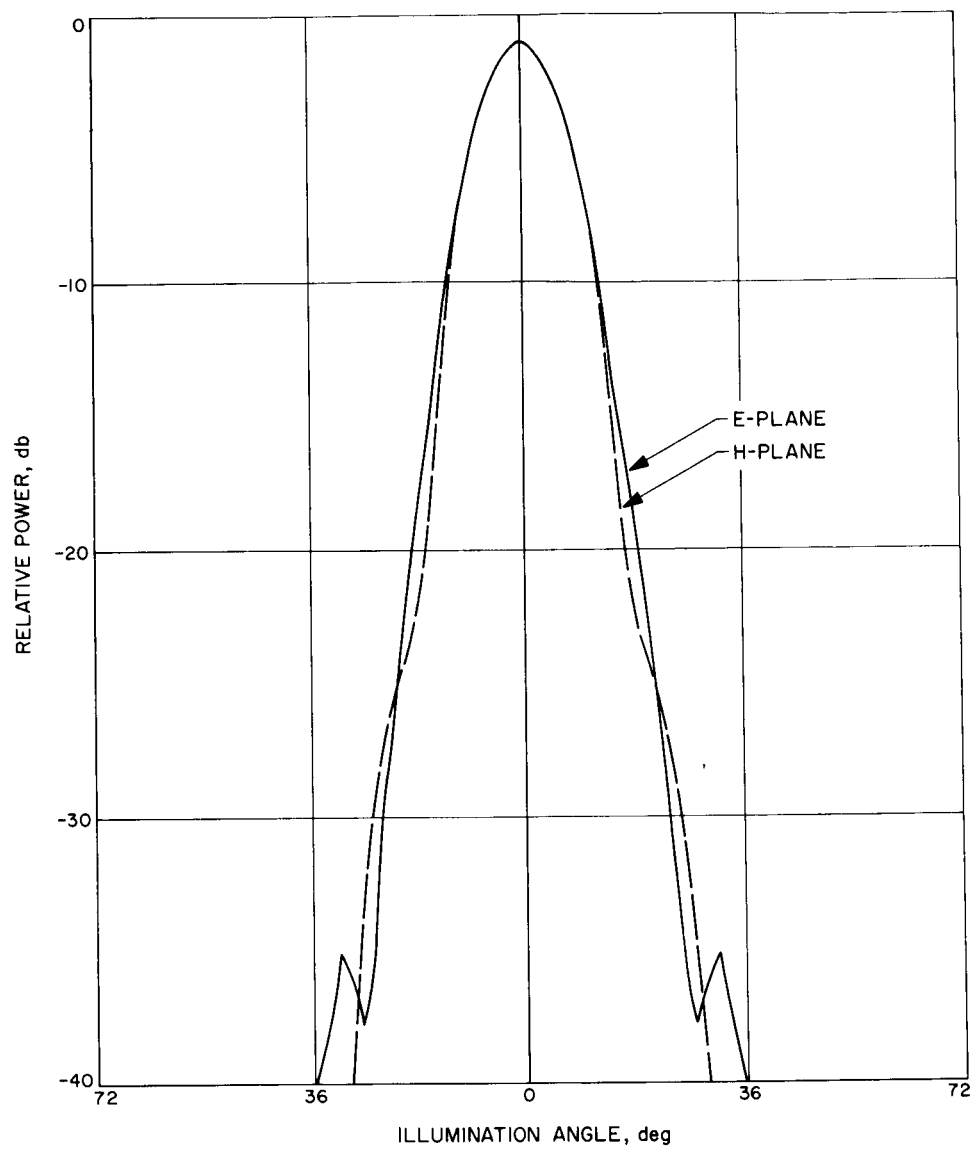
Fig. 8. Broadband dual mode horn radiation pattern, 2295 MHz
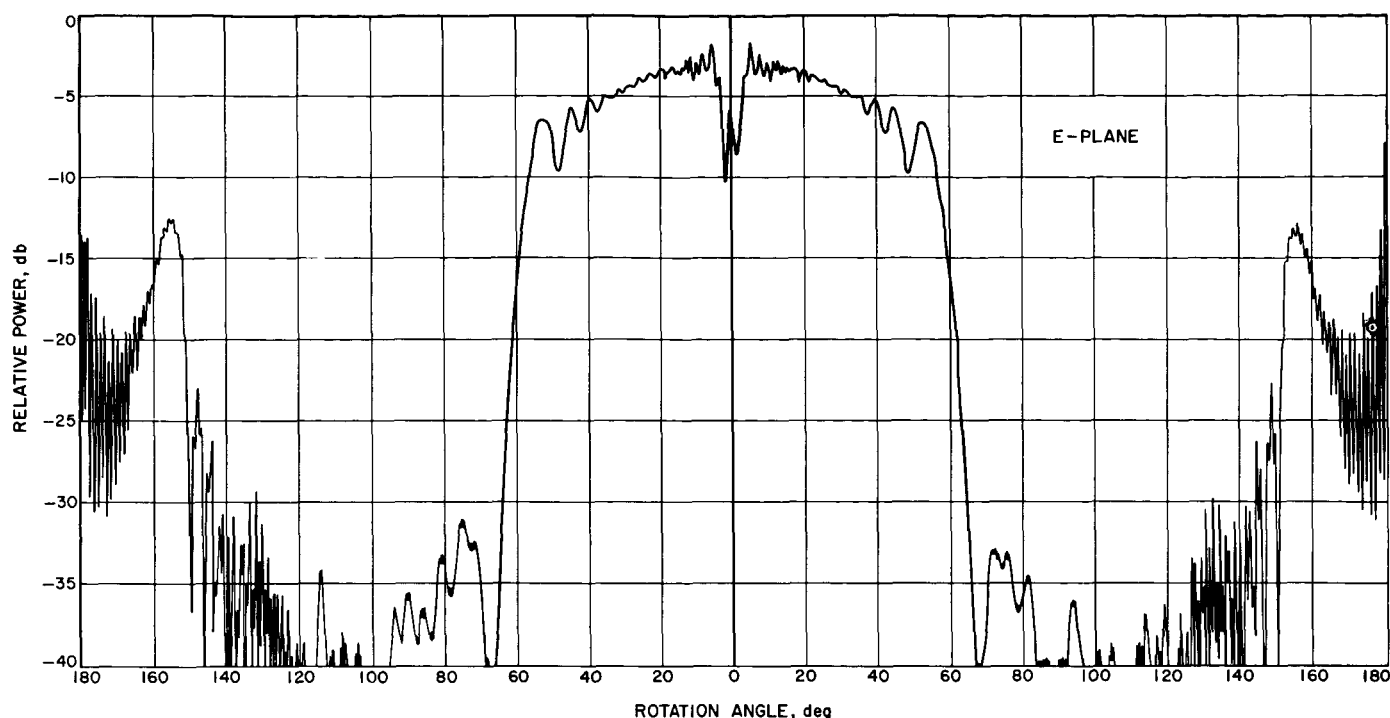
Fig. 9. Model hyperboloid scattered pattern, 2295 MHz

scattering program generates subreflector fields and has demonstrated outstanding agreement with experimentally determined subreflector amplitude and phase patterns, performed on a scale model basis (Fig. 9). The scattered patterns are then input to the efficiency program a second time. Results of this procedure are summarized in Table 1. In Table 1, surface tolerance loss represents restricted

environmental conditions of low winds and thermal gradients on the structure. The antenna gain, the weighted mean of the calculated and direct measured gain, is +61.81 ±0.32 db, (2σ). Table 2 shows calculated and measured antenna noise temperature at zenith.

Far-field radiation patterns of the 210-ft reflector at 2295 MHz have been obtained using the *Surveyor I* spacecraft (Ref. 9) and are shown in Figs. 10 and 11. The noise performance of the 210-ft reflector may be found in subsection II. D of this report.

Table 1. Calculated and measured aperture efficiency and gain

Item	Associated gain at 2295 MHz, db	Aperture efficiency factor, %
Theoretical maximum	+63.75	100
Illumination factor, including spillover and subreflector blocking	−1.15	76.8
Quadripod scattering loss, 80% opaque	−0.62	86.8
Surface tolerance loss, 0.057-in. rms (restricted environment)	−0.08	98.4
Predicted total[a]	+61.90 ± 0.18 (2σ)	65.4
Measured total[b]	+61.62 ± 0.27 (2σ)	61.3
Weighted mean	+61.81 ± 0.32 (2σ)	64.0
Original specification[c] (0.25-in. rms Precision 1 operation)	60.7	

[a]Ref. 5

[b]Ref. 6

[c]Engineering Planning Document No. 5, Rev 4, Jet Propulsion Laboratory, Pasadena, April 1963.

Table 2. Calculated and measured antenna noise temperature

Item	Associated zenith antenna noise temperature, deg K 2295 MHz
Direct spillover to ground, 0.3%	0.8
Quadripod scattering to ground, 80% opaque, isotropic	2.8
Atmospheric and extra atmospheric noise[a]	6.0
Losses	Negligible
Predicted total, feedhorn output	9.6
Measured total, feedhorn output	9.6

[a]Based on private correspondence with Dr. D. C. Hogg of Bell Telephone Laboratories, Holmdel, New Jersey.
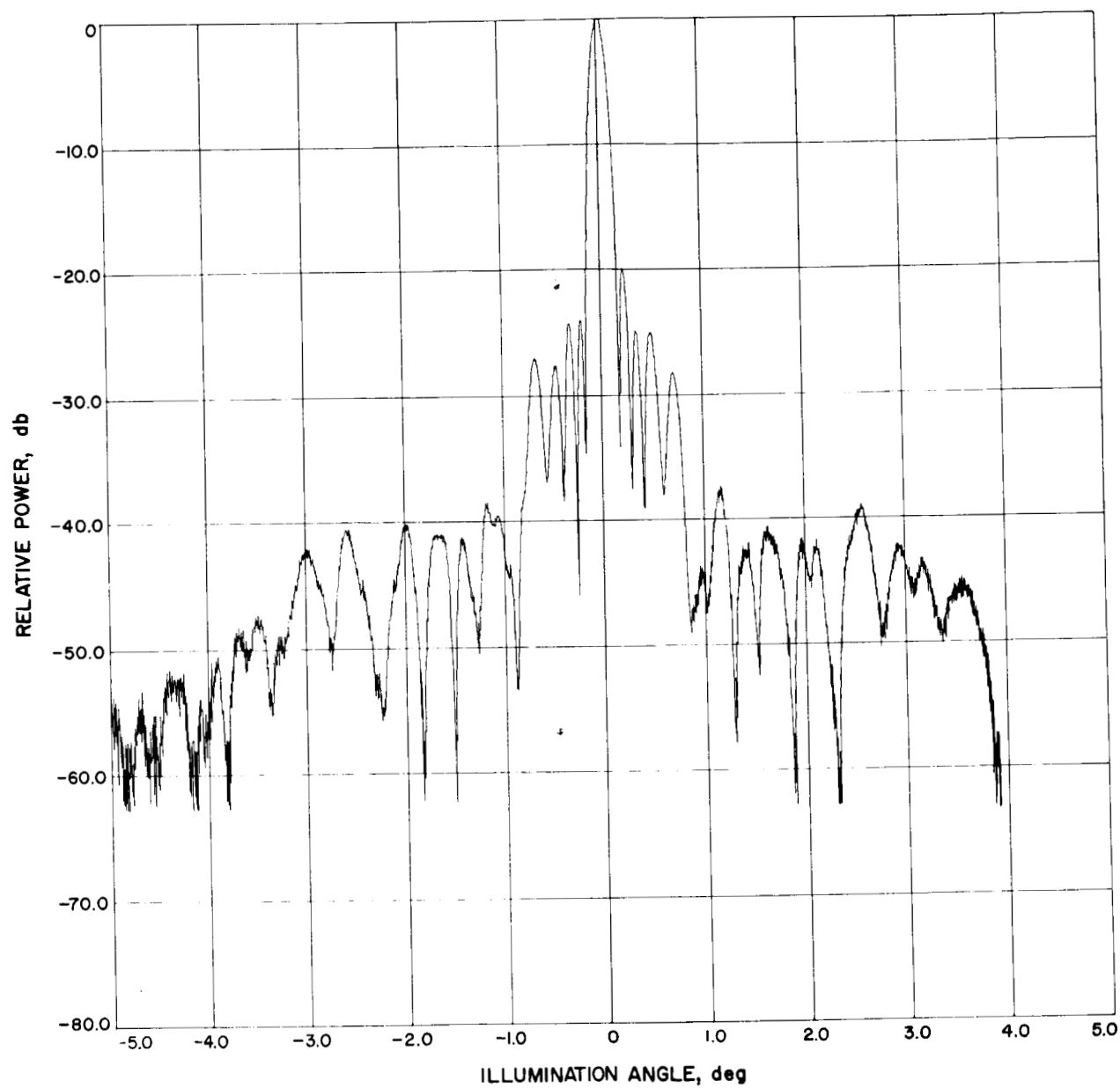
Fig. 10. Mars DSS azimuth radiation pattern
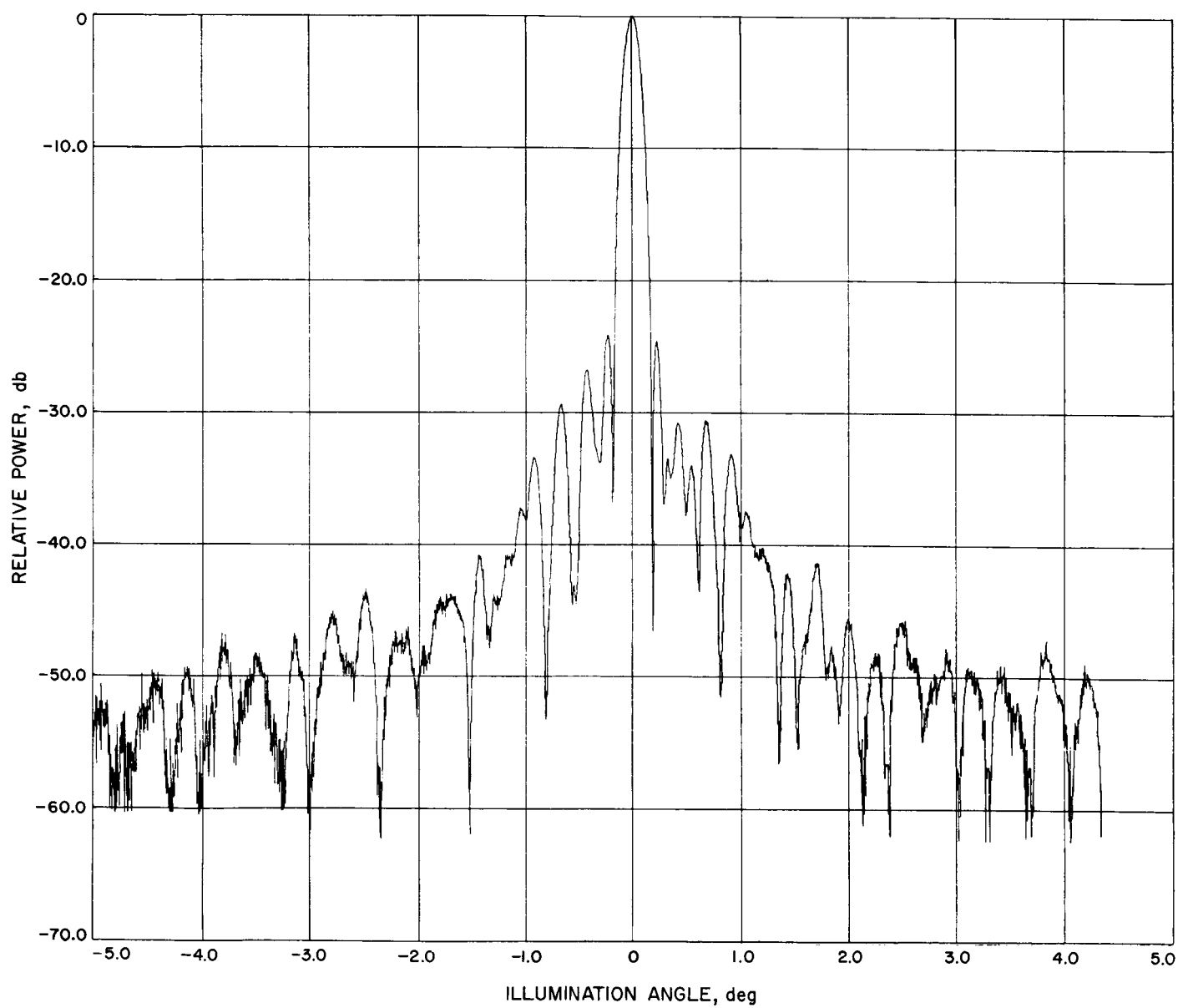
Fig. 11. Mars DSS elevation radiation pattern
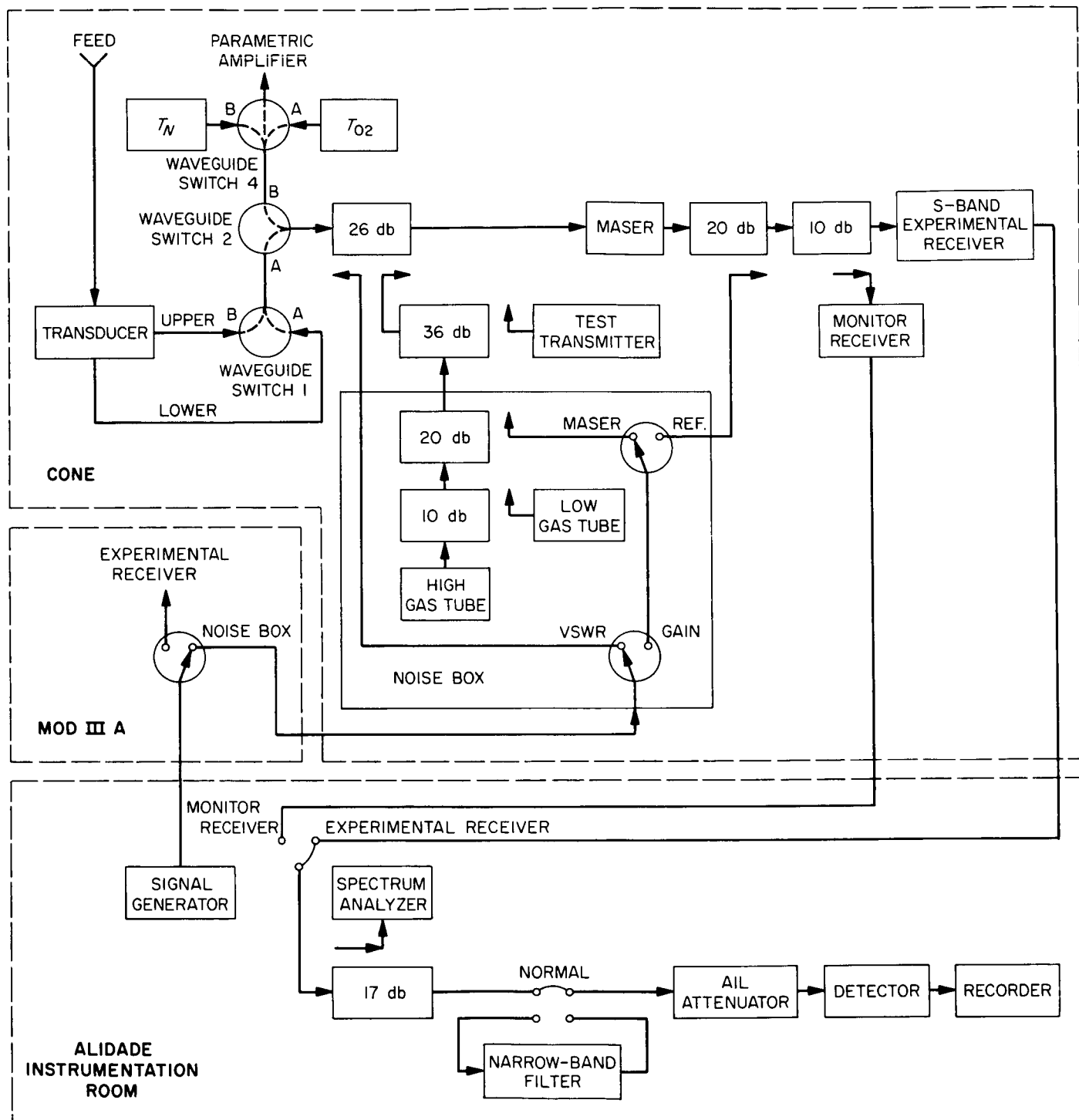
Fig. 12. A simplified block diagram of the RF instrumentation

C. Maser System

Recent advances in traveling wave maser (TWM) technology as well as in closed cycle refrigerators (CCR) are reflected in the system recently installed in the listening cone at the advanced antenna system.

The TWM is electronically tunable over a 125-MHz band, from 2,275 to 2,400 MHz; at least 35 db gain is available over the band. The pump klystron, at present, needs to be changed, for best results, in going from the lower frequency end to the higher.

Precision machining of the comb structure as well as improvement in the quality of the ruby have contributed to the versatility of the new TWM. Magnetic field staggering is also used to increase the bandwidth of the TWM.

The center conductor of the input coax has been conductively cooled to a point midway between the TWM and the ambient temperature input flange. This has reduced the TWM noise temperature to $7 \pm 0.5°K$.

The CCR also represents a technical achievement. The new refrigerator consists of an A. D. Little paramp cooler (Model 340 L), which has been modified to a 4.3°K machine by the addition of a Joule-Thompson expansion stage. One watt of refrigeration is available for cooling the TWM. Cool-down time is approximately 7 hr without the use of liquid nitrogen precooling, and may be reduced to 3½ hr by the use of liquid nitrogen.

Details of both the TWM and CCR are reported in Ref. 10.

D. System Temperature

1. Instrumentation description and quiescent performance characteristics. The RF instrumentation for the Mars station 210-ft antenna multifrequency feedcone provides for remote measurements of system effective noise temperatures, waveguide reflection coefficients, and maser gain. Provision is also made for antenna gain, radio source flux density and AGC curve calibrations.

The complete block diagram of the multifrequency feedcone is discussed in Ref. 11. A simplified block diagram of the RF instrumentation is shown in Fig. 12. The instrumentation racks installed in the alidade control room are
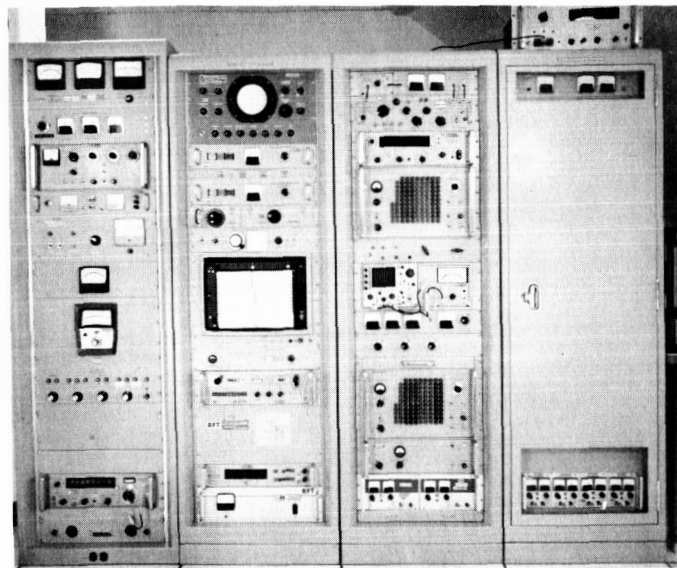
Fig. 13. RF instrumentation racks installed in alidade control room

shown in Fig. 13. Figures 14 and 15 show the cone interior.

Maser gain is measured by comparing a CW signal from the signal generator which is switched first in front and then behind the maser. Reflectometer measurements are made by comparing the CW signal injected into the maser and into the load under evaluation, respectively. The side arm of the 26-db waveguide coupler at the maser input is provided with a waveguide-to-coax transition with a built-in isolator and tuning screws (MMC Model SR 8126) to match up the reflectometer.

Noise instrumentation is provided by switching in waveguide between the antenna and the cryogenic loads and by two gas tube noise sources of approximately 37° and 4°K. For long term stability, the noise box is mounted separately from the maser with a waveguide run to permit removal for maintenance or other reasons without disturbing the noise instrumentation or reflectometer.

The liquid nitrogen load assembly (Model SR8135) was manufactured for JPL by the Maury Microwave Corporation. Design details are discussed in Ref. 12.

The waveguide ambient load assembly is equipped with a digital temperature readout having an absolute accuracy of approximately 0.1°C. The temperature sensing thermometer is imbedded in a copper heat sink, which surrounds the terminating element for the ambient load.
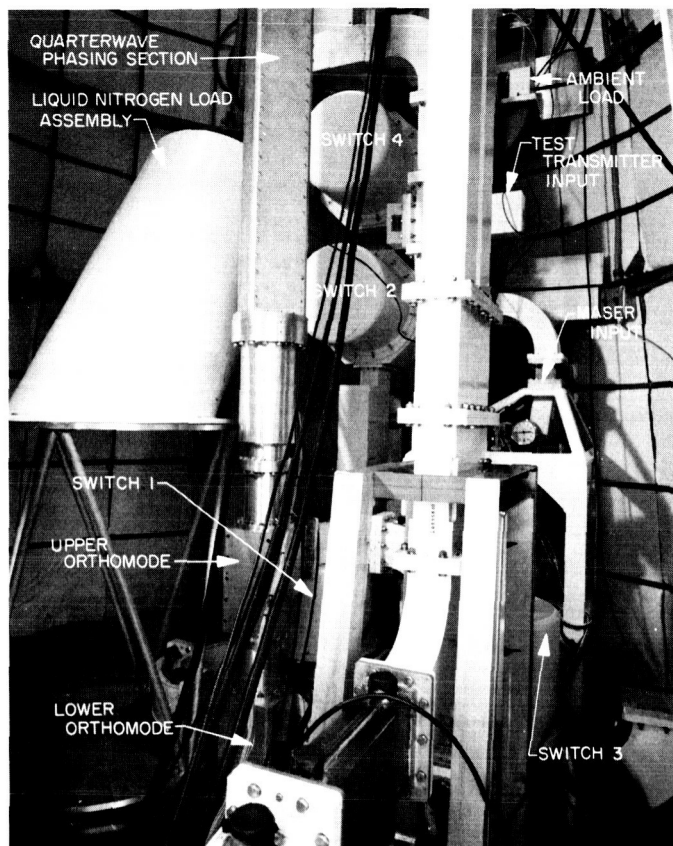
Fig. 14. Lower section of cone interior

Fig. 15. Upper section of cone interior

The heat sink is also thermally connected to the waveguide walls. The ambient load waveguide was filled with polystyrene foam to prevent gas convection in the waveguide system from causing erroneous ambient load temperature readings.

2. Insertion loss calibrations. Reflection coefficient and insertion loss measurements were made for the critical interconnecting transmission lines shown in Fig. 16. Both the DC potentiometer (Ref. 13) and the AC ratio (Ref. 14) insertion loss test sets were used for the insertion loss measurements. Photographs of the maser input and horn output reference flanges may be seen in Figs. 14 and 15, respectively.

Parameter measurements for the cone transmission lines are summarized in Table 3. The probable errors (PE) in the tables represent the best estimate of the total probable error due to various possible sources (Ref. 15): (1) insertion loss equipment; (2) mismatch; (3) reflection coefficient measurement; and (4) measurement dispersion. It is assumed that the errors are random and vary independently.

3. Noise temperature calibrations. Prior to installation of the multifrequency feedcone on the 210-ft diameter antenna, noise temperature calibrations, and preliminary RF cone instrumentation checkout tests were made at JPL on the roof of Building 238. The measurement techniques and error analysis are reported in Ref. 16. An overall measured average of 6.2 ±0.1°K was found for the cone zenith antenna temperature, as defined at the antenna reference flange (Fig. 16).

After the calibrations at JPL, the multifrequency feedcone was shipped to the Mars station at Goldstone and installed on the 210-ft antenna. To check the stability of the antenna and receiver noise temperatures over a period of time, calibration was performed weekly. The weekly calibration, which required the liquid nitrogen cooled waveguide load assembly, depended on the Y-factor measurement technique. These calibrations determined: (1) receiver noise temperature and probable error; (2) antenna noise temperature and probable error; (3) system noise temperature; (4) gas tube excess noise temperatures; and (5) follow-up receiver noise temperature. The noise temperatures are calculated for both maser input and antenna output reference flange cases.
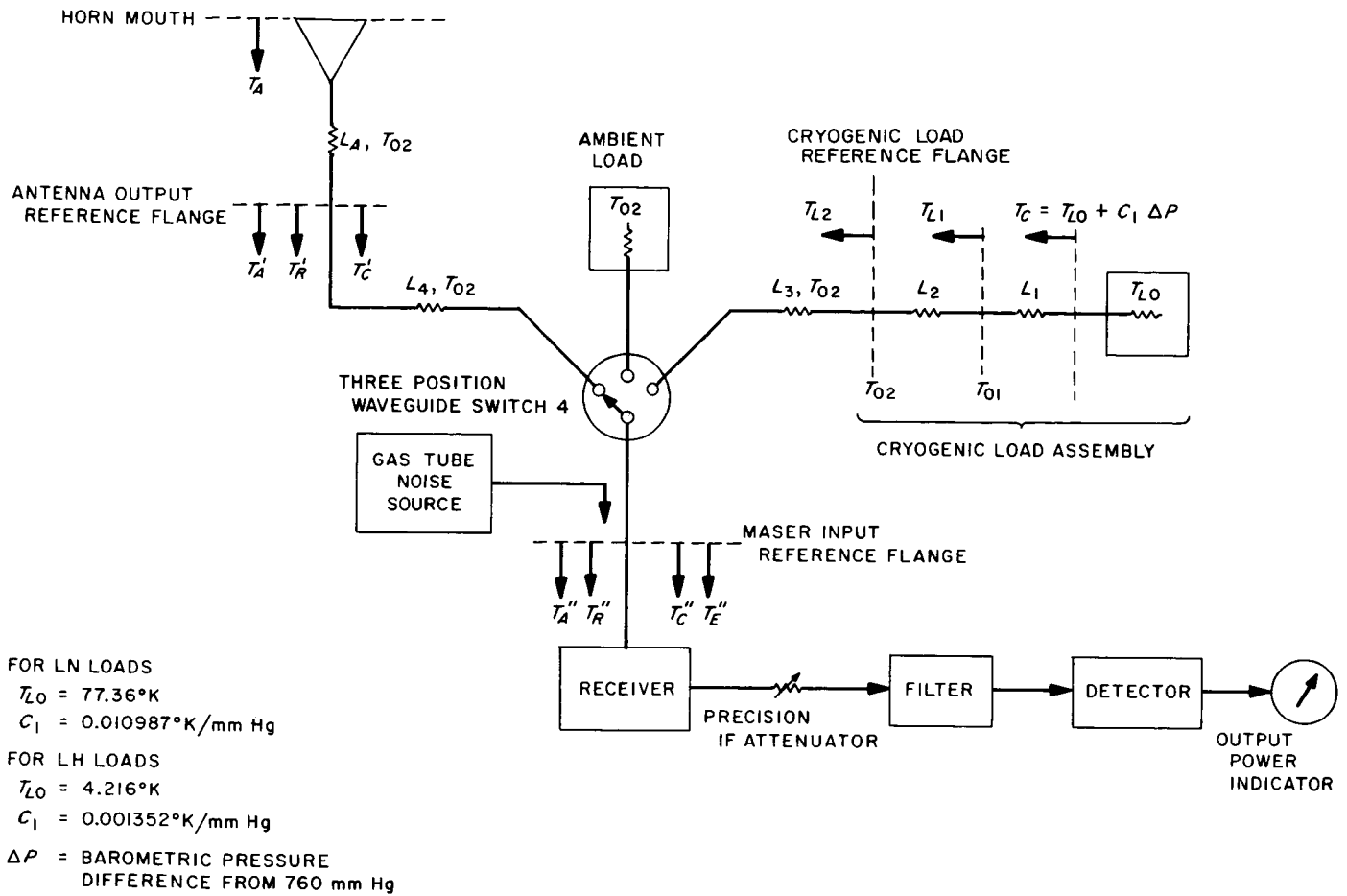
Fig. 16. Receiving system noise temperature reference planes

FOR LN LOADS
$T_{LO} = 77.36°K$
$C_1 = 0.010987°K/mm\ Hg$

FOR LH LOADS
$T_{LO} = 4.216°K$
$C_1 = 0.001352°K/mm\ Hg$

ΔP = BAROMETRIC PRESSURE
DIFFERENCE FROM 760 mm Hg

Table 3. Calculated and measured transmission line parameters of AAS multifrequency feedcone

Part A. Antenna transmission lines

$\Gamma_G = 0$ Γ_1 $\Gamma_L = 0$

a_{11} a_{12}

a_{21} a_{22}

Maser input Ref. flange ①   Antenna output Ref. flange ②a

$A = 10 \log_{10} \dfrac{1}{|a_{21}|^2}$

$A_D = 10 \log_{10} \left[\dfrac{1 - |a_{11}|^2}{|a_{21}|^2} \right]$

Frequency, MHz	Input/output flange (Fig. 15)	$VSWR_1 \pm PE$	$|a_{11}| \pm PE$	Attenuation[a] $A \pm PE$, db	Dissipative loss[b] $A_D \pm PE$, db
2295	① / ②a Via upper orthomode	1.077 ±0.011	0.0372 ±0.0050	0.1761 ±0.0023	0.1701 ±0.0028
2388	① / ②a Via upper orthomode	1.109 ±0.011	0.0519 ±0.0050	0.1724 ±0.0036	0.1607 ±0.0042
2295	① / ②a Via lower orthomode	1.063 ±0.011	0.0306 ±0.0050	0.1496 ±0.0015	0.1456 ±0.0020
2388	① / ②a Via lower orthomode	1.058 ±0.011	0.0282 ±0.0050	0.1371 ±0.0023	0.1336 ±0.0026

Part B. Liquid nitrogen load line

$\Gamma_G = 0$ Γ_1 $\Gamma_L = 0$

n_{11} n_{12}

n_{21} n_{22}

Maser input Ref. flange ①   Liquid nitrogen load Ref. flange ③

$A = 10 \log_{10} \left[\dfrac{1}{|n_{21}|^2} \right]$

$A_D = 10 \log_{10} \left[\dfrac{1 - |n_{11}|^2}{|n_{21}|^2} \right]$

Frequency, MHz	Input/output flange (Fig. 15)	$VSWR_1 \pm PE$	$|n_{11}| \pm PE$	Attenuation $A \pm PE$, db	Dissipative loss $A_D \pm PE$, db
2295	① / ③	1.021 ±0.002	0.0104 ±0.0010	0.0627 ±0.0007	0.0622 ±0.0007
2388	① / ③	1.022 ±0.002	0.0109 ±0.0010	0.0876 ±0.0007	0.0871 ±0.0007

[a]The terms attenuation and dissipative loss are defined in Ref. 17.

[b]Measurements of reflection coefficient and attenuation were made with the antenna line in the linear polarization configuration. This linear polarization configuration was produced by rotating the quarter wave phasing section 45 deg from the normal circular polarization position.

Table 3. (contd)

Part C. Ambient load line

$$A = 10 \log_{10} \left[\frac{1}{|u_{21}|^2} \right]$$

$$A_D = 10 \log_{10} \left[\frac{1 - |u_{11}|^2}{|u_{21}|^2} \right]$$

Maser input Ref. flange ①   Ambient load Ref. flange ④

Frequency, MHz	Input/output flange (Fig. 15)	VSWR₁ ±PE	$\|u_{11}\| \pm PE$	Attenuation A	Dissipative loss A_D
2295	① / ④	1.032 ±0.002	0.0157 ±0.001	See footnote[c]	See footnote[c]
2388	① / ④	1.035 ±0.002	0.0172 ±0.001	See footnote[c]	See footnote[c]

[c] These measurements were not required. For noise temperature calculations, the ambient load line is essentially at the same physical temperature as the ambient load.

Based on the data taken on days 87, 94, and 98 (GMT, 1966), the overall average noise temperature values for the advanced antenna system (AAS) using the multifrequency feedcone are listed in Table 4. The probable error of each average includes only relative measurement precision errors. A detailed description of the techniques and data reduction are given in Ref. 16.

The receiving system noise temperature performance was evaluated on a daily basis during routine pre- and post-calibrations from March 17 to April 12, 1966. The measurement technique consisted of switching the waveguide switch S3 between the antenna, pointed at zenith, and the ambient load. Waveguide switch S1 was left in

position A through the lower waveguide run to the mode transducer, providing right-hand circular polarization. The AIL attenuator was adjusted to give the same noise level on the recorder when switched between the antenna and ambient load. Measurement data also include the follow-up receiver noise temperature, maser gain and reflectometer measurements of the ambient load and antenna. A computer program has been written to simplify data reduction. The daily maser gain and reflectometer readings (defined as the difference between a signal applied at the maser input and that reflected from the termination) of the waveguide ambient load and antenna are shown in Fig. 17.

Although there appears to be some correlation between the reflectometer readings on the ambient load and antenna, indicating some systematic error in the measurements, the system is satisfactory for this application. Divergent reflectometer readings between the antenna and ambient load would indicate an unstable situation in either the ambient load or antenna. Correlated changes indicate problems in the reflectometer. The data reduction is further described in Ref. 16.

An error analysis of the daily system temperature technique (Ref. 17) shows that an overall measurement probable error of less than 1% should be expected.

Table 4. Summary of AAS/multifrequency feedcone noise temperatures (weekly calibration data)

Noise source	Reference flange	Average noise temperature ±PE, °K
Antenna via lower orthomode	Antenna output	9.6 ±0.1
	Maser input	19.1 ±0.1
Receiver	Maser input	8.2 ±0.2
Follow-up receiver contribution	Maser input	0.6
High gas tube	Maser input	37.4 ±0.5
Low gas tube	Maser input	4.3 ±0.1
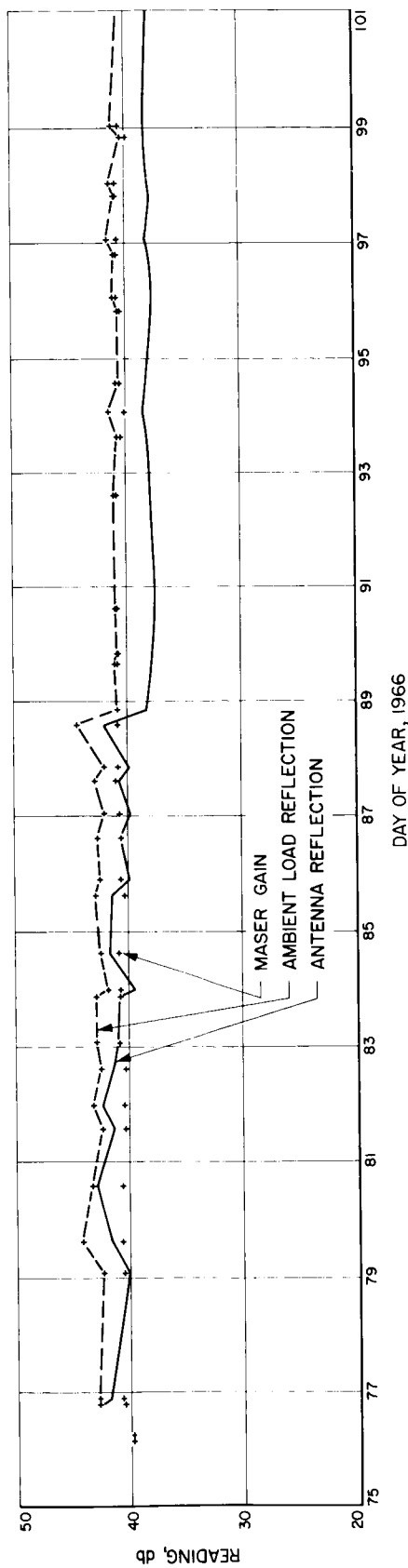
Fig. 17. Daily maser gain and reflectometer readings of waveguide ambient load and antenna
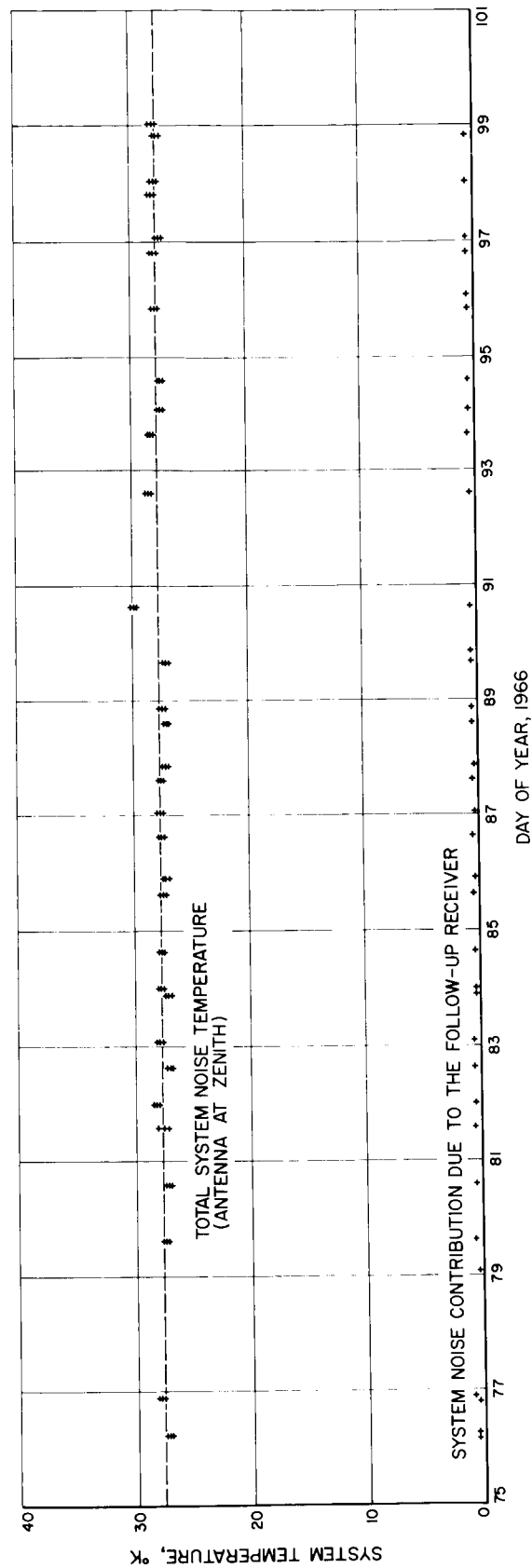
Fig. 18. Daily zenith temperature measurements for operational period

A plot of the daily zenith temperature measurements for the operational period is shown in Fig. 18. The average of all these data points is (27.7 ±0.4 PE) °K. The probable error (Ref. 18) refers to the daily statistical variation. The overall system temperature measurement accuracy probable error $PE_{T_{SA}}$ for a daily calibration is typically 0.3°K. The average of the daily measurement errors $PE_{T_{SA}}(M)$ from the data sheets is 0.03°K. The actual statistical variation in the system temperature (0.4°K), which is considerably greater than the (0.03°K) daily resolution is probably an actual receiver temperature change not necessarily due to the measurement system. The maser gain was not peaked each day in order to determine long term gain stability. It is shown (Ref. 15) that the maser temperature is somewhat sensitive to tuning.

4. Operational system temperature. In contrast to the occultation effects upon the *Mariner IV* signal, the proximity of the Sun to the antenna beam (to within approximately 0.8 deg or 6 beamwidths) caused significant increases in system noise temperature. This temperature was monitored by the usual instrumentation techniques at roughly 1 hr intervals through the observation period, March 17 through April 12, both as a reference for autocorrelator signal-to-noise ratio data concurrently obtained, and as independent data. System temperature also was used during the experiment to influence the choice of operating time during a given day. (Much of the period was restricted to half-day operation due to

other commitments of the antenna, then in final stages of completion and initial shakedown.) Typical plots of one day data are given in Figure 19.

Solar flux contribution to system noise temperature is complicated by the ground antenna radiation pattern in the (θ, ϕ) space. Fig. 20 shows the coordinate system with ∠SEP (Sun-Earth-Probe) equal to θ. Although the feed radiation patterns of the 210-ft system are very highly rotationally symmetric, the presence of the quadripod feed support members introduces secondary radiation pattern ϕ dependence. Figure 21 shows the 210-ft reflector with the 30-deg quadripod geometry employed.
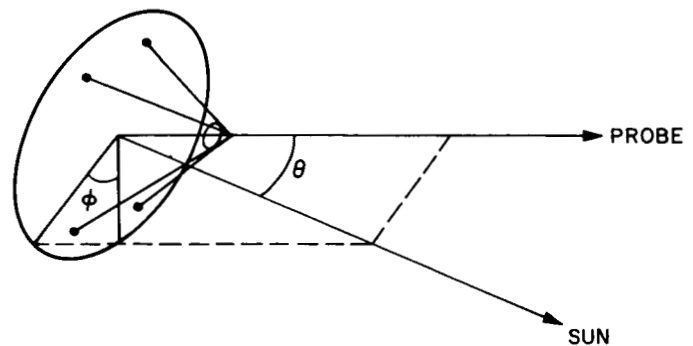
Fig. 20. Coordinate system
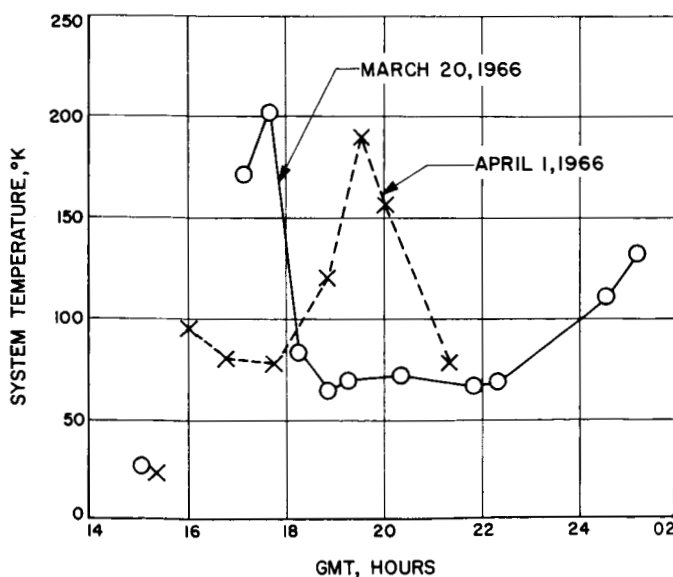
Fig. 19. Typical temperature calibrations for sample days
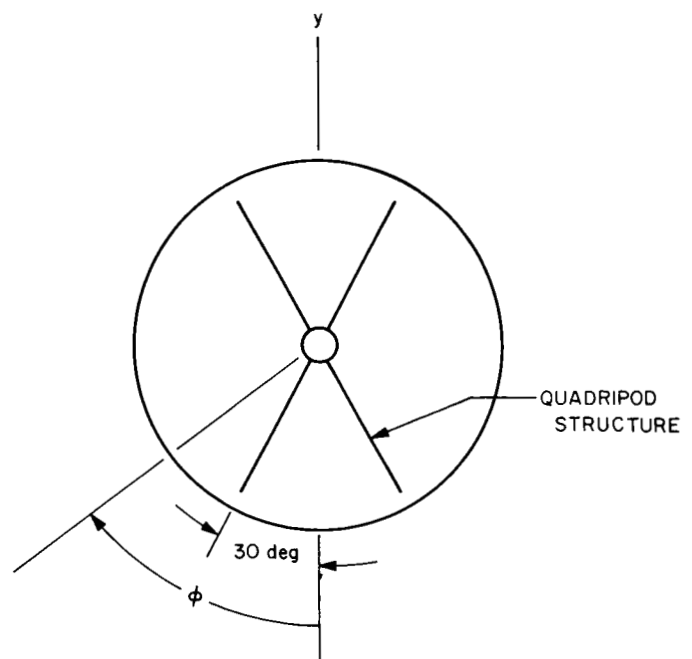
Fig. 21. Mars station reflector with 30-deg quadripod geometry

Figure 22 shows a composite of all receive system noise temperature measurements made with the 210-ft system pointed at the *Mariner IV* probe as a function of SEP, for the period March 17 to April 12. During this time SEP closed from 1.6 deg to a minimum of 0.8 deg and out to a maximum of 1.8 deg. Also shown in Fig. 22 are three predictions of receive system noise temperature. The first represents a pre-experiment estimate intended to place an upper bound. The second and third predictions are based on experimental far-field radiation patterns obtained using the Goldstone Venus 30-ft modeled reflector. This reflector includes a very accurately scaled model of the prototype quadripod.

Solar flux contribution to system noise temperature is given by

$$T = \frac{1}{2} \frac{S}{k} A_s \qquad (1)$$

where

$T =$ Solar flux contribution, °K

$S =$ Total solar flux density, 1×10^{-20} w/m^2/Hz (Ref. 19)

$k =$ Boltzmann constant, 1.3803×10^{-23} w/°K/Hz

$A_s =$ Sidelobe effective aperture, m^2.

Side lobe effective aperture for the extended solar source (mean angular diameter of 0.533 deg) was obtained by numerical integration of the scale model radiation patterns. On-axis effective aperture was taken to be $+61.9$ db/isotropic for a point source. Two radiation patterns were considered independently, as though each pattern were rotationally symmetric; the elevation plane pattern ($\phi = 0$ deg) and a plane normal to one of the quadripod members ($\phi = 60$ deg). These planes represent minima and maxima, respectively, for sidelobe effective aperture. Fig. 22 suggests a region in the (θ, ϕ) space in the neighborhood of $\theta = 0.8$ deg, where the sidelobe effective aperture is approximately 5 db less than in the $\phi = 0$-deg plane, while minimum measured system temperatures in the region $1.0 < \theta < 1.8$ deg are within approximately 1 db of predictions.

A brief study of the entire set of data points (approximately 140) revealed that significant variations occurred not only on a day-to-day basis but also during a given day, as shown above. The first step in data reduction was to plot daily temperature minima as a function of operating day. This curve appears as Fig. 23. The fact that operating time during a given day did not always include

Fig. 22. Composite of all receive-system noise temperature measurements made with the antenna pointed at the *Mariner IV* probe
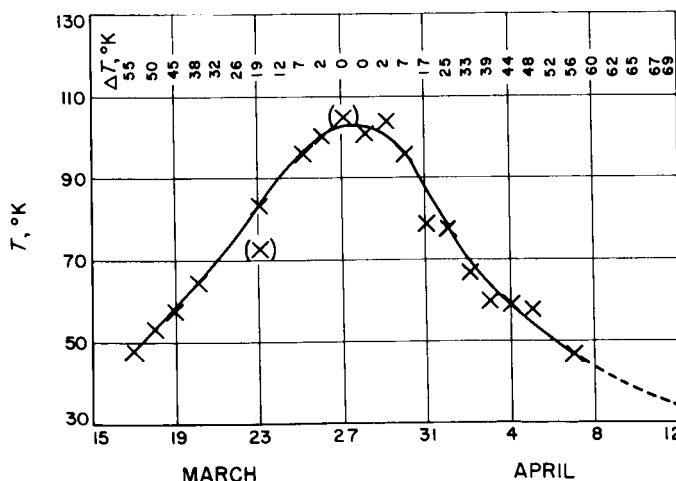
Fig. 23. System noise temperature (daily minima on *Mariner IV*). ΔT = normalizing factor for Fig. 24
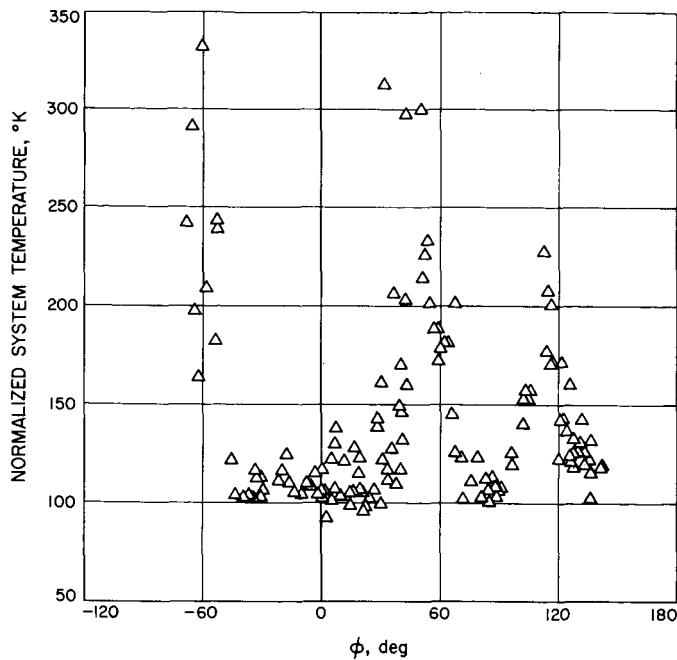
Fig. 24. Normalized system noise temperature measurement on *Mariner IV* between March 17 and April 4, 1966

a true minimum is evident in the missing data points; however, enough were available to plot the curve shown.

This SEP (polar) dependence of the data can be removed for further data analysis by a daily normalization. Normalization was accomplished by adding to each day's temperature data the difference from Fig. 23 between the daily minimum and the maximum (midoccultation) minimum. This normalization is such that a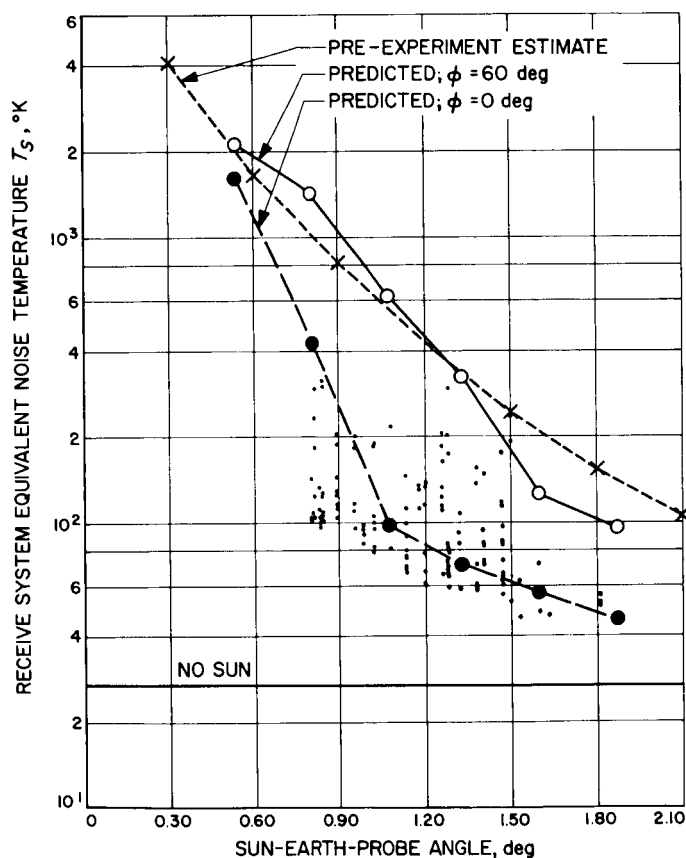ll data may now be considered as having been collected on March 28. The angular dependence of the data around the principal

axis of the antenna beam was then established as follows. The spacecraft to Sun vector, as viewed from the antenna, rotates around the beam (pointing) axis with respect to a fixed reference on the dish. This angular variation is evidenced by the familiar movement of the quadripod shadow upon the face of the reflector. This is the angle ϕ defined in Fig. 21.

Normalized data are presented in Fig. 24 as a function of the spin angle ϕ. The three prominent peaks, occurring at approximately -60, $+60$ and $+120$ deg, confirm first order side lobes 90 deg removed from the quadripod legs (Fig. 21). Figure 25, when overlaid on Fig. 24, provides a cross reference of ϕ to time-of-day and date. The absence of a fourth symmetrical side lobe (at -120 deg) is due to the geometry of the spacecraft trajectory.

This normalized curve serves to provide reference temperatures in reducing the data obtained with the autocorrelator by allowing interpolation and extrapolation to points not recorded during the experiment. Further, interpretation with respect to antenna pattern must include consideration of the fine sidelobe structure in the (θ, ϕ) space. That is, the solar diameter of approximately 0.53 deg results in an averaging effect over more than one sidelobe in (θ, ϕ).

E. Ephemeris

1. Tracking data. The spacecraft ephemeris used during the solar occultation experiment is based on orbit determination from two-way coherent phase-locked doppler data taken between July 17, 1965 and September 30, 1965. The tracking pattern from the various stations is as follows:

DSS station	Location	Beginning date	Ending date	Number of compressed 600-sec points
11	Goldstone Pioneer, California	7/19/65	7/27/65	15
42	Canberra, Australia	7/17/65	8/17/65	79
41	Woomera, Australia	8/20/65	9/12/65	211
51	Johannesburg, South Africa	7/17/65	7/28/65	19
12	Goldstone Echo, California	8/04/65	9/30/65	293
61	Madrid, Spain	8/03/65	9/30/65	462
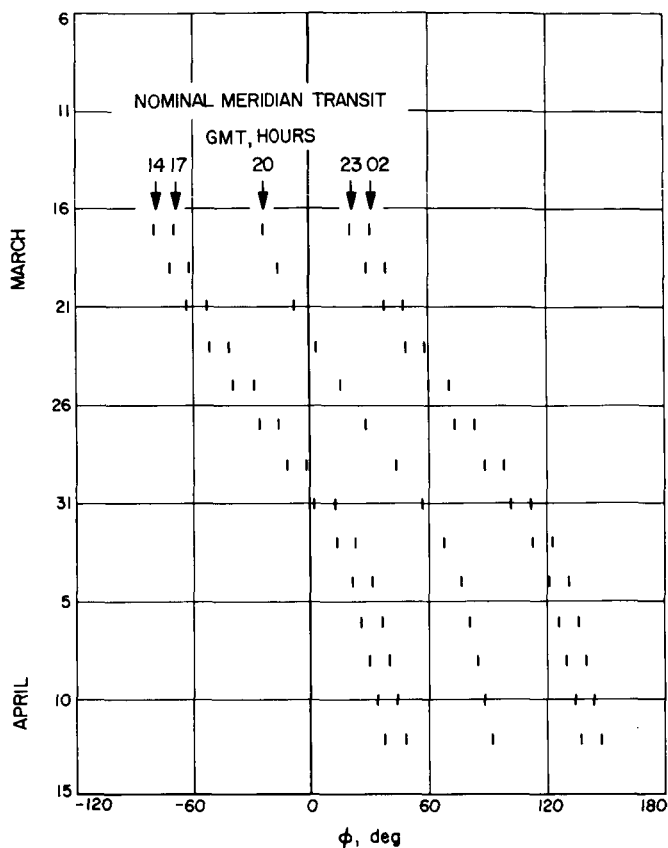
Fig. 25. Time vs conversion for normalized system noise temperature chart

No doppler data were obtained after October 1. It had been planned to update the orbit estimate with the Goldstone spectral plot data. However, the large spectral broadening of the signal masked any orbit errors which may have been present.

Encounter data and pre-encounter data were not included in the orbit fit because of the inability of the single precision orbit program to adequately model all the physical parameters involved in such a solution. The effects of some of these, such as the astronomical unit and the solar radiation pressure, are highly correlated. Other parameters, such as the Mars–Earth ephemerides, are not accurately known; unfortunately, the orbit program version used is not capable of solving for these latter quantities.

2. Orbit estimate. The comparatively small amount of postencounter data does not allow a strong solution for the astronomical unit or for small forces. For this reason the astronomical unit (149,597,500 km), which best fits the *Mariner IV* doppler tracking data near Mars encounter was used. The spacecraft reflectivity coefficient $\gamma = 0.19$, from pre-encounter tracking, was adopted, where the

solar radiation force is given by

$$F = \frac{A}{R^2}(1 + \gamma)$$

where

A = the effective area of the spacecraft exposed to the Sun

R = the Sun-probe distance

The orbit estimate is based on a weighted least-squares fit of the previously mentioned data with the JPL single precision orbit determination program.[2] Perturbations from all major planets, with the exception of Uranus, Neptune, and Pluto, are included. The solution consists of the determination of the geocentric position and velocity of the probe in true-of-date equatorial rectangular coordinates,

$$x, y, z, \dot{x}, \dot{y}, \dot{z},$$

and the geocentric station coordinates,

r_i = the geocentric radius of the ith station,

θ_i = the geocentric longitude of the ith station, for DSS stations 11, 42, 41, 51, 12, and 61. These parameters were as follows:

Parameter	Value	Standard deviation
x, km	-215952520.0	680.0
y, km	-33355757.0	634.0
z, km	-14082417.0	598.0
$\dot{x}$, m/sec	-11254.923	0.062
$\dot{y}$, m/sec	-25693.434	0.252
$\dot{z}$, m/sec	-10080.637	0.617
r_{11}, km	6372.0325	0.0198
θ_{11}, deg	243.15072	0.00038
r_{42}, km	6371.7108	0.0458
θ_{42}, deg	148.98138	0.00033
r_{41}, km	6372.6173	0.01538
θ_{41}, deg	136.88759	0.00027
r_{51}, km	6375.5133	0.0196
θ_{51}, deg	27.68551	0.00035
r_{12}, km	6371.8842	0.0248
θ_{12}, deg	243.19456	0.00025
r_{61}, km	6369.9353	0.0185
θ_{61}, deg	355.75110	0.00027

[2]M. R. Warner and M. W. Nead, SPODP — *Single Precision Orbit Determination Program*, JPL Technical Memorandum No. 33-204, February 15, 1965.

The probe position and velocity, mapped to March 1, 1966, 0^h UT, are as follows:

Parameter	Value (March 1, 1966, 0^h UT)	Standard deviation
x, km	323301780.0	339.0
y, km	−90077767.0	2889.0
z, km	−31115780.0	4724.0
$\dot{x}$, m/sec	12634.654	0.235
$\dot{y}$, m/sec	50951.929	0.127
$\dot{z}$, m/sec	21267.782	0.457

3. Ephemeris. Figure 26 is a sample of the Goldstone Mars station (DSS 14) spacecraft ephemeris generated by the ODP for March 20, 1966. The station centered quantities are:

Time = hour, minute, second of GMT

R = spacecraft slant range, km

DR = spacecraft slant range rate, km/sec

EL = elevation angle of the probe, deg

AZ = azimuth angle of the probe, deg

Dec = equatorial declination of the spacecraft, deg

HA = equatorial hour angle of the spacecraft, deg

$C1$ = doppler shift of signal received from probe beacon plus 1 MHz, Hz

$CC3$ = two-way doppler shift plus 1 MHz, Hz

4. Error sources. On March 1, 1966 the geocentric range vector lay near the x direction. The mapped-out range-rate uncertainty is accordingly approximately 0.24 m/sec or 4 Hz S-band, 1-σ on that date. Errors resulting from uncertainties in the solar radiation pressure should be comparatively small. Telemetry on May 21, 1966 indicated 3.22 lb of attitude control gas remaining compared with 4.08 lb on October 1, 1965 and 5.18 lb at launch (November 28, 1964). Thus, 3.7×10^{-3} lb/day was the gas consumption rate between October 1, 1965 and May 21, 1966.

F. Ephemeris Tuned Oscillator System

1. Introduction. The ephemeris tuned oscillator (ETO) was developed to obtain improved performance and in-

creased flexibility over previously developed programmed oscillators (Ref. 20). The system was also intended as an initial attempt to control and monitor the operation of electronic equipment by computer.

The primary feature of interest in the *Mariner IV* Sun occultation experiment is the spectra of the received signals. The signal frequency, of course, is altered by the doppler shift. *Mariner IV* had a diurnal doppler shift of over 14 kHz, and an orbital shift many times larger.

In order to obtain faithful spectra, ephemeris tuning of the receiver must be very precise. Any fluctuations, or phase jitter, of the ETO serve to degrade the quality of the spectra.

2. Description of operation. The ETO system shown in Fig. 27 controls and distributes the output frequency of a Hewlett-Packard (H-P) 5100A/5110A frequency synthesizer. A Scientific Data Systems (SDS) 920 Computer and integrated circuit logic provide remote, programmed control of the synthesizer. A rubidium vapor frequency standard is the reference for the system.

The H-P frequency synthesizer can provide frequencies from 0–50 MHz in 0.01 Hz steps. The nominal output frequency is selected by local pushbutton control or by remote programming. Variations about the nominal output frequency are accomplished by digitally controlling a search oscillator in the 10-Hz decade. A more detailed explanation of the H-P synthesizer operation is given in Ref. 21.

The most significant digits of the output frequency are set by computer control of the decade switches. A separate manual control is maintained for test purposes.

Fine frequency tuning of the synthesizer is controlled by remotely controlling the search oscillator. This is done by the digital-to-analog (D/A) converter followed by an integrating amplifier (Fig. 27). The output of the integrator is sufficiently noise-free to obtain a search oscillator resolution of one part in 200,000 (Ref. 19). Binary inputs into the D/A converter represent a rate at which the search oscillator is to change. The range of the D/A converter is ±1000 increments. Each increment causes a frequency sweep of 5 Hz/sec in the search oscillator range of 3 to 4 MHz. At the synthesizer output this represents a rate capability of up to 0.5 Hz/sec in increments of 0.5 mHz/sec.

TIME	R		DR	EL	AZ	DEC	HA	C1	CC3
200000	.33096723	09	-.35543207 01	55.826	181.841	1.084	1.034	948355.24	945056.88
200500	.33096616	09	-.35460372 01	55.775	184.064	1.085	2.285	948418.73	945183.47
201000	.33096509	09	-.35377609 01	55.684	186.279	1.086	3.535	948482.15	945310.17
201500	.33096403	09	-.35294955 01	55.554	188.481	1.087	4.786	948545.49	945436.92
202000	.33096297	09	-.35212451 01	55.395	190.667	1.088	6.037	948608.72	945563.66
202500	.33096192	09	-.35130136 01	55.178	192.832	1.089	7.287	948671.80	945690.34
203000	.33096086	09	-.35048049 01	54.934	194.973	1.091	8.538	948734.70	945816.88
203500	.33095982	09	-.34966230 01	54.653	197.087	1.092	9.789	948797.41	945943.23
204000	.33095877	09	-.34884716 01	54.336	199.170	1.093	11.039	948859.88	946069.33
204500	.33095773	09	-.34803548 01	53.985	201.220	1.094	12.290	948922.07	946195.12
205000	.33095669	09	-.34722761 01	53.599	203.233	1.095	13.541	948983.98	946320.53
205500	.33095564	09	-.34642398 01	53.181	205.210	1.096	14.791	949045.56	946445.52
210000	.33095460	09	-.34562494 01	52.732	207.147	1.098	16.042	949106.79	946570.02
210500	.33095357	09	-.34483087 01	52.252	209.043	1.099	17.293	949167.64	946693.97
211000	.33095253	09	-.34404216 01	51.743	210.898	1.100	18.543	949228.08	946817.31
211500	.33095150	09	-.34325916 01	51.205	212.711	1.101	19.794	949288.08	946939.59
212000	.33095048	09	-.34248228 01	50.641	214.481	1.102	21.045	949347.60	947061.95
212500	.33094946	09	-.34171186 01	50.051	216.209	1.103	22.295	949406.64	947183.12
213000	.33094843	09	-.34094829 01	49.437	217.894	1.104	23.546	949465.15	947303.45
213500	.33094741	09	-.34019190 01	48.799	219.538	1.106	24.797	949523.10	947422.88
214000	.33094639	09	-.33944308 01	48.139	221.139	1.107	26.047	949580.48	947541.36
214500	.33094537	09	-.33870218 01	47.457	222.700	1.108	27.298	949637.25	947658.84
215000	.33094434	09	-.33796952 01	46.755	224.221	1.109	28.549	949693.38	947775.24
215500	.33094334	09	-.33724547 01	46.035	225.703	1.110	29.799	949748.86	947890.52
220000	.33094232	09	-.33653039 01	45.296	227.146	1.111	31.050	949803.65	948004.63
220500	.33094131	09	-.33582460 01	44.539	228.552	1.112	32.301	949857.72	948117.51
221000	.33094032	09	-.33512843 01	43.766	229.922	1.114	33.551	949911.05	948229.10
221500	.33093930	09	-.33444223 01	42.978	231.258	1.115	34.802	949963.63	948339.36
222000	.33093830	09	-.33376633 01	42.175	232.559	1.116	36.053	950015.41	948448.23
222500	.33093731	09	-.33310100 01	41.358	233.829	1.117	37.303	950066.38	948555.66
223000	.33093631	09	-.33244662 01	40.528	235.067	1.118	38.554	950116.52	948661.60
223500	.33093531	09	-.33180346 01	39.685	236.274	1.119	39.805	950165.79	948765.99
224000	.33093432	09	-.33117180 01	38.831	237.454	1.121	41.055	950214.17	948868.80
224500	.33093333	09	-.33055203 01	37.965	238.605	1.122	42.306	950261.65	948969.96
225000	.33093233	09	-.32994436 01	37.089	239.730	1.123	43.557	950308.20	949069.44
225500	.33093135	09	-.32934912 01	36.203	240.829	1.124	44.807	950353.80	949167.18
230000	.33093037	09	-.32876654 01	35.307	241.904	1.125	46.058	950398.41	949263.13
230500	.33092937	09	-.32819698 01	34.402	242.956	1.126	47.309	950442.04	949357.27
231000	.33092838	09	-.32764062 01	33.489	243.986	1.127	48.559	950484.65	949449.52
231500	.33092741	09	-.32709790 01	32.568	244.995	1.129	49.810	950526.22	949539.86
232000	.33092641	09	-.32656869 01	31.640	245.984	1.130	51.061	950566.74	949628.25
232500	.33092544	09	-.32605364 01	30.704	246.953	1.131	52.311	950606.18	949714.63
233000	.33092447	09	-.32555280 01	29.761	247.904	1.132	53.562	950644.53	949798.97
233500	.33092348	09	-.32506645 01	28.813	248.838	1.133	54.813	950681.77	949881.23
234000	.33092252	09	-.32459482 01	27.858	249.755	1.134	56.063	950717.88	949961.37

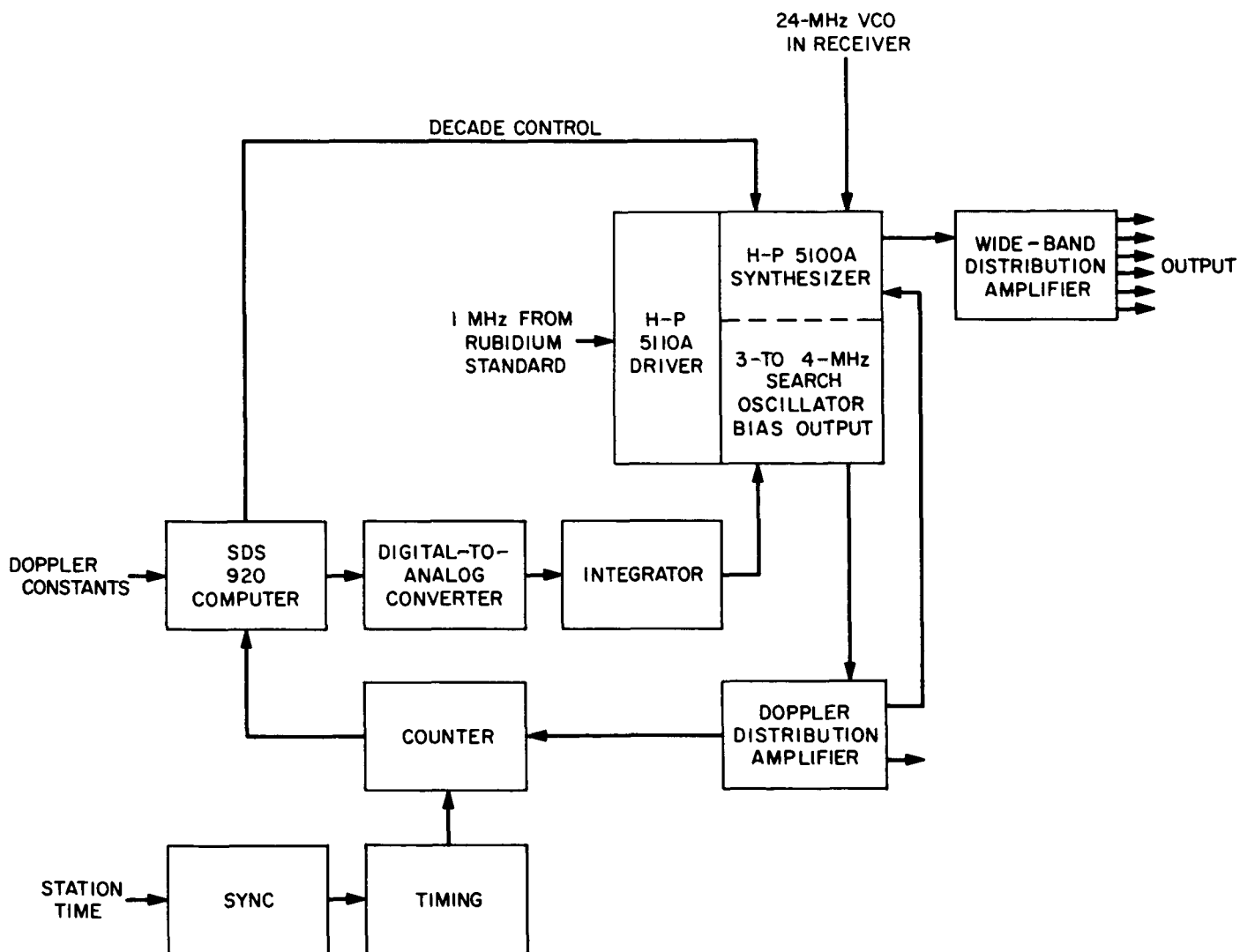**Fig. 26. Sample of DSS 14 spacecraft ephemeris**

Fig. 27. Ephemeris tuned oscillator

The exact frequency of the search oscillator is determined by a counter. A register in the counter continuously counts the frequency of the search oscillator. At periodic intervals of 1 sec, the computer can read the instantaneous count of this register. Average frequency is computed by taking the difference between the present and past counter reading. The computer arithmetic is such that even when the counter recycles through zero, a correct difference can be obtained.

The sync function permits the computer to synchronize the timing logic to within 2 μsec of the leading edge of the 1-sec station time tick.

The control program for the ETO accomplishes the following:

(1) Accepts data in the form of polynomial constants for the evaluation of the received frequency.

(2) Determines the receiver frequency and translates it into ETO requirements once a second.

(3) Tunes the ETO to the required frequency and controls the ETO to track the required frequency.

(4) Provides communication between the ETO system and the operator to determine proper operation and signal any malfunction, real or apparent, without interrupting the operation of the ETO.

An outline of the control program is given in Ref. 22.

3. Performance characteristics. A photograph of the system, as installed in the Mars station alidade control room, appears in Fig. 28. The performance of the system is summarized in Table 5. The statistics apply to the
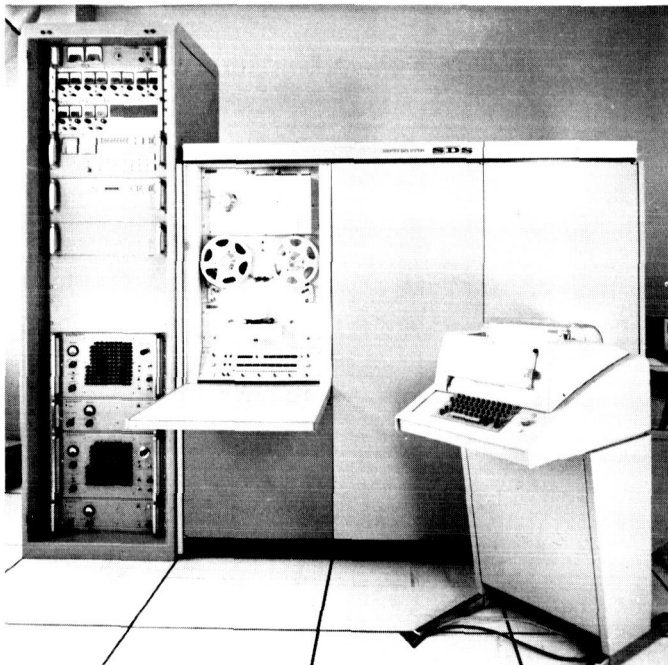

Fig. 28. ETO installation

Table 5. ETO performance characteristics

Performance characteristic	Search oscillator	Synthesizer output	S-band		Units
			Actual	Required by experiment	
Phase noise, $2B_L = 3Hz$	—	0.05	3.2[a]		deg-rms
Frequency stability, σ	3.0	0.0003	0.02		Hz
Frequency control accuracy	1.72	0.000172	0.011		Hz
Spectral line width, −6 db	—	0.0083	0.53		Hz
Total doppler range	—	100 kHz to 50 MHz	±5 MHz		—
Minimum rate change	5	0.0005	0.032	—	Hz/sec
Maximum rate change	±5000	±0.5	±32	±0.43	Hz/sec
Continuous doppler coverage	10^6	100	6400	12,000	Hz
Continuous viewing time	—	—	4.4	11.5	hr
Maximum No. of decade changes for complete view time	—	—	2	—	—
Sampling period	—	—	1	—	sec

[a] ETO contribution only.

Mariner IV Sun occultation experiment. The search oscillator was used in the 10-Hz column so that its effect on the synthesizer output is reduced by a factor of 10^4. The ETO output frequency was multiplied by 64 to obtain the receiver S-band frequency.

The contribution of the ETO to overall system phase noise was measured in a strong signal phase-locked loop at 35 MHz with a double-sided noise bandwidth of 3 Hz. The worst case situation exists when the computer is maintaining the search oscillator at a constant frequency. Under these conditions the phase noise was measured to be 0.05 deg rms. When multiplied to S-band, this phase noise represents 3.2 deg rms. This is not appreciably worse than when the search oscillator is not used. Therefore, the digital control of the ETO does not increase the system phase noise.

The ability of the digital logic to control the output frequency is determined by making a histogram of the frequency deviation of the search oscillator. The histogram appears in Fig. 29. The standard deviation of this graph is less than ⅓ mHz, or a stability of better than 1 part in 10^{11} at 35 MHz for a 1-sec averaging time. This represents a standard deviation of 0.02 Hz at an S-band frequency of 2300 MHz.

The nonzero mean of the histogram is caused by a residual offset in the D/A converter. With the present method of frequency control this represents a limit to the accuracy of setting the output frequency of the ETO. This accuracy represents 1 part in 10^{11}.

The line width of the ETO is that of the H-P synthesizer. This has been measured at X-band (Ref. 23) and corresponds to a -6-db line width of 0.53 Hz at S-band.

The ETO was able to provide the doppler rates and the doppler coverage necessary for the Sun occultation experiment. The single limitation is the range of continuous doppler coverage. With the search oscillator in the tens of hertz column, the range of continuous doppler coverage
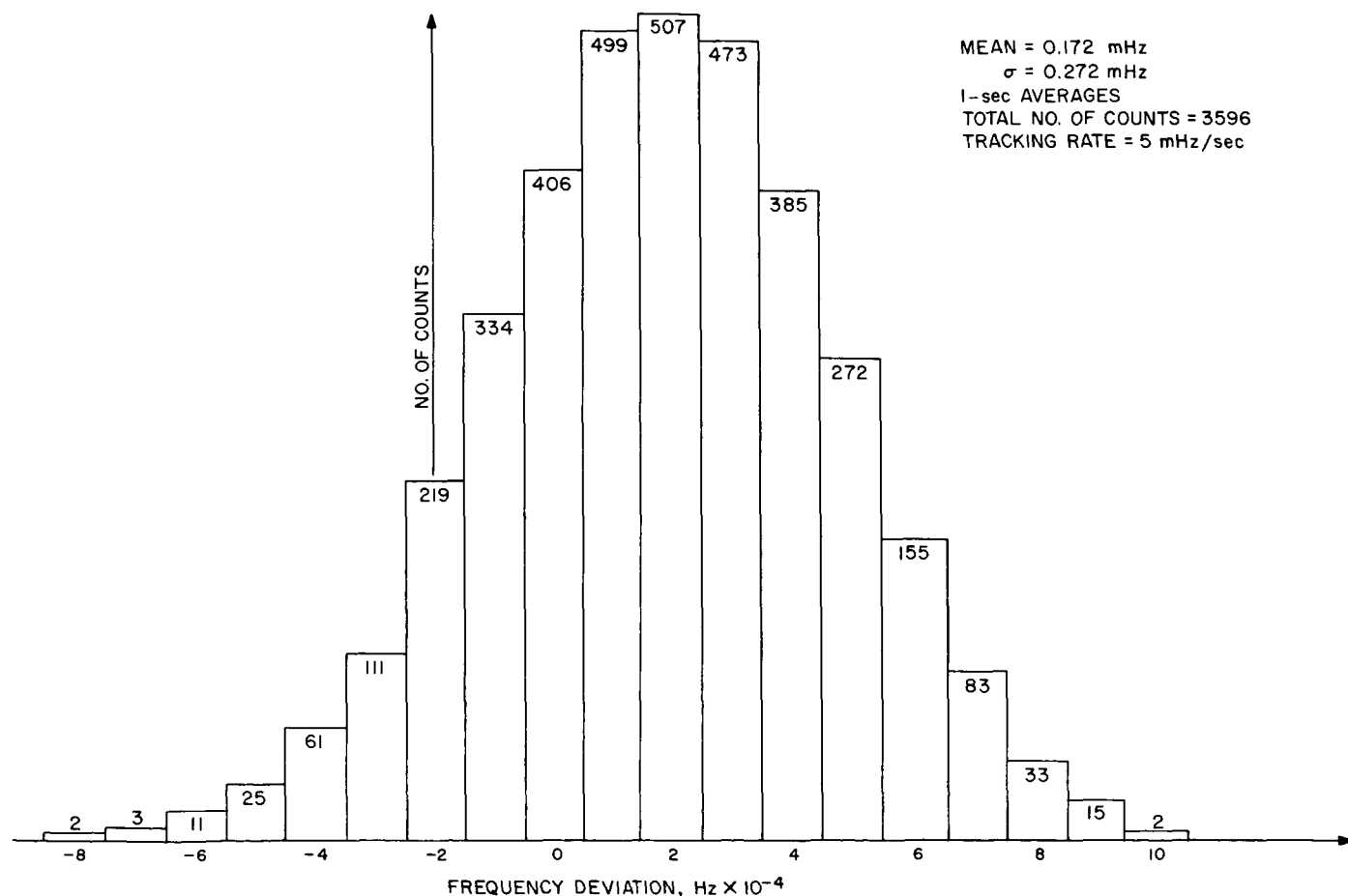

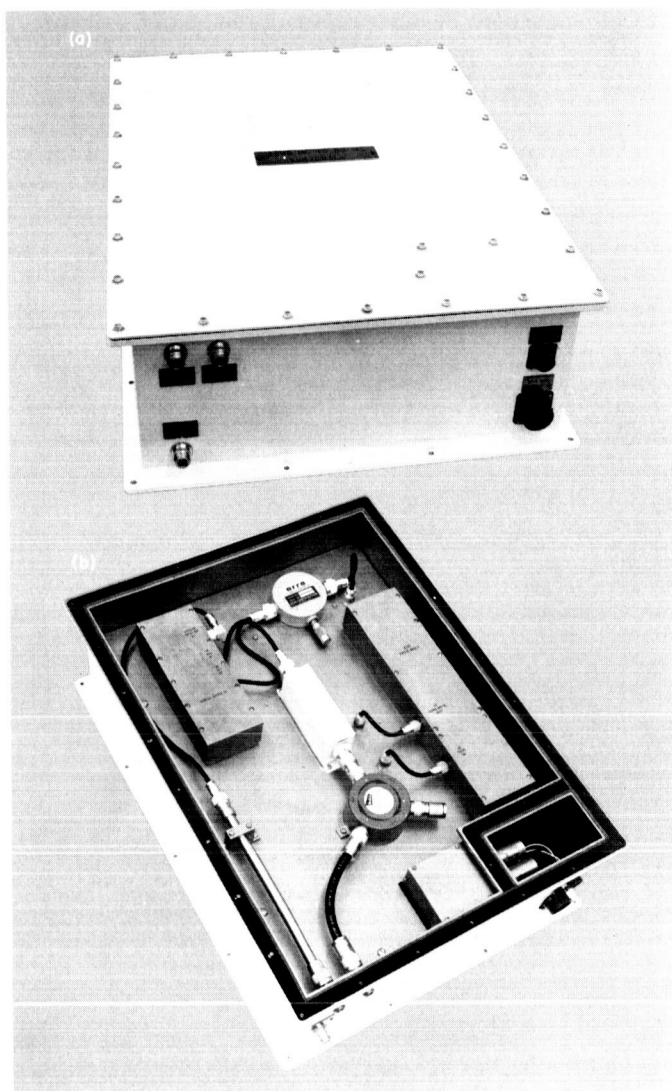**Fig. 29. Histogram of ETO frequency stability**

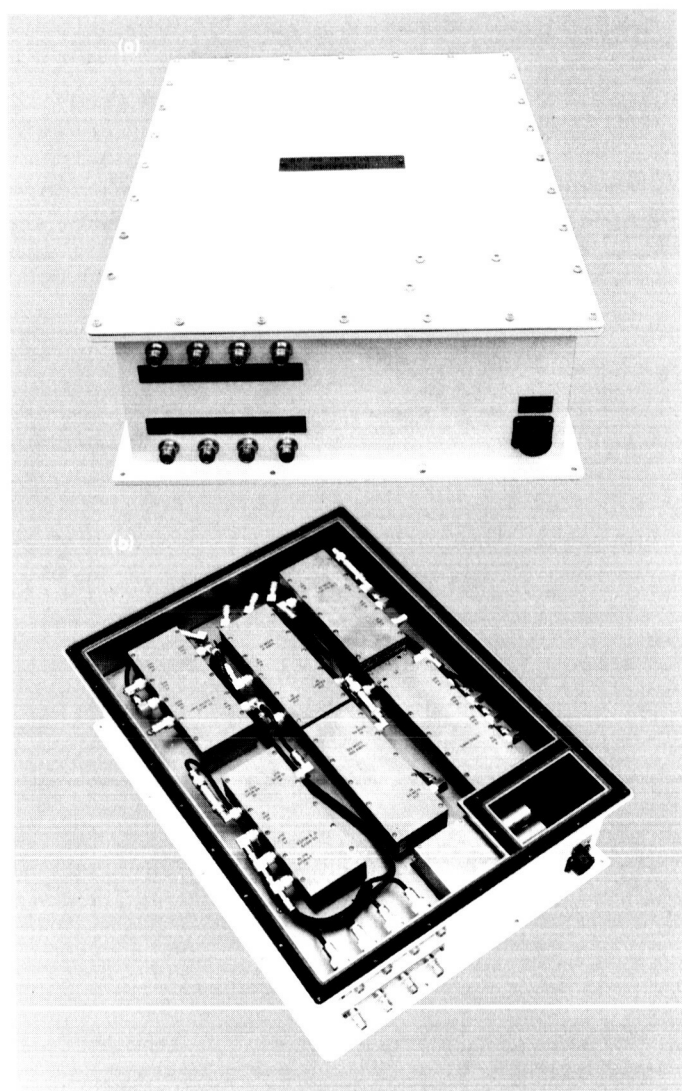Fig. 30. 2295- to 50-MHz converter:
(a) exterior; (b) interior

Fig. 31. 50-MHz to 1050-Hz converter:
(a) exterior; (b) interior

is 100 hz. The minimum time for switching is 5 sec with an absolute maximum switching time of 105 sec. The average switching time is approximately 10 sec. For noncoherent spectrum analysis this switching time is small compared to total integration time.

G. Receiver

Initial planning for postencounter tracking of *Mariner IV* at the Goldstone Mars station included modification of the Goldstone duplicate standard receiver for use with an ephemeris tuned local oscillator (ETO) for open-loop tuning and an autocorrelator for signal processing. These changes were to consist of:

(1) Cabling to allow injection of 70-MHz ETO output into the standard ×32 frequency multiplier;

(2) Provision for a special ×12 frequency multiplier to supply a stable 60-MHz second local oscillator (to be derived from the 5-MHz output of the frequency and timing subsystem); and

(3) Addition of a stable third local oscillator (commercial synthesizer), balanced mixer, and special IF amplifier to provide an output to the autocorrelator.

When it became apparent that the station implementation schedule would not provide a standard receiver until late spring of 1966, an experimental receiver for this purpose was decided upon instead. Figures 30–32 are views of the antenna-mounted and control room equipment. The block diagram is presented in Fig. 33. The "cone area" portion of the block diagram follows that of the conventional tracking receiver block diagram. The first and second local oscillator frequency multipliers and third mixer were special designs for this application, while the third local oscillator and excitation for the test transmitter were provided by commercial frequency synthesizers, chosen primarily for their flexibility in output frequency. A major portion of the signal gain was provided by means of a variable gain, narrow band (500 Hz) 455-kHz IF amplifier as used in the planetary radar receiver. Finally, the output video amplifier was used solely to isolate 60 Hz interference in
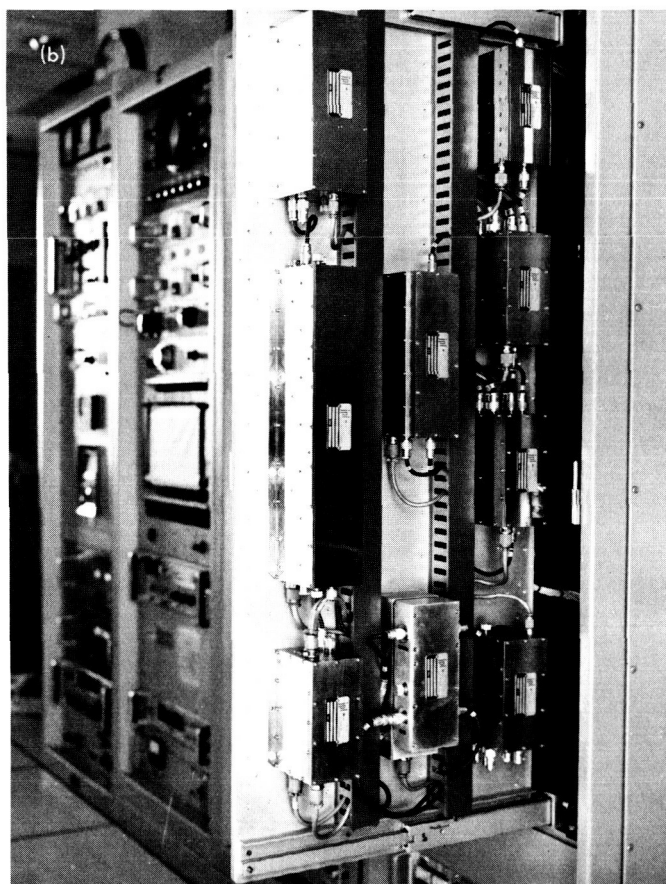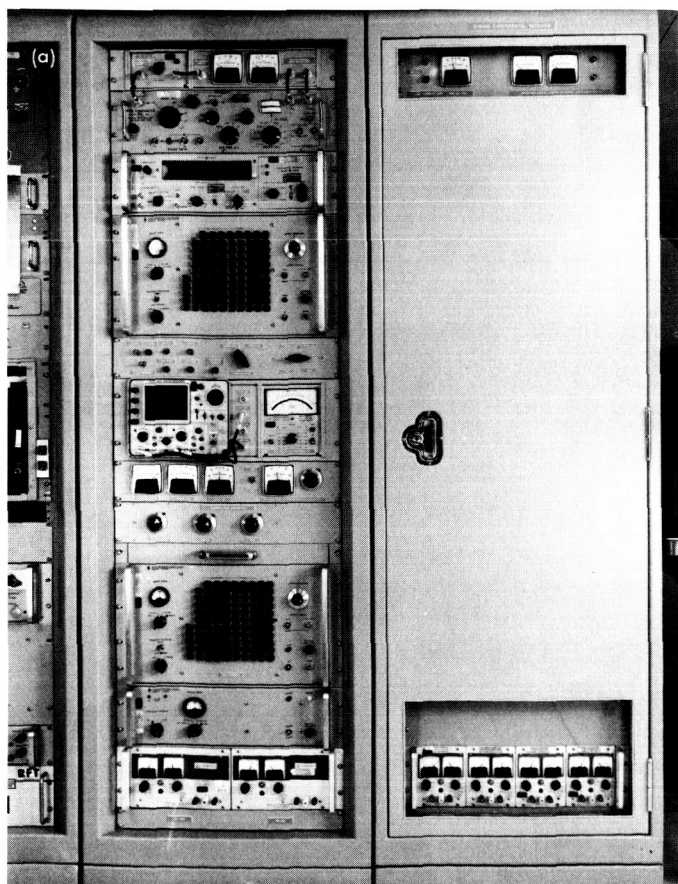

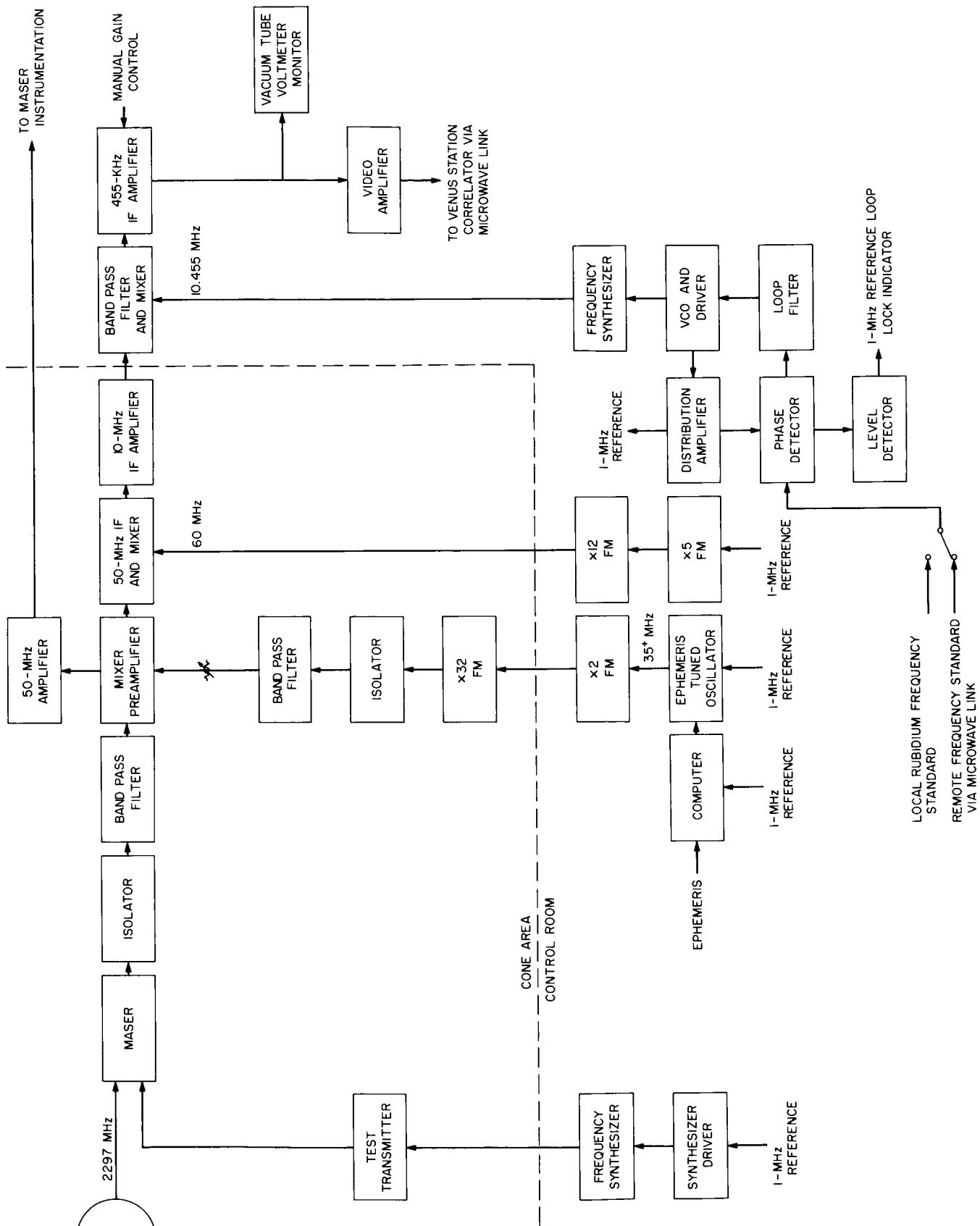**Fig. 32. S-band experimental receiver: (a) exterior; (b) interior**
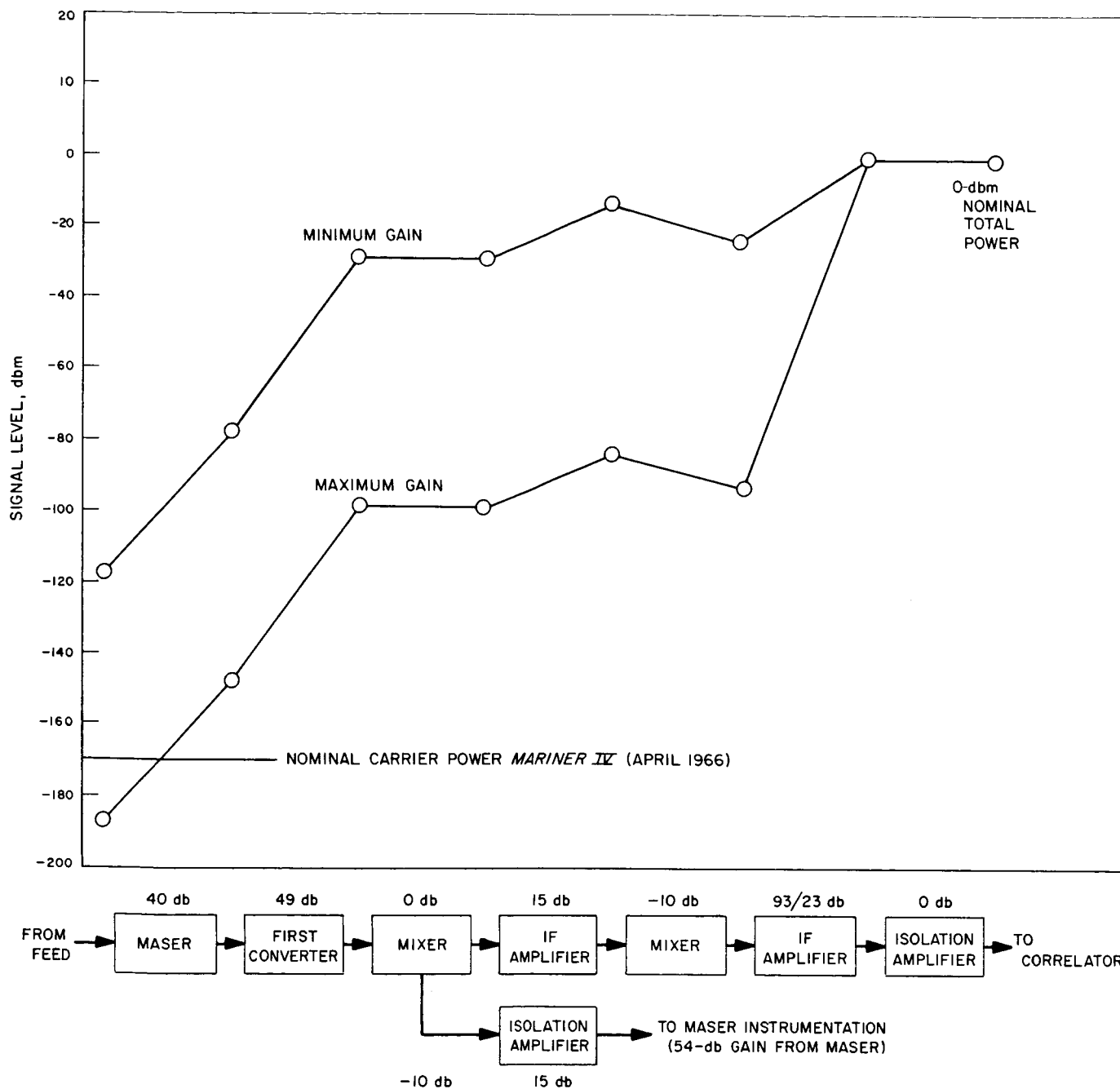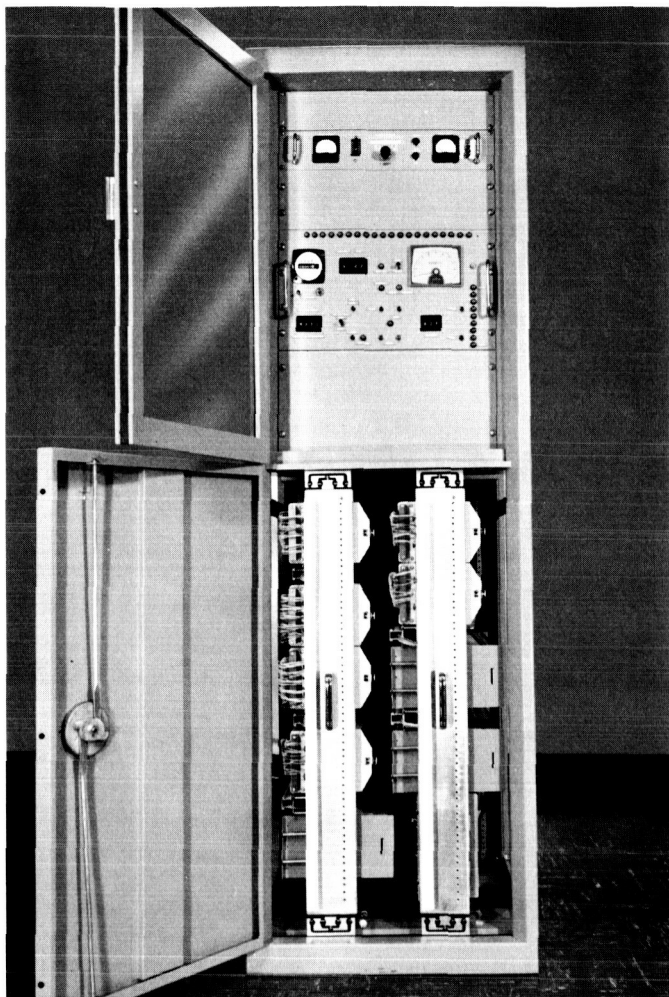
Fig. 33. Experimental receiver

Fig. 34. Signal profile

Fig. 35. Nine-channel autocorrelator

the interface with the microwave link. The resulting gain distribution is shown in Fig. 34.

Additionally, a 1-MHz clean-up loop and distribution system were utilized in connection with the microwave link from Venus station to establish a common frequency reference with the transmitter and correlator (refer to subsection II. J. in this report). The receiving system, as described above, was installed and initially tested in the "3A" cone adapter and alidade control room, and was used in the antenna calibration and Sun occultation activities commencing March 16, 1966.

H. Spectrum Analyzer

The equipment used to obtain the power spectrum of the received *Mariner IV* signal was the nine-channel autocorrelator, shown in Fig. 35, and an SDS 930 computer.

First, the autocorrelation function coefficients of the signal are accumulated in real time within the autocorrelator. After an accumulation time of up to several hours, the computer reads out these coefficients and by means of the Fourier transformation computes the power spectrum.

The nine-channel autocorrelator has two modes of operation. One mode provides nine separate channels, each containing storage for 51 autocorrelation lag points. Used in this mode, the autocorrelator has the capability of measuring the spectra of nine independent signals. In the second mode of operation, which was used in this occultation experiment, the nine channels are cascaded to form a single channel autocorrelator with 459 lag points.

Figure 36 is a block diagram of the nine-channel autocorrelator. Control of the autocorrelator by the computer is accomplished by means of a series of binary coded computer commands. These commands are decoded by the command decoder logic from which they are routed to either the autocorrelation control and output logic, the digital-to-analog (D/A) converter, or the pen-control logic. Commands to the autocorrelation control and output logic perform such functions as starting and stopping correlation, and outputting the accumulator storage one bit at a time simultaneously from each of the nine channels.

Each channel contains a recirculating delay line storage for 50 autocorrelation (lag) points plus the lag point for zero argument. Each lag point occupies 20 bits of binary storage, which provides a count capacity of 1.05 million samples. Fifty lag points allow the derived power spectrum to be resolvable to one-fiftieth of the total system band-pass. In the cascaded mode of operation, the maximum resolution is the system bandwidth divided by 459.

The timing and sampling logic provide accurate timing pulses for the correlator logic and for sampling of the input signal. High accuracy is obtained by tying the logic to an atomic standard by means of a 1-MHz reference signal.

Plotting of the computed power spectrum curve is accomplished by means of computer commands to the D/A converter and pen-control logic. The D/A converter provides position information for both the x and y axes of the X-Y recorder, and the pen-control logic permits the computer to raise or lower the X-Y recording pen on the recording paper. Further details of the nine-channel autocorrelator may be found in Ref. 24. Table 6 summarizes the correlator capability and lists the constants used in the experiment. The filter entry refers to a plug-in band pass
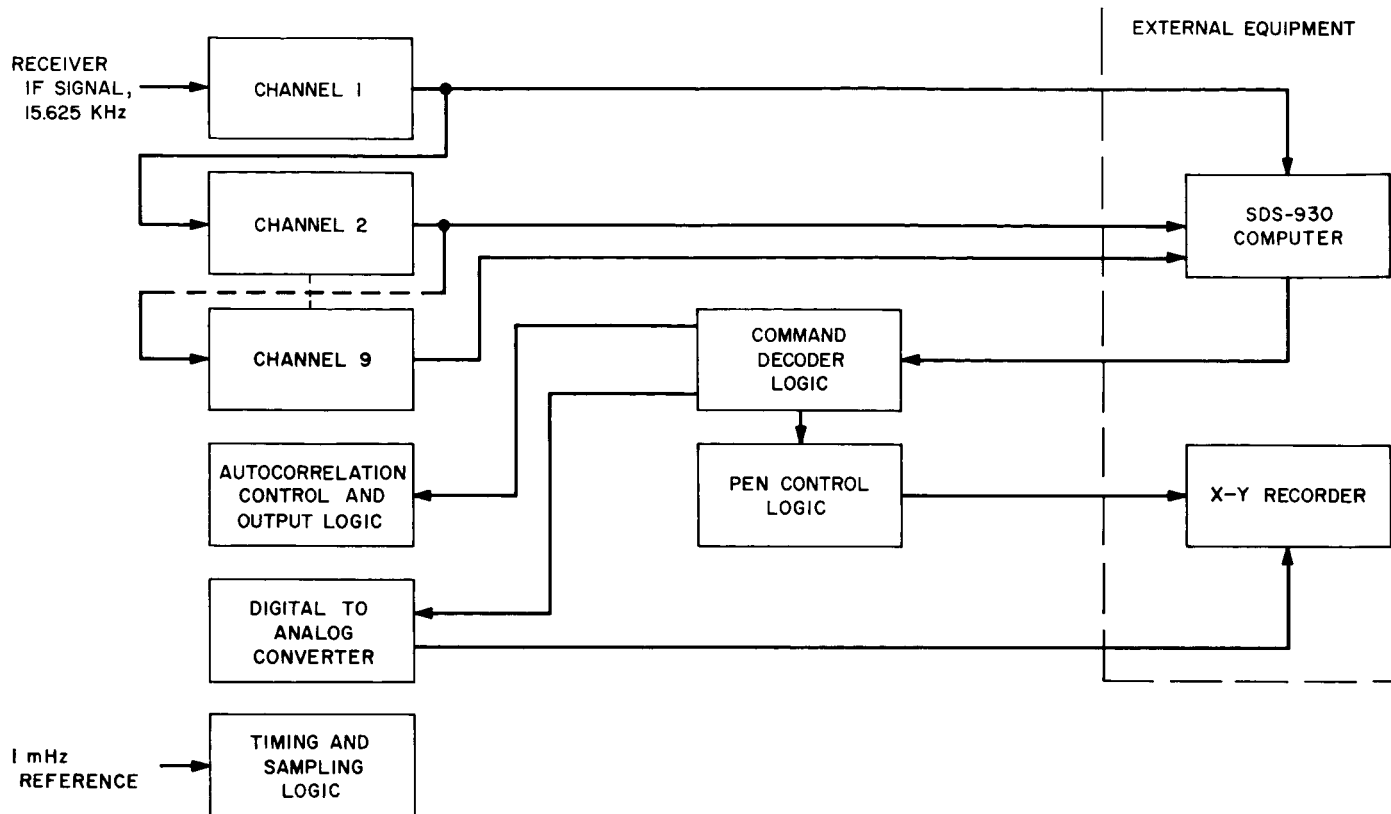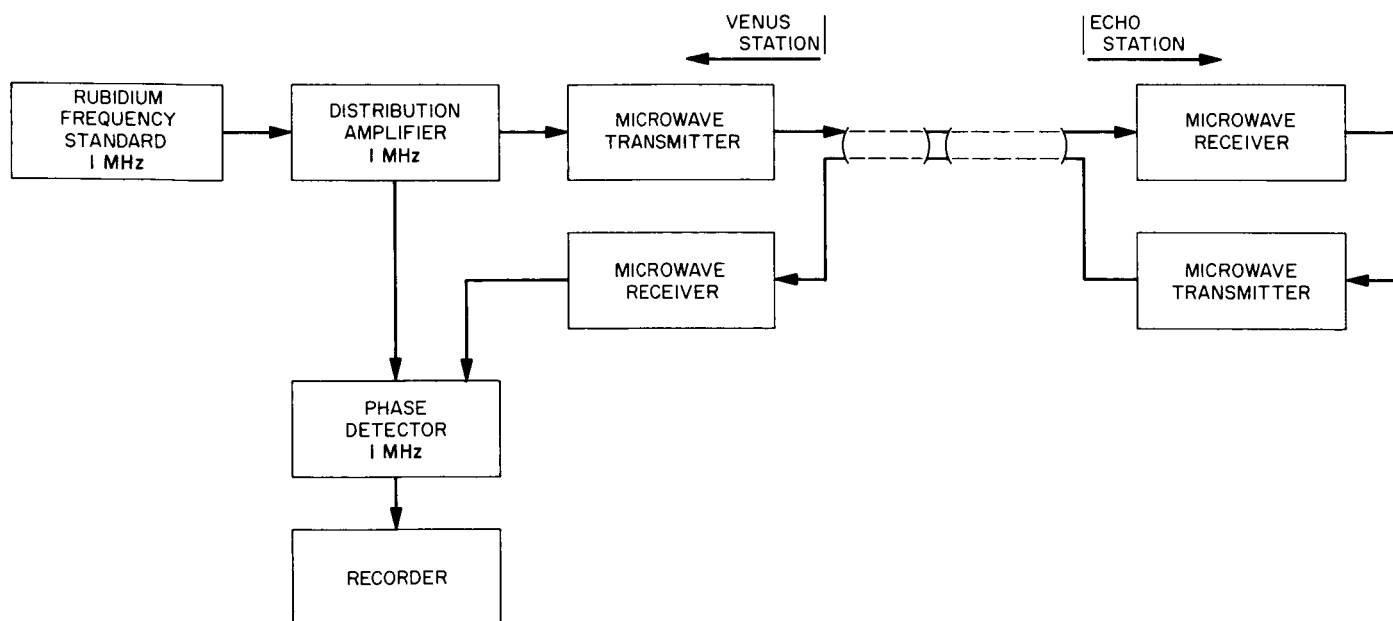
Fig. 36. Autocorrelator block diagram

Fig. 37. Test setup to measure wind modulation

Table 6. Autocorrelator constants

Parameter	Sampling rate		Experiment	
	Maximum	Minimum	One way	Two way
Sampling rate, samples/sec	961.54	49.02	58.70	235.85
Sampling period, μ sec	1040	20400	17040	4240
Autocorrelator bandwidth, Hz	480.77	24.51	29.34	117.92
Filter bandwidth, Hz	—	—	25	100
Maximum cascaded mode resolution, Hz	1.05	0.053	0.064	0.26
Maximum integration time, hr	0.30	5.95	4.97	1.24

filter within the channel used to limit received noise, prevent noise spectrum folding, and provide the overall receiver band pass characteristic.

I. Frequency Standard

The choice of a frequency reference standard for the experiment employed the same criteria (good short term and long term stability with high reliability) that resulted in the selection of the rubidium standards for the DSN. These units are described in Refs. 25 and 26. The stability data are reproduced in Table 7.

Table 7. Stability data for rubidium vapor standards

Averaging time	Stability of two units, Hz at S-band
50 msec	$\pm 5 \times 10^{-11} \pm 0.12$
500 msec	$\pm 2 \times 10^{-11} \pm 0.05$
5 sec	$\pm 0.5 \times 10^{-11} \pm 0.012$
8 min	$\pm 0.4 \times 10^{-11} \pm 0.009$
40 min	$\pm 0.4 \times 10^{-11} \pm 0.009$

Table 7 shows that, for the round trip and integration times used in this experiment, the error in frequency measurement due to the frequency reference standard amounts to only ± 9 mHz. Moreover, these two standards operated almost continually for nearly 3.5 yr with only one failure per unit. The frequency standards operate with frequencies nominally based on the A1 time scale.

Since the most recent data on *Mariner IV*, i.e. the monthly measurements of frequency used one of these standards at the Venus station, the data for setting the required frequencies at the exciter (Venus station) and receiver (Mars station) were based on that standard, and that standard was used during the experiment. The reference frequency was sent from the Venus station to the Mars station via the microwave link and filtered by means of a narrow-band clean-up loop for use as the fre-

quency standard for the Mars station to eliminate any errors from long term drift which might occur using two separate standards.

The second standard was installed in the frequency time standard at the Mars station during this experiment for use in case of failure either of the operating standard at the Venus station or of the microwave link. This second standard was adjusted to within 1×10^{-12} of the frequency of the operating standard by means of the doppler extracting hardware. This standby unit was not required during the experiment.

J. Microwave Link

A microwave link was established to facilitate communications and data handling between the Mars station and the other Goldstone tracking stations.

This link consists of two paths — Venus to Echo, and Echo to Mars — and was first used to furnish a coherent reference frequency between the Venus and Mars stations for the *Mariner* occultation experiment. Before the Echo-to-Mars microwave link was completed, preliminary investigations were made on the existing Venus-to-Echo link. As originally installed, the Venus-to-Echo path suffered severe phase transients caused by automobile interference. This path was changed, and the problem of traffic modulation was eliminated. However, tests indicate that a 1-MHz signal can have 0.1-deg peak-to-peak phase transients caused by wind modulation. Figure 37 shows the test setup to measure both wind and traffic modulation.

The terminal microwave equipment used on the Venus-to-Echo path ($P_0 = 100$ mw, vacuum tube receiver) was investigated to determine methods of minimizing phase noise. The drive level into the transmitter modulator was found to be critical. Too much drive causes the reflex klystron to generate noise, and too little signal reduces the signal-to-noise ratio. Further, there is less noise when
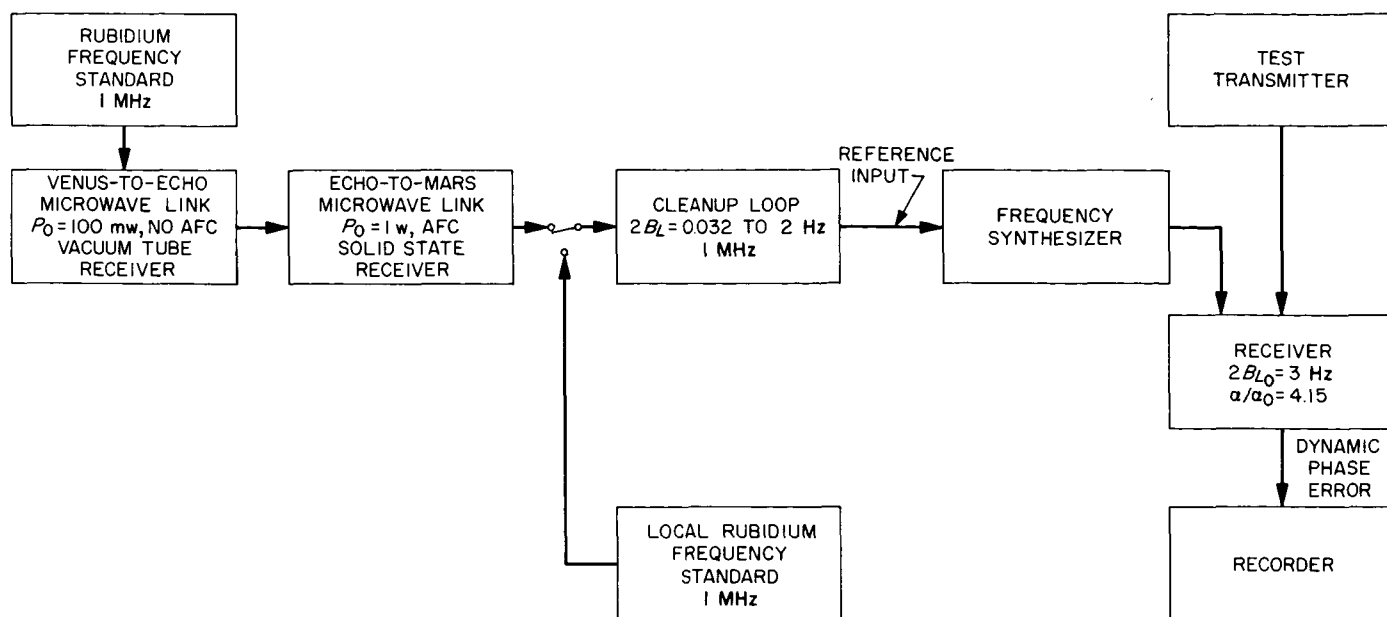
Fig. 38. Test setup to measure receiver jitter as a function of 1-MHz reference source
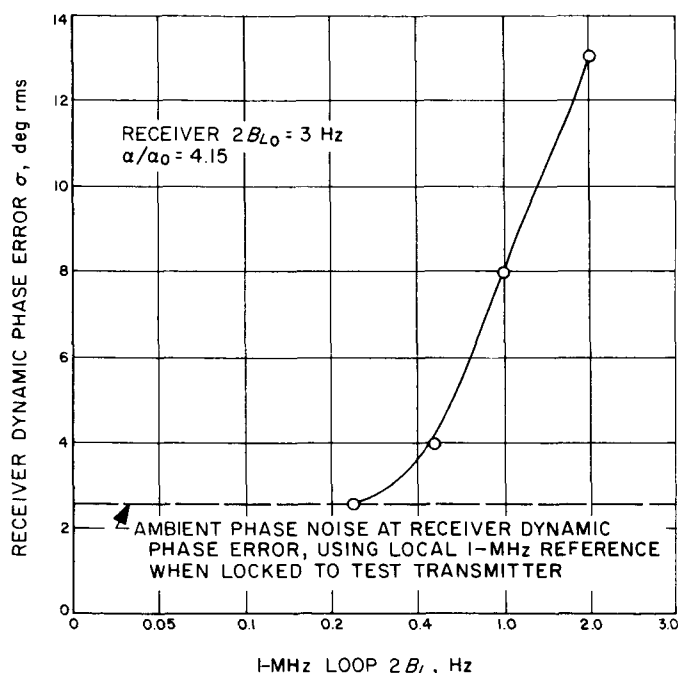

Fig. 39. Jitter on dynamic phase error of receiver as a function of 1-MHz clean-up loop bandwidth

the relay point is connected so that the receiver drives the transmitter directly than when the de-emphasis and pre-emphasis circuits that are part of the microwave system are used.

The complete path was investigated and connected as shown in Fig. 38. The bandwidth of the 1-MHz cleanup loop was optimized by observing the dynamic phase error (DPE) of the receiver (when the receiver was locked to a local test transmitter). The results of this test (Fig. 39) indicate that a $2B_L$ of 0.25 Hz or less will allow the Venus 1-MHz rubidium frequency standard to be used with no degradation to the Mars-receive system. The 1-MHz cleanup loop is presently operating with a design $2B_L$ of 0.032 Hz.

The 100-mw equipment used in the present microwave link between Venus and Echo has no automatic frequency control (AFC) on the transmitter. The resultant circuit outages have created a reliability problem. This problem has apparently been eliminated in the new, solid state, 1-w equipment used between Echo and Mars. Added flexibility is available in the new equipment since it has a 6½-MHz bandwidth, in contrast to the 4½-MHz bandwidth of the 100-mw system.

III. Experimental Procedure and Data

The superior conjunction of *Mariner IV* occurred while the 210-ft antenna was being constructed. However, because of the splendid cooperation of the Rohr Company, it was possible to perform the experiment in spite of this difficulty. The observations were "interleaved" with finishing work on the main azimuth bearing. Consequently, less

than half of each view period was available for gathering data. Sometimes this was the first half, while work was being done on west sections of the bearing. When east sections needed attention, *Mariner IV* was observed during the lowering part of the pass. Sometimes, of course, this interleaving was not possible and data were lost. Altogether, data were taken during 15 different days.

Two separate experiments were performed each day, time and construction work permitting. The first mode was one-way operation. That is, the ground transmitter was switched off and *Mariner IV* transmitted from its free-running crystal oscillator. This signal passed through the solar corona once, and the resulting spectrogram shows the amount of spectral broadening induced upon the signal by the corona. For eleven days, starting on the day of closest angular approach to the Sun, one-way spectrograms were obtained. These are reproduced here as Figs. 40 through 50. The frequency scale is the same for each, ±14.7 Hz full scale. Zero frequency corresponds

to the doppler shift of the known orbit of *Mariner IV*. Some extra noise, caused by the system bandpass not extending into this region, is to be seen on the left edge of these spectrograms and should be disregarded.

The integration time for these spectrograms varied from 30 min to 1 hr, with 45 min being typical. The fluctuations on the spectrograms show the random noise, which is still left after such integration. The frequency resolution of these spectrograms is 0.245 Hz. That is, if a perfect sinusoid were observed, the resulting spectrum would be 0.245 Hz wide at the half power points. This is more resolution than needed for most of the spectra; less resolution would result in smaller noise fluctuations.

As can be seen from these data, the spacecraft oscillator was subject to an unpredictable component of frequency drift. Any such drift, during the integration time, is effective in broadening the spectrum of the signal. To determine the extent of this effect, six spectrograms were taken
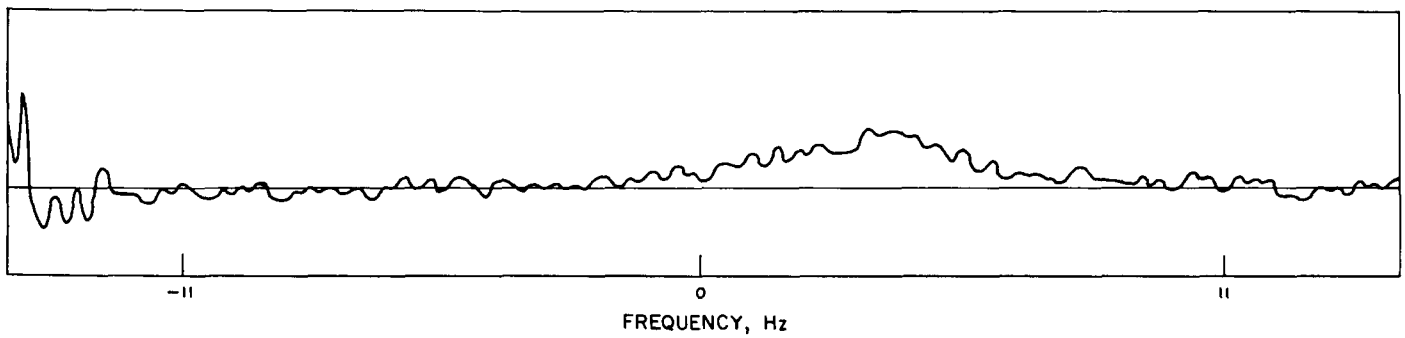

FREQUENCY, Hz
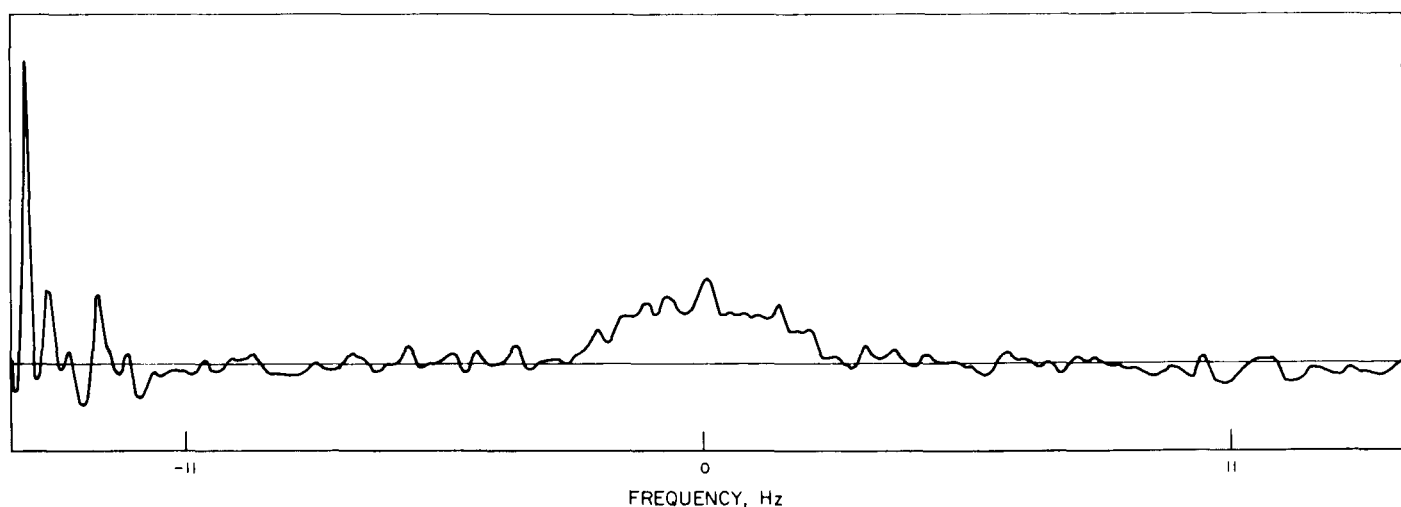
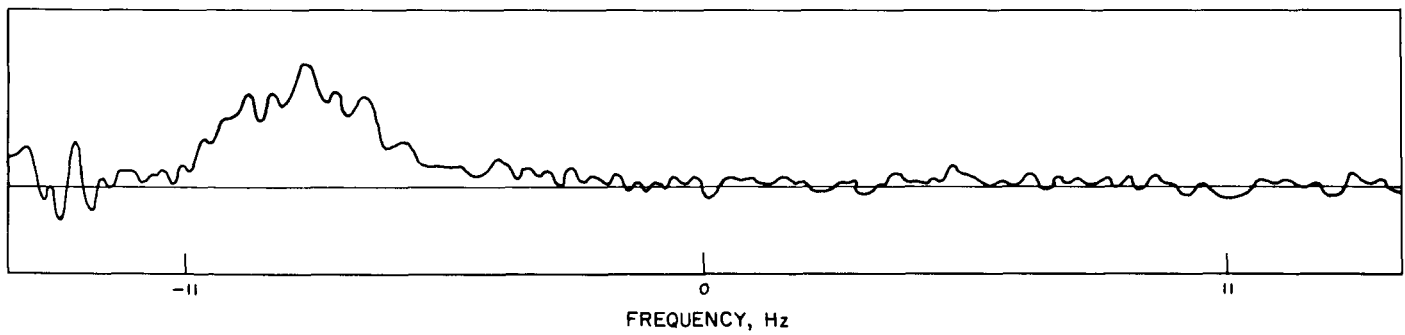**Fig. 40. March 27, 1966 one-way spectrogram**

FREQUENCY, Hz
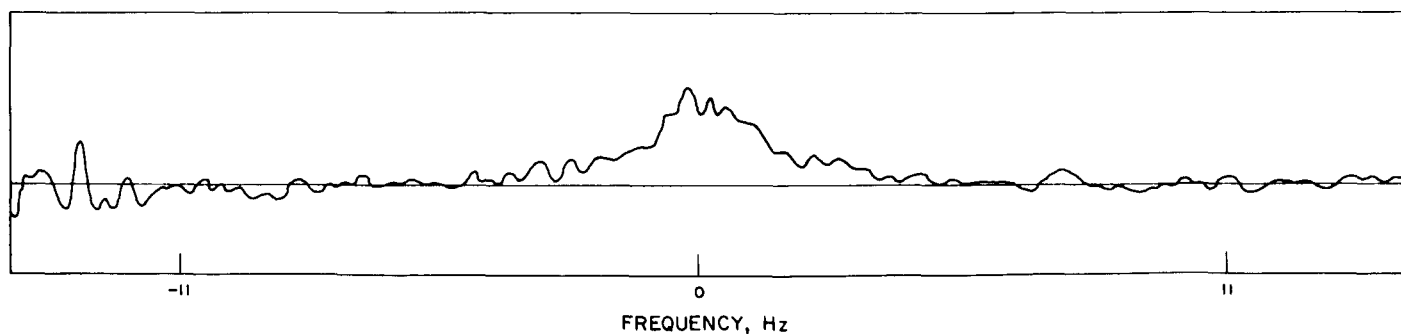
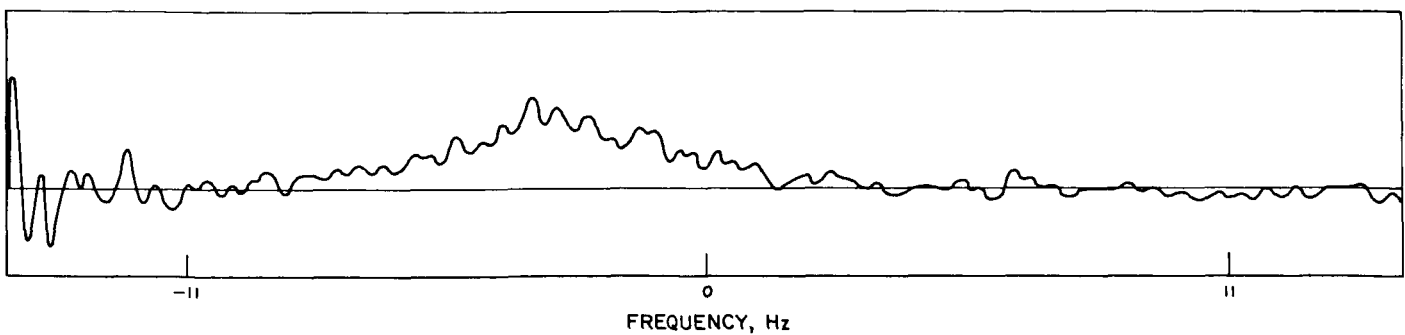**Fig. 41. March 28, 1966 one-way spectrogram**
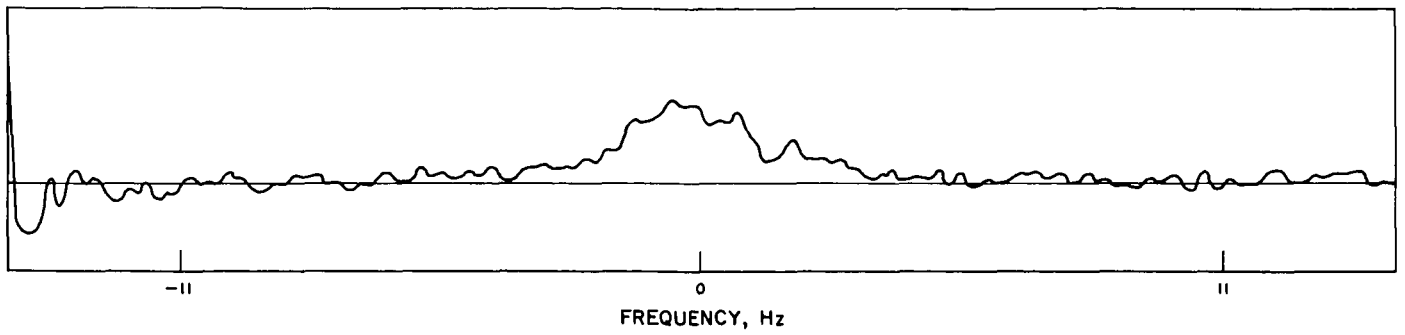
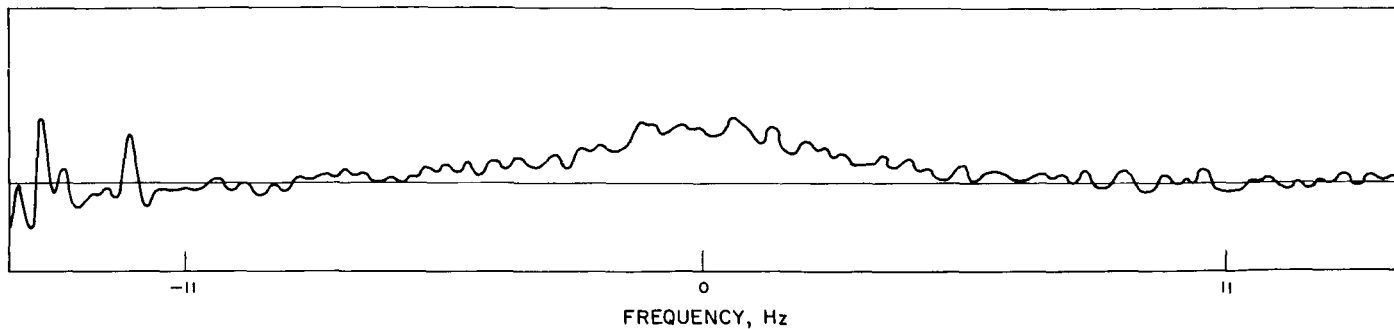**Fig. 42. March 29, 1966 one-way spectrogram**
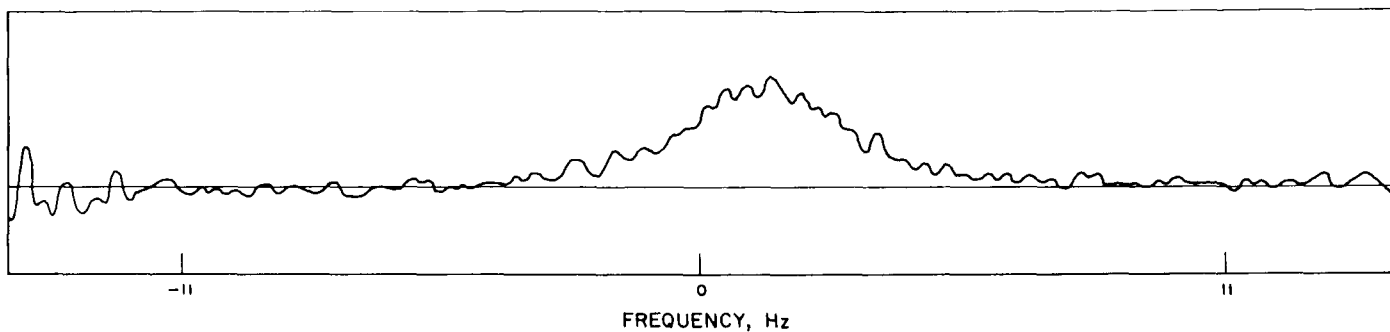

Fig. 43. March 30, 1966 one-way spectrogram

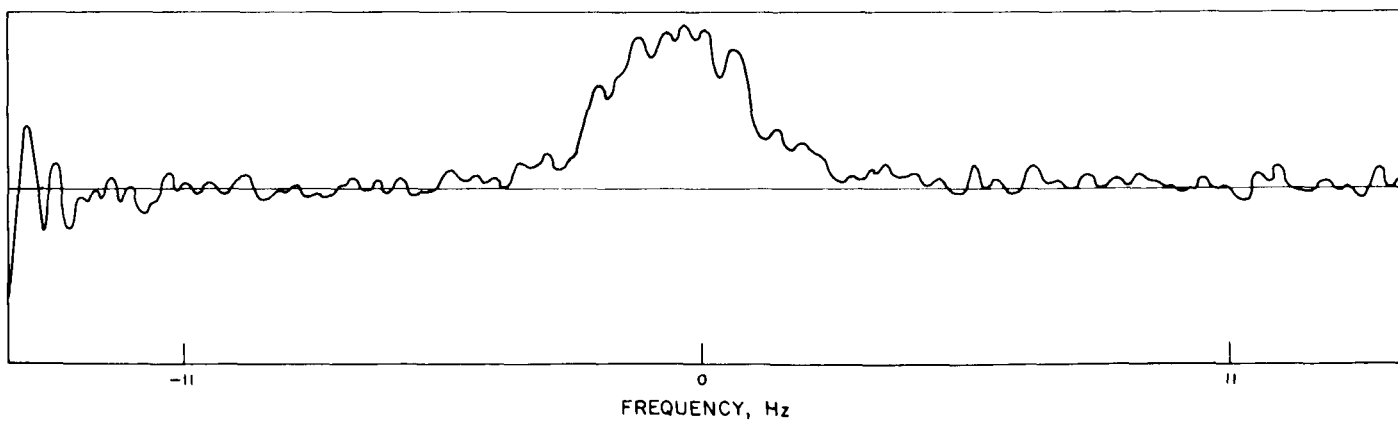**Fig. 44. March 31, 1966 one-way spectrogram**

Fig. 45. April 1, 1966 one-way spectrogram
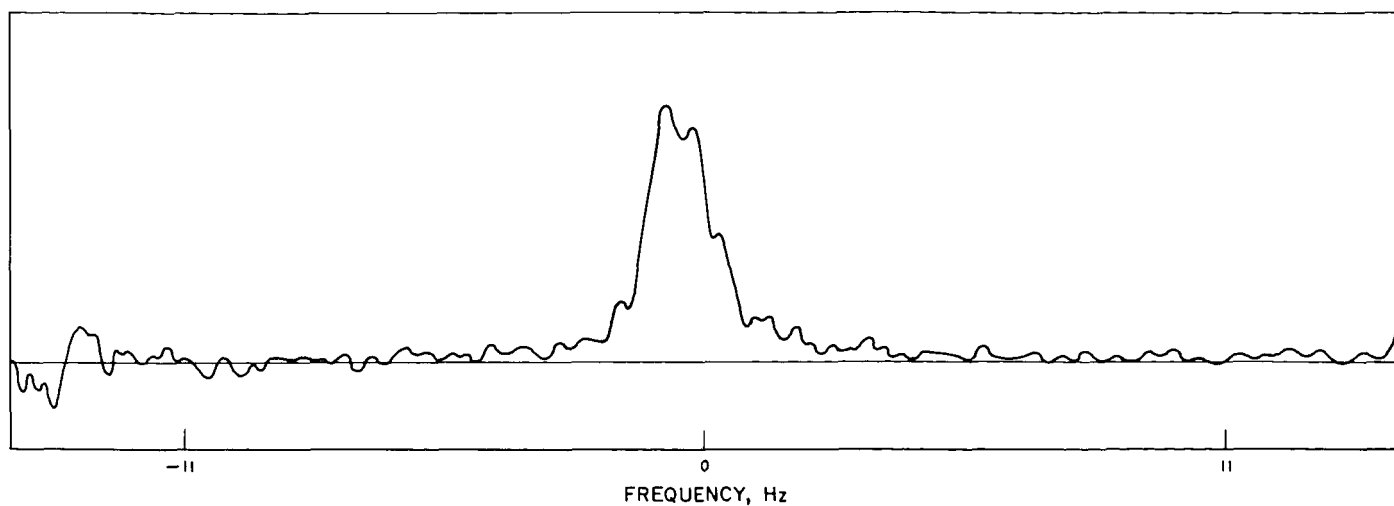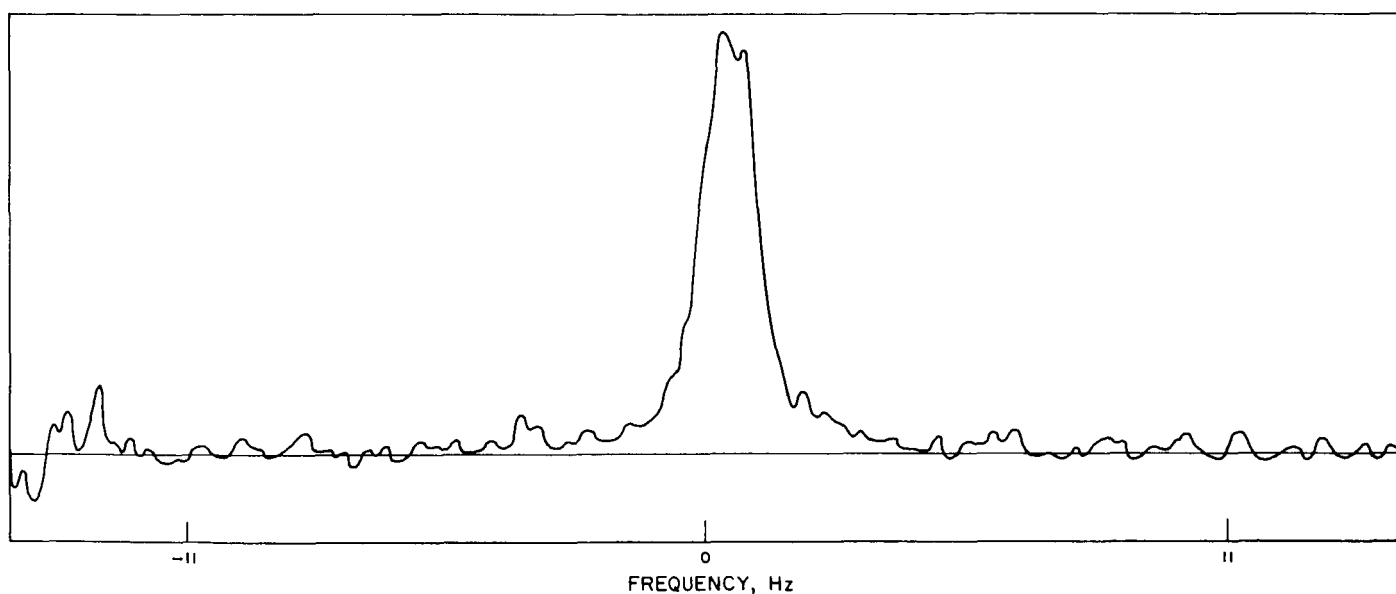
Fig. 46. April 3, 1966 one-way spectrogram

Fig. 47. April 4, 1966 one-way spectrogram

Fig. 48. April 5, 1966 one-way spectrogram

FREQUENCY, Hz

Fig. 49. April 6, 1966 one-way spectrogram

FREQUENCY, Hz

**Fig. 50. April 7, 1966 one-way spectrogram**

May 3, when the *Mariner IV* transmission path was far from the solar corona. These spectrograms are reproduced as Figs. 51 and 52. They were taken under essentially the same conditions as the first set and can help calibrate the effect of oscillator drift on the spectral widths of the signals.

The second type of measurement was two-way spectra. In this mode of operation, the spacecraft transmitter was phase-locked to the ground transmitter. To achieve this up-link lock, the ground transmitter was tuned very slowly past the calculated frequency of the spacecraft receiver.

The slow tuning, plus the 30-min time-of-flight, used up much of the precious available time. In order to use the time efficiently, one-way spectral measurements were made during the tuning process.

The two-way operation removed the troublesome drift in the spacecraft transmitter, but substituted another form of uncertainty in its place. The signal received by the spacecraft had passed through the solar corona, and consequently was spectrally broadened similar to the spectrograms of Figs. 40 through 50. The spacecraft could track

FREQUENCY, Hz
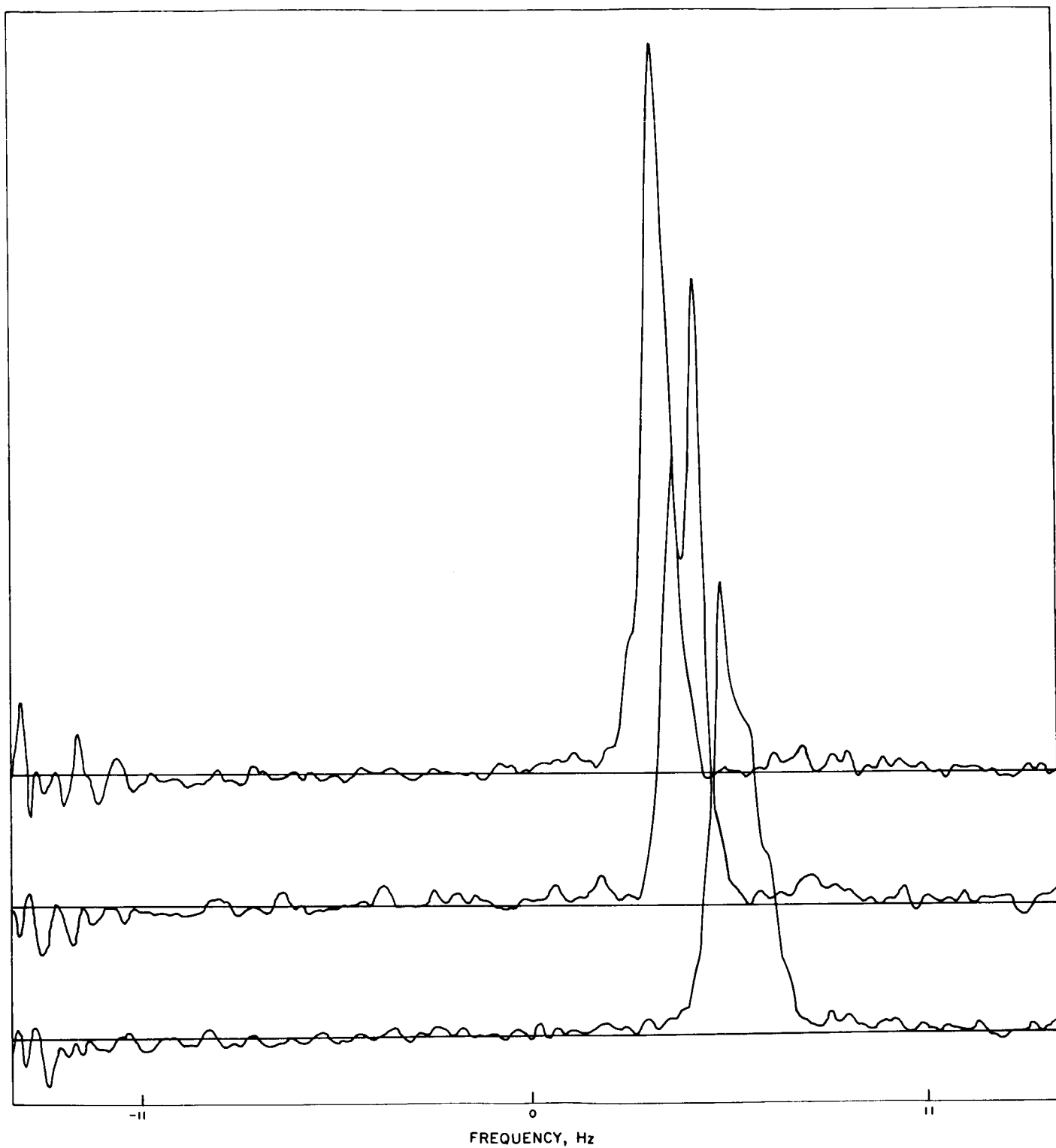
Fig. 51. First set of one-way spectrograms, May 3, 1966
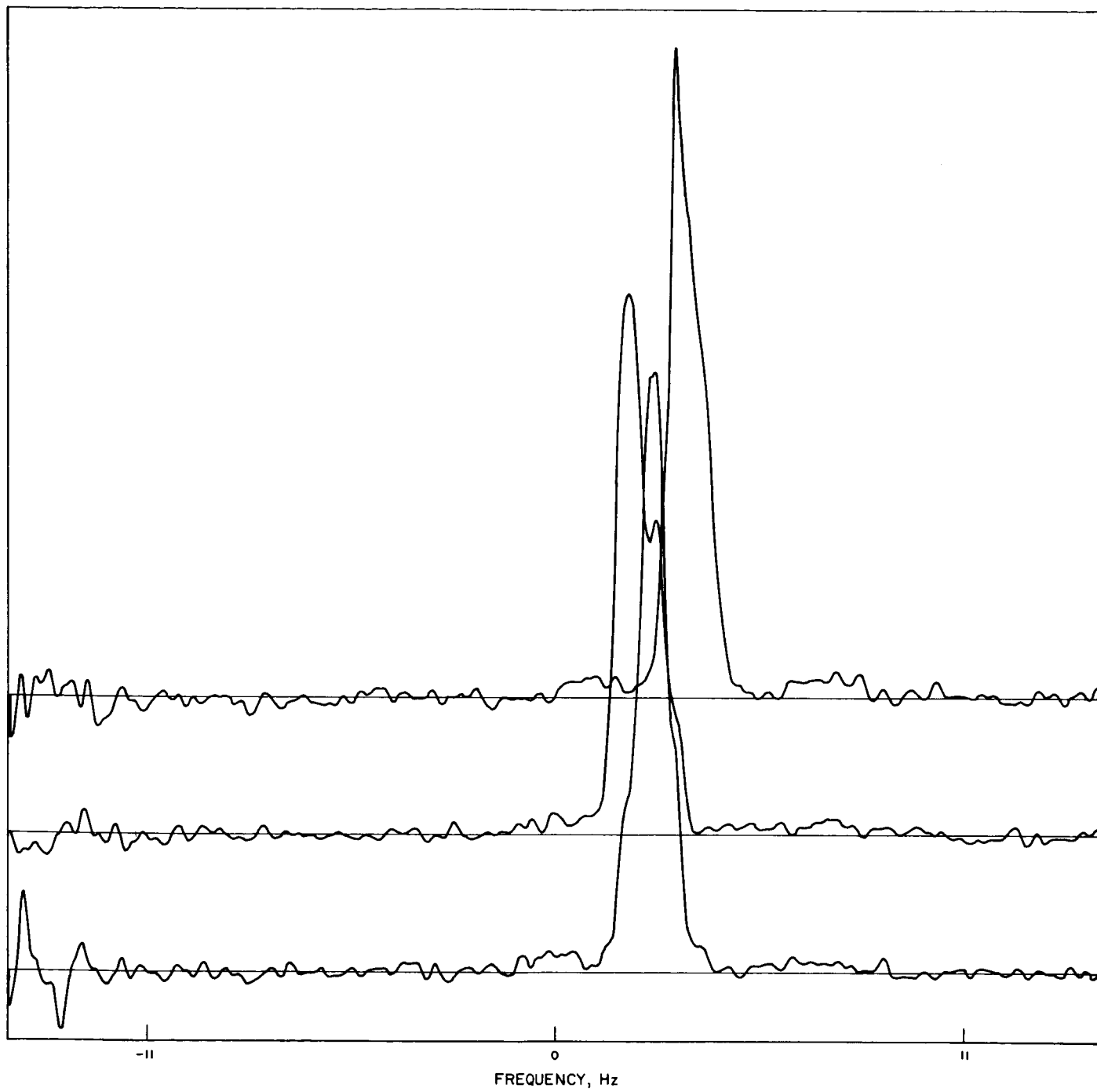
Fig. 52. Second set of one-way spectrograms, May 3, 1966

any phase variations of the signal, but none of the amplitude variations. Of course, the "mix" of amplitude and phase fluctuations generated by the corona is not known.

The reradiated signals passed through the corona a second time and were recorded as spectrograms. In all, seventeen two-way spectrograms were taken. They are reproduced here as Figs. 53 through 69. These spectrograms cover 118 Hz full scale and have a frequency resolution of 0.984 Hz. The increased scale of the spectrograms was needed to accommodate the much greater spectral width of the two-way signals. Integration time for these observations was, again, approximately 45 min.

The observed spectral broadening can be attributed not only to two trips through the solar corona but also to one trip through the spacecraft. Additional spectral broadening is also caused by any inaccuracies of ephemeris tuning and instabilities of the oscillators of the system.

A passive link test was designed to test for system instabilities. For this test, the ground transmitter was beamed to the receiver via three passive reflectors which were placed on local peaks between the two stations. The third reflector contained a transponder similar to the one carried on board *Mariner IV*. This was necessary in order to obtain the same frequency multiplication, 240/221.

FREQUENCY, Hz
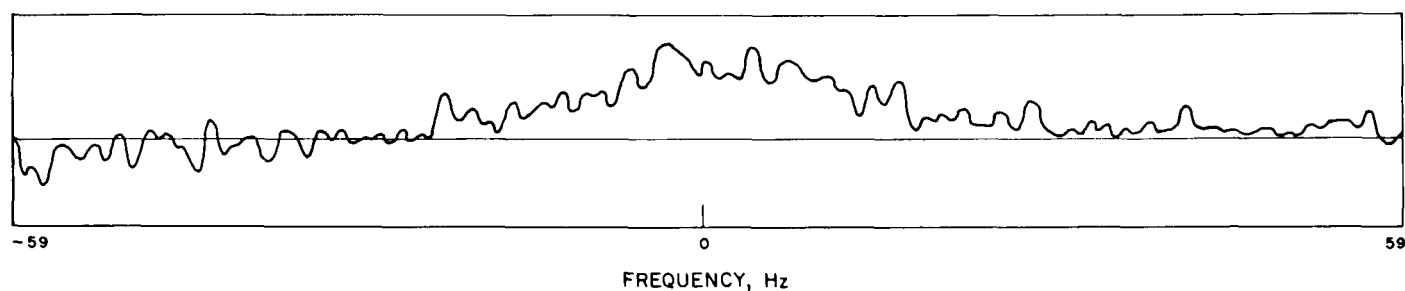
Fig. 53. March 26, 1966 two-way spectrogram

FREQUENCY, Hz
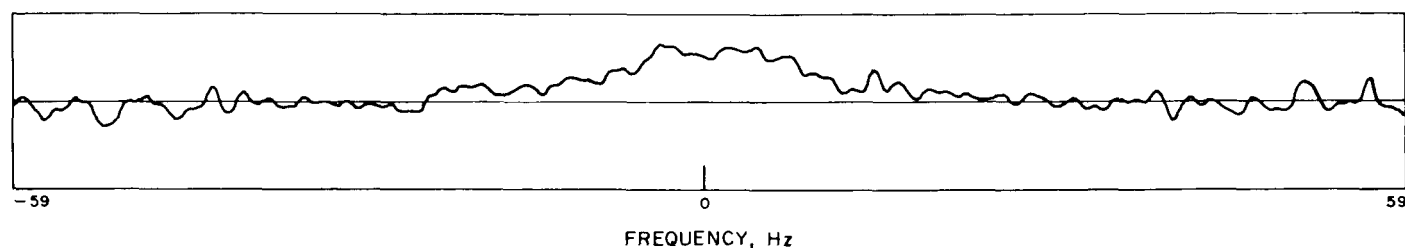
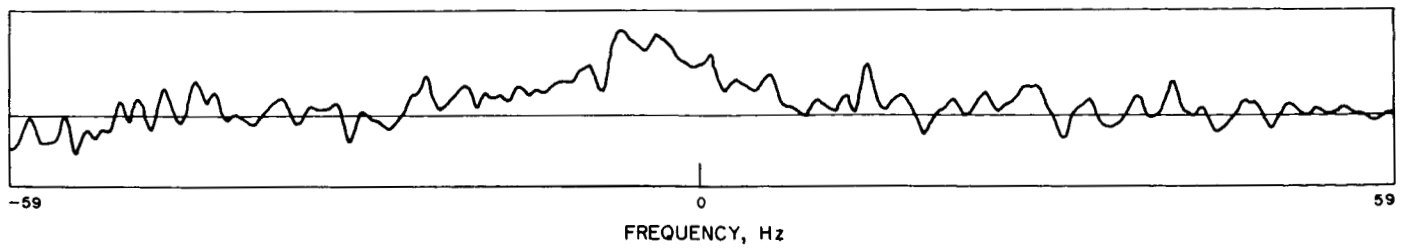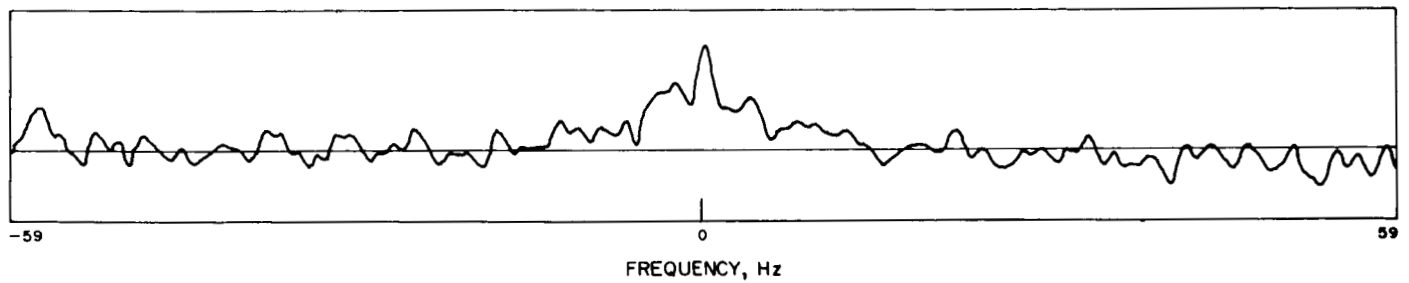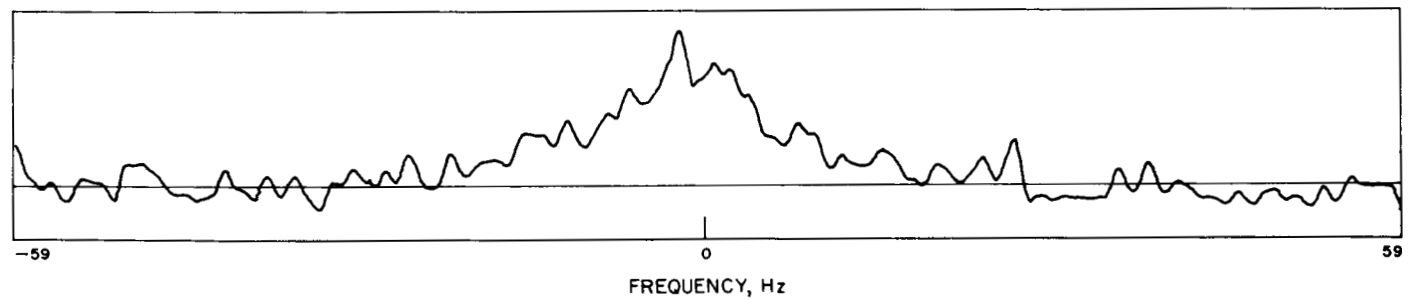**Fig. 54. March 27, 1966 two way spectrogram**

FREQUENCY, Hz
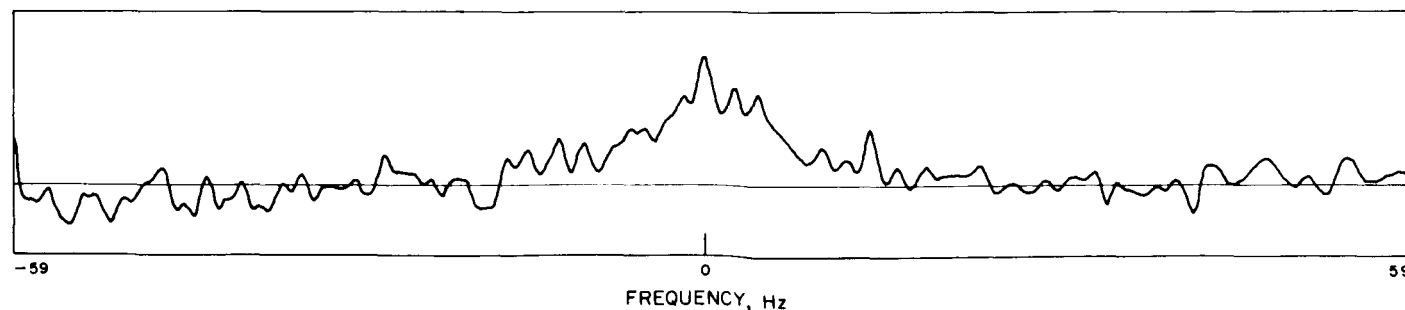
Fig. 55. March 28, 1966 two-way spectrogram

Fig. 56. March 29, 1966 two-way spectrogram

Fig. 57. March 31, 1966 two-way spectrogram

Fig. 58. April 3, 1966 two-way spectrogram (first transmission)
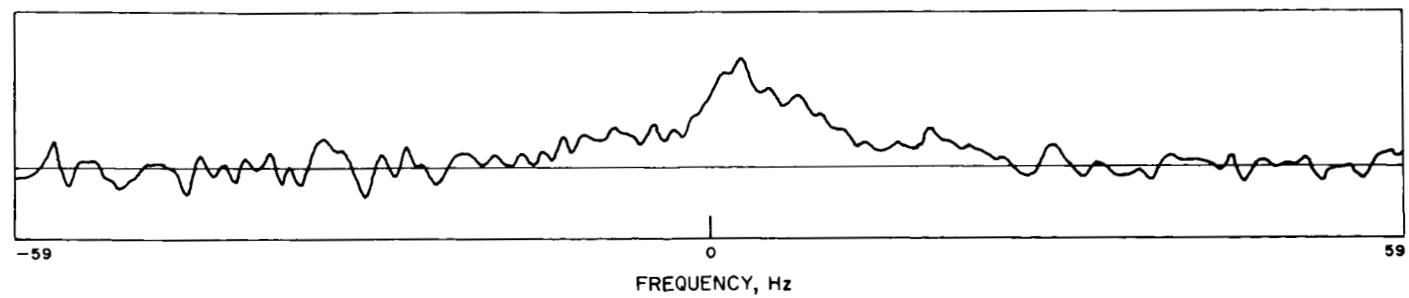
Fig. 59. April 3, 1966 two-way spectrogram (second transmission)

-59   0   59

FREQUENCY, Hz
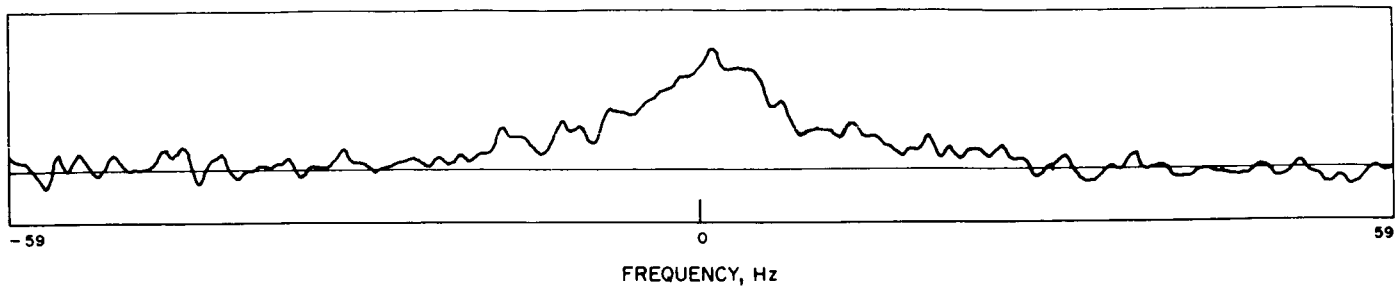
Fig. 60. April 3, 1966 two-way spectrogram (third transmission)

-59   0   59

FREQUENCY, Hz
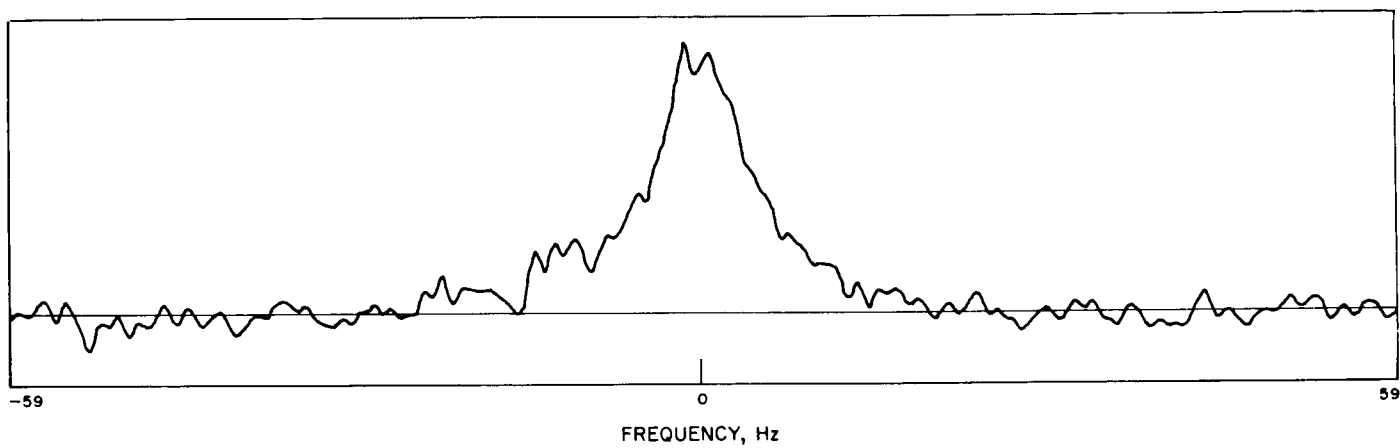
Fig. 61. April 4, 1966 two-way spectrogram

-59   0   59

FREQUENCY, Hz

Fig. 62. April 5, 1966 two-way spectrogram

FREQUENCY, Hz

Fig. 63. April 6, 1966 two-way spectrogram

FREQUENCY, Hz

Fig. 64. April 7, 1966 two-way spectrogram
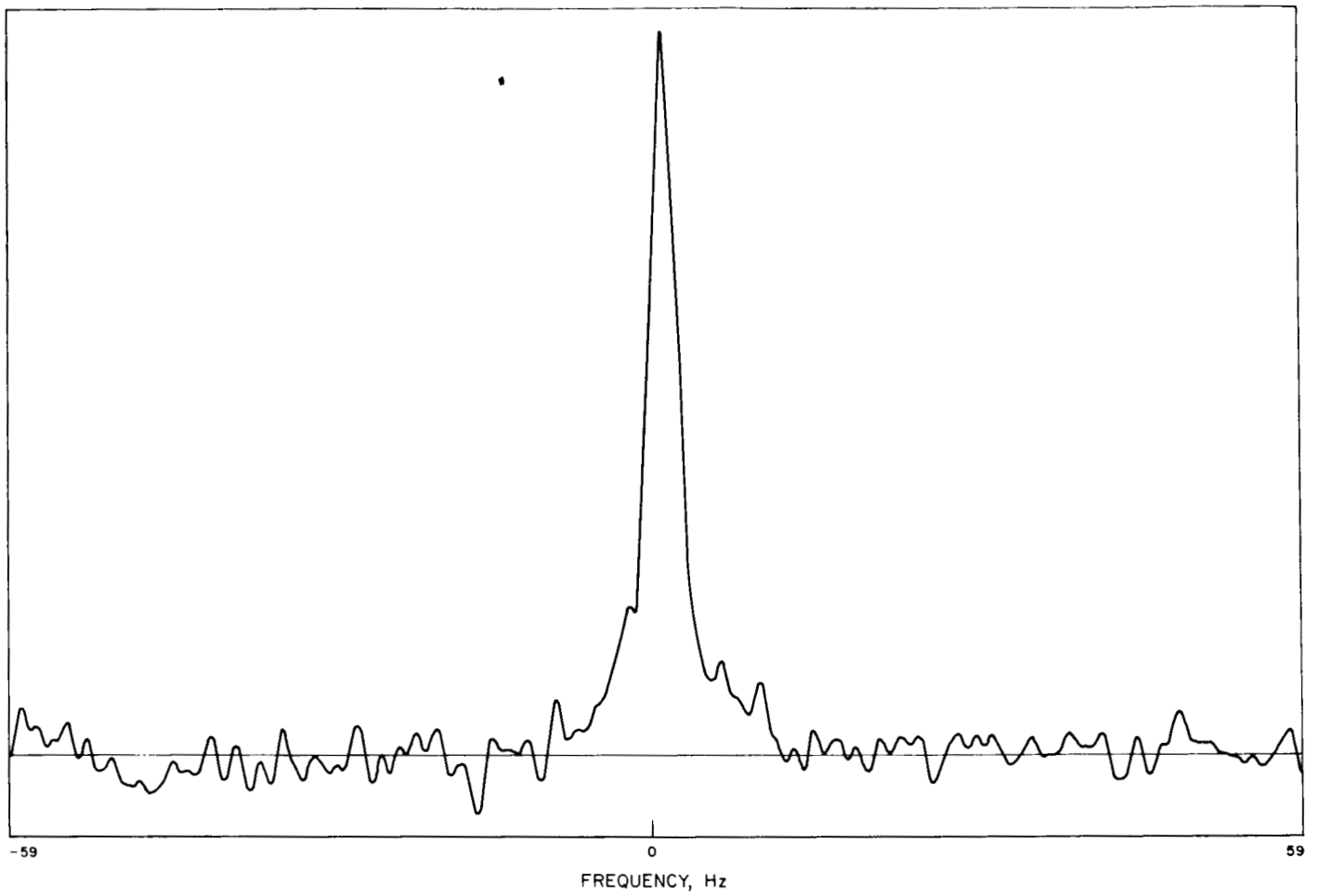
Fig. 65. April 8, 1966 two-way spectrogram

FREQUENCY, Hz
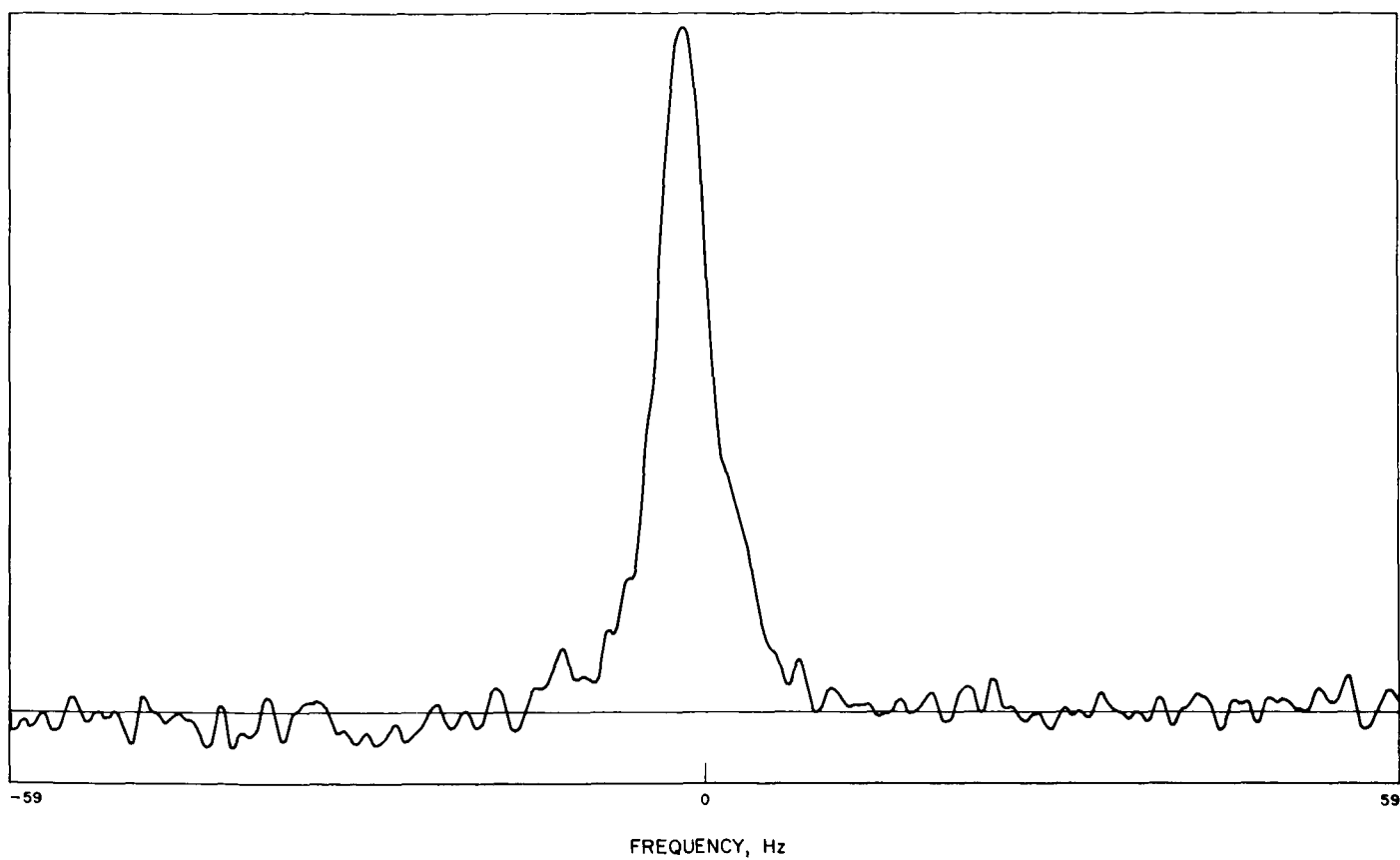
Fig. 66. April 11, 1966 two-way spectrogram
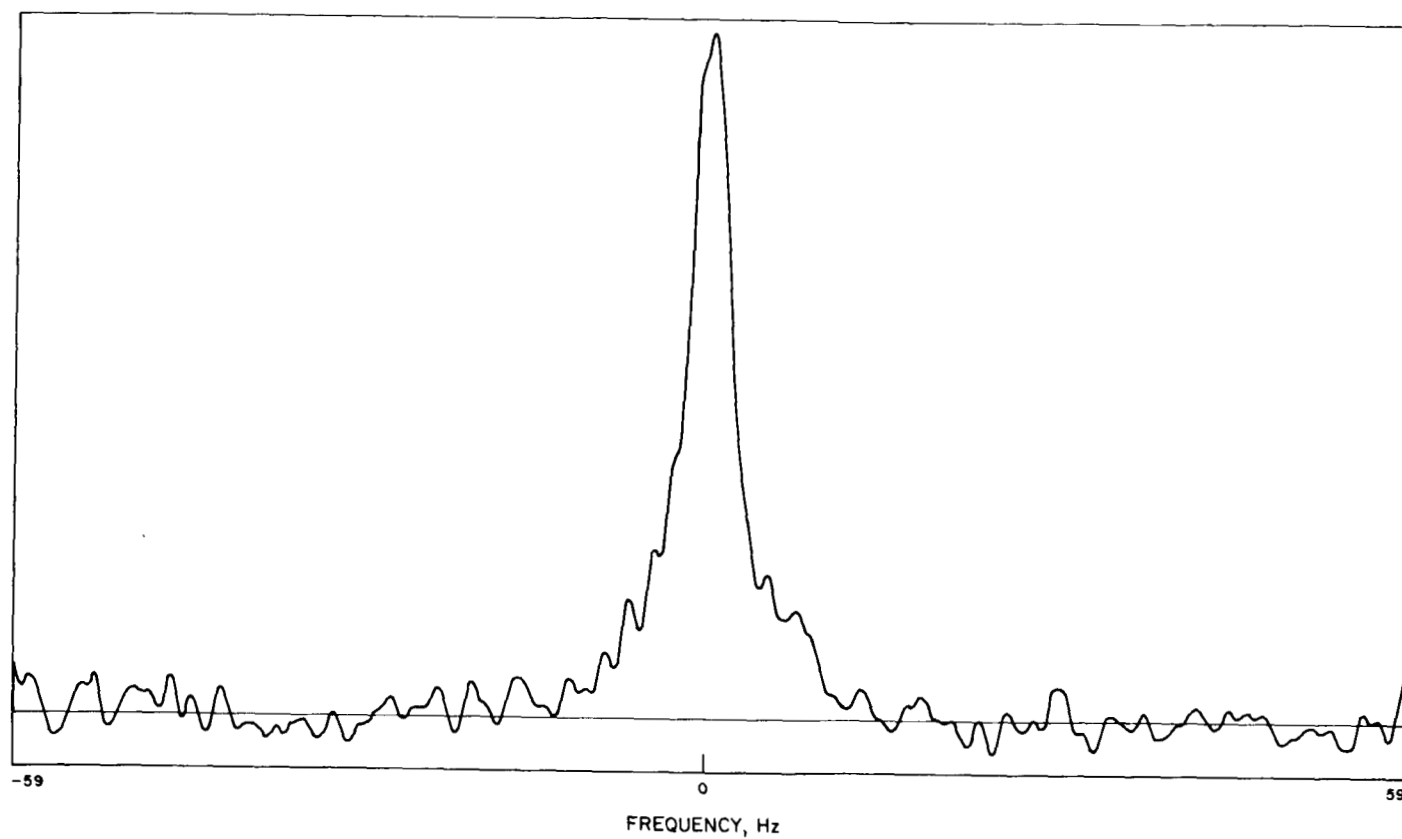
FREQUENCY, Hz

Fig. 67. April 12, 1966 two-way spectrogram (first transmission)

-59

0

FREQUENCY, Hz

59
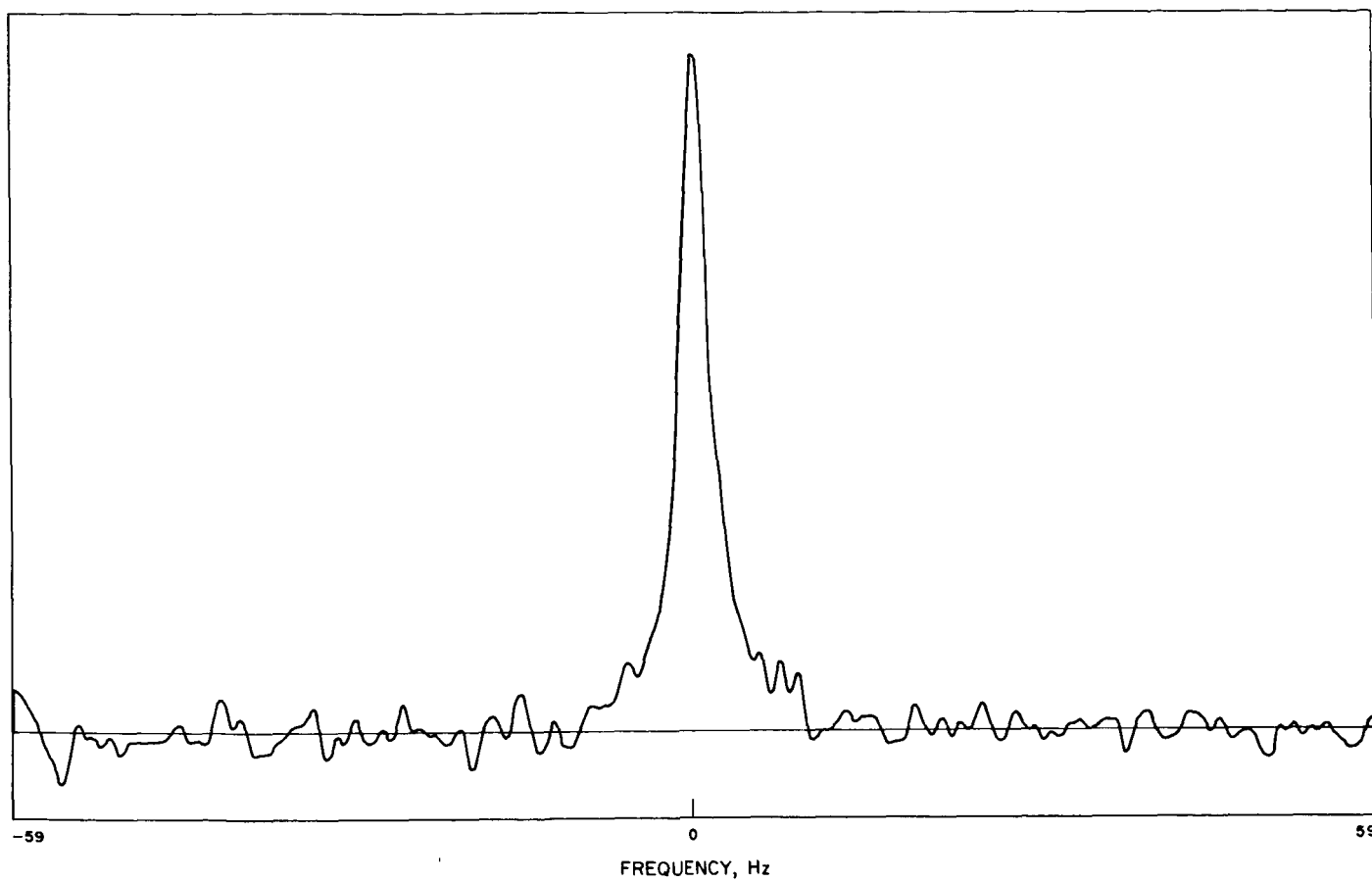
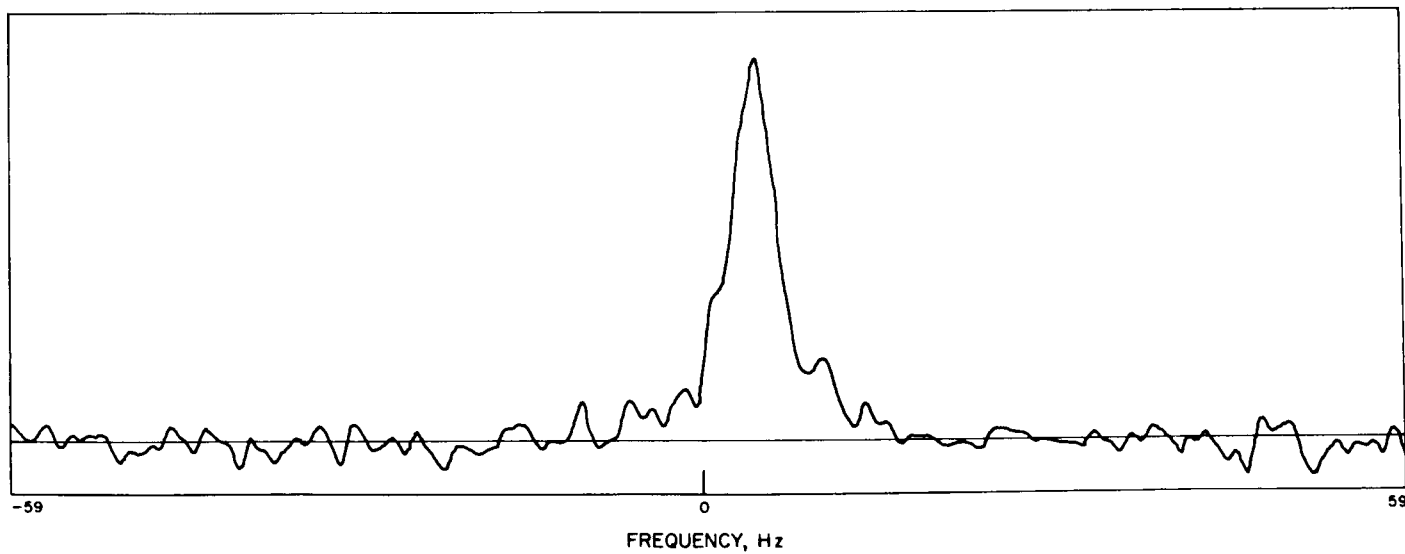**Fig. 68. April 12, 1966 two-way spectrogram (second transmission)**

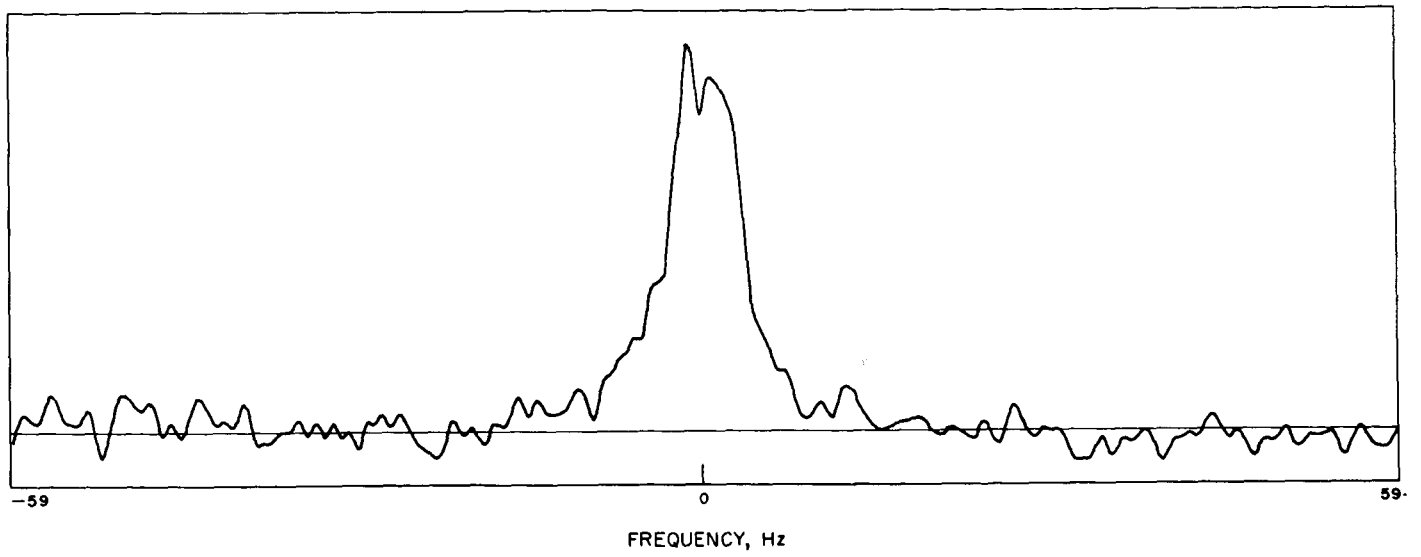−59   0   59

FREQUENCY, Hz

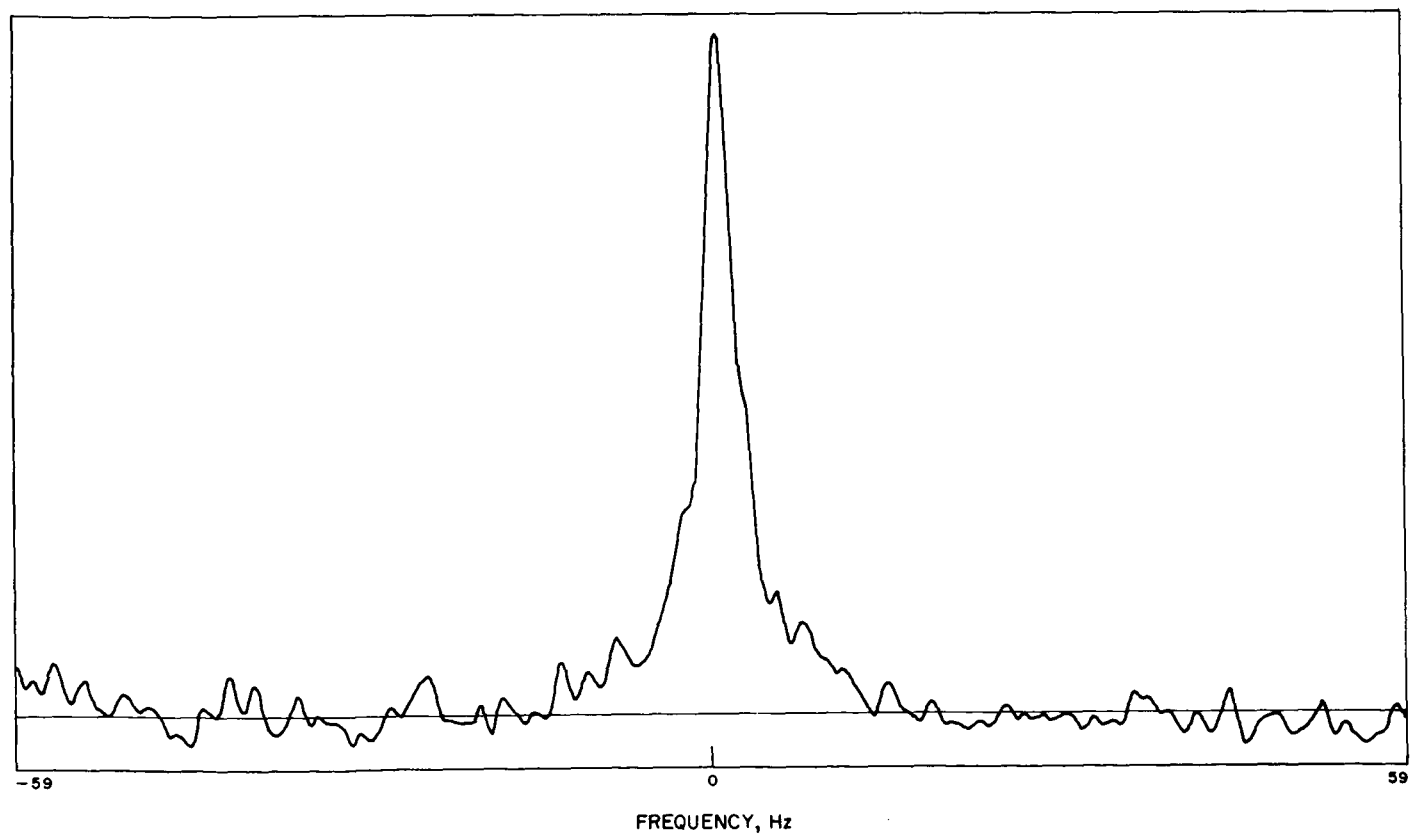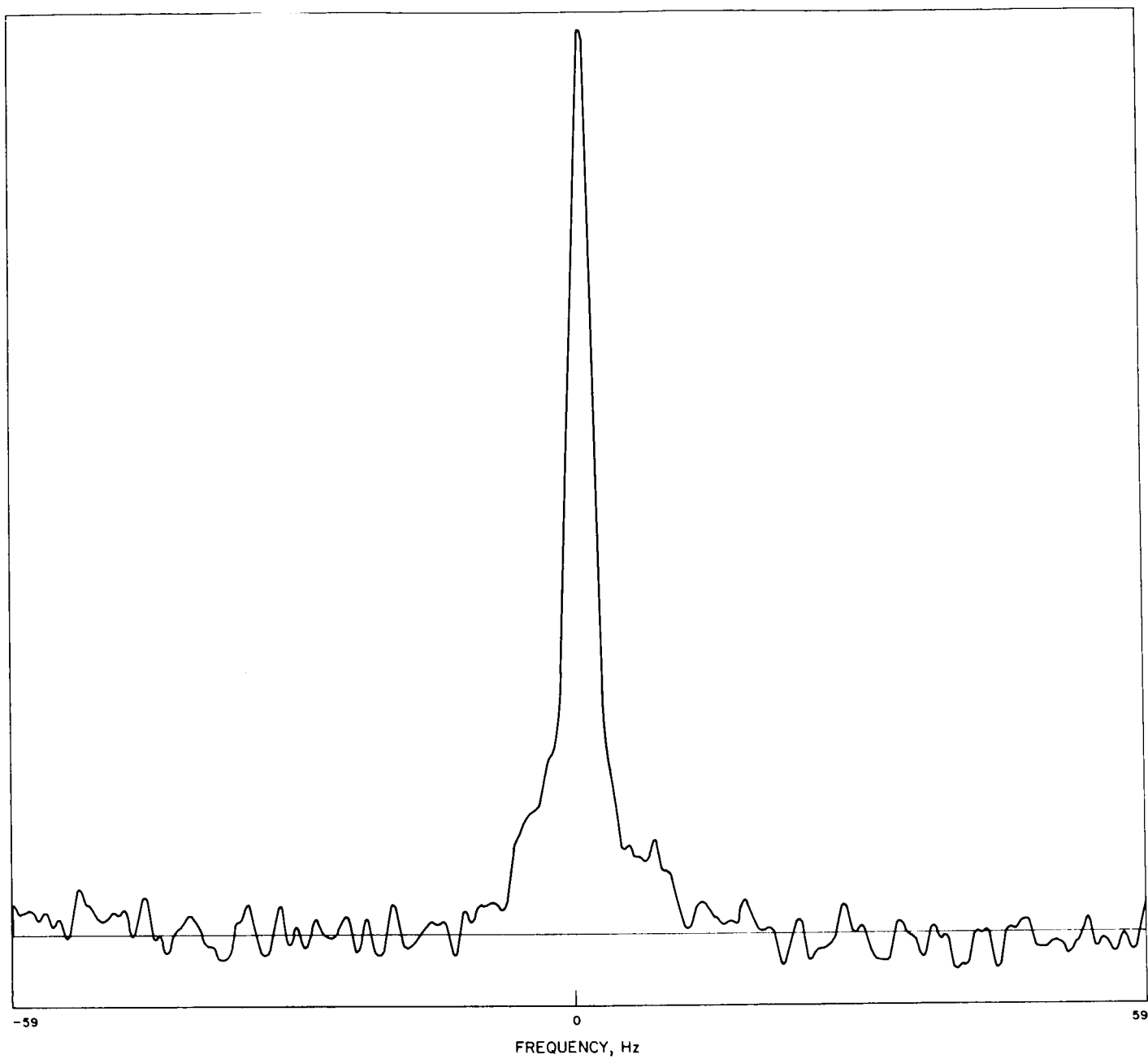**Fig. 69. April 12, 1966 two-way spectrogram (third transmission)**

Figure 70 is the resulting spectrogram. The frequency scale is the same as for the one-way spectrograms, but the resolution is increased to 0.128 Hz. This spectrogram demonstrates that the frequency jitter of the entire system, exclusive of the ephemeris tuning, was less than 0.28 Hz.

A further test was made June 5, when the *Mariner IV* link was far from the influence of the Sun. On that day, a two-way spectrogram was made under essentially the same conditions as before. This spectrogram, Fig. 71, has the same frequency scale and resolution as the passive link test. It shows a combined spectral broadening, caused by the entire system including ephemeris tuning and spacecraft interaction, of only 0.32 Hz. Thus, essentially all of the broadening of the one-way and the two-way spectra may be attributed to the effects of the solar corona and *Mariner IV*.

IV. Additional Experiment

B. B. Lusignan (Ref. 27) predicted theoretically that relativistic electrons in the solar wind could alter the

polarization ellipse of an electromagnetic wave passing through. It was noted[3] that this phenomenon could cause significant loss of signal if circular polarization were employed in the *Mariner IV* S-band telemetry link. Although the phenomenon was predicted to have a negligible effect on the *Mariner IV* S-band communication system (Ref. 28), the suggestion of using the precision instrumentation of the NASA-JPL deep space network to attempt to identify the predicted phenomena was followed.

From January 19 through July 28 measurements were made to determine the ratio of right hand circularly polarized (RCP) to left hand circularly polarized (LCP) signal received at the Goldstone Pioneer station. This was accomplished by measuring the calibrated automatic gain control (AGC) voltage in the normal matched mode (RCP) then switching the receiver input to the mismatched (LCP) port of the antenna and again measuring the AGC voltage. On all occasions the signal level measured in the LCP mode was at least 17 db below the RCP mode or else below the receiver threshold. The LCP signal measured

---

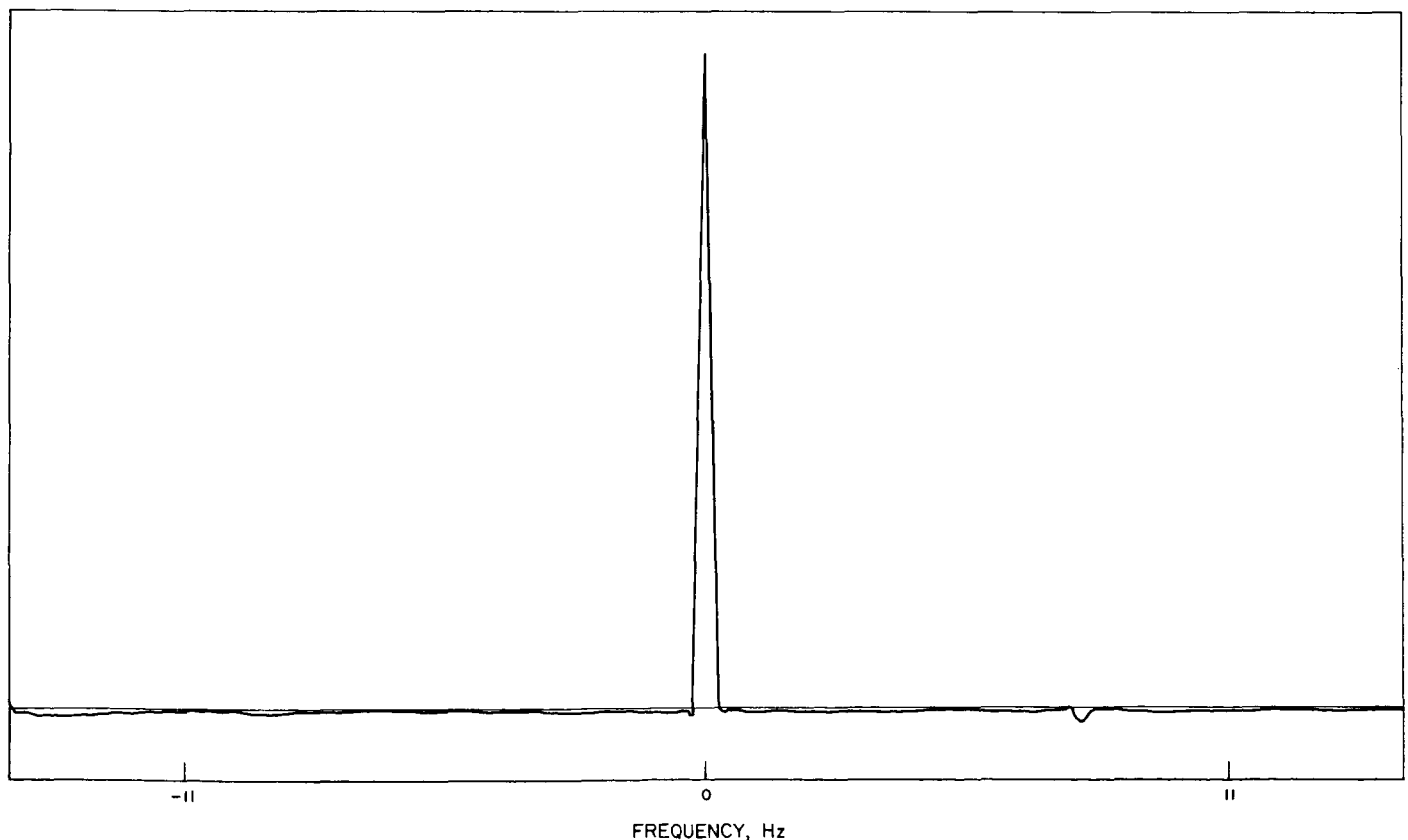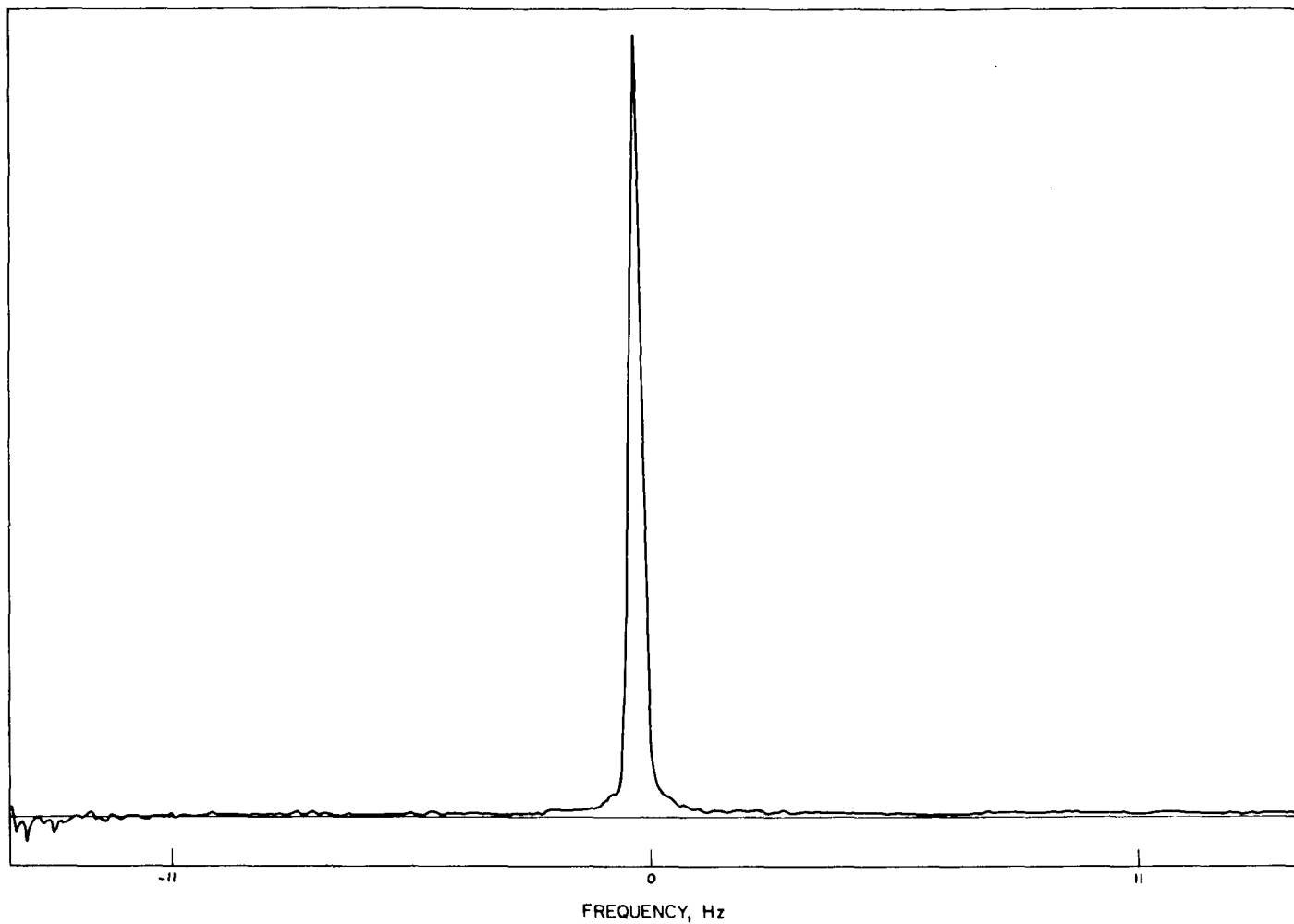[3]Letter from V. R. Eshleman to J. Clark, November 15, 1963.

FREQUENCY, Hz

Fig. 70. March 27, 1966 passive link test

FREQUENCY, Hz

Fig. 71. June 5, 1966 two-way spectrogram

could be completely accounted for by the combination of ellipticity of the spacecraft antenna and the 0.5-db ellipticity of the receiving antenna.

On April 1, 1966, as *Mariner IV* was approximately 327.7 gigameters from the Earth, the angle formed between the center of the Sun, the Earth, and the probe was only 1.05 deg. The spacecraft was tracked using the 210-ft antenna and the programmed local oscillator receiver. The LCP signal was below the threshold of detectability, which was estimated to be 10 db below the matched RCP mode. Figure 72(a) shows the spectrum of the RCP signal integrated for a total of 30 min. A bandwidth of 25 Hz was employed, and the receiver was tuned with a programmed local oscillator. Figure 72(b) shows the spectrum of the LCP signal integrated for a period of 77 min. There is no apparent signal present in the LCP case, and it appears that one would have been detected had it been no more than 10 db less than the RCP signal.

Cross-polarized feed-through of the ortho-mode transducer and the ellipticity of the 210-ft feed system should have given a spurious cross-polarized signal of no more than 25.6 db down from the matched circular mode.

Adding this to the cross-polarized signal from the spacecraft omnidirectional antenna, which had an ellipticity of 2.3 db, the total cross-polarized signal at the observed orientation angle, ignoring the medium, should be between 14.6 and 21.8 db down from the RCP mode, which would be below the detection threshold.

In the April 1 experiment the RCP signal was located and observed in a 400-Hz bandwidth. The bandpass was then narrowed to 25 Hz and the signal was sought on RCP and LCP. The spacecraft was transmitting on its auxiliary oscillator. The oscillator might have drifted in frequency, but, based on data taken during the rest of the solar occultation measurements, this seems unlikely. As a check, the last 18 min of the view period were used to measure LCP in the 100-Hz filter. No signal was detectable in either the 25- or 100-Hz filter for LCP.

The anisotropic nature of the solar wind can be explained by considering the effect of two linearly polarized waves propagating in a direction normal to the velocity vector of a relativistic electron, Ref. (27). One wave is polarized perpendicular as to the velocity vector and the
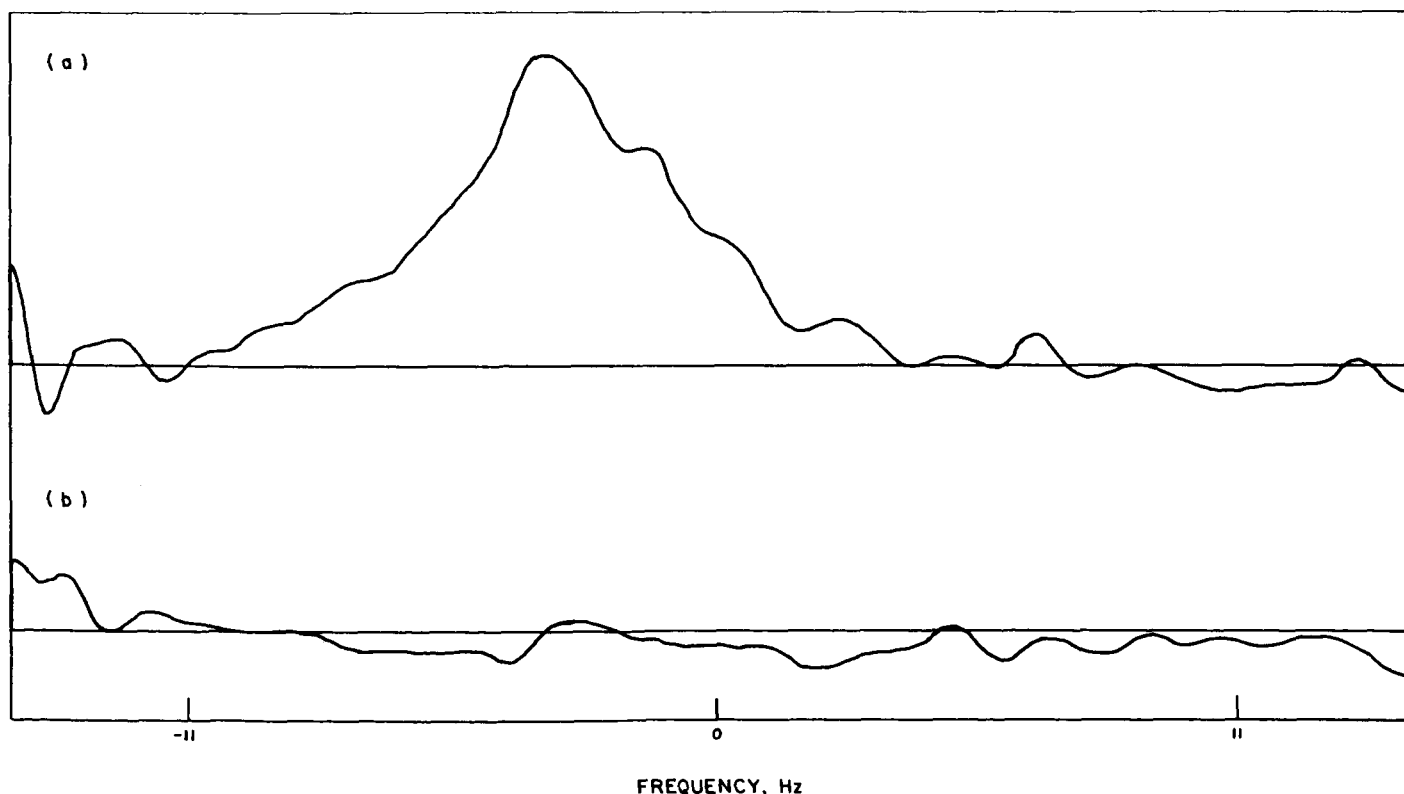

FREQUENCY, Hz

Fig. 72. *Mariner IV* depolarization measurements: (a) spectrum of the RCP signal; (b) spectrum of the LCP signal

other parallel. The accelerations produced by the perpendicularly polarized wave on the electron make the electron's mass appear to be simply its rest mass. The mass seen by the wave polarized parallel to the velocity vector, however, is modified by a relativistic correction. The electron will, therefore, have an elliptical rather than circular oscillation superimposed on its linear velocity. This will result in a circularly polarized signal giving rise to the opposite sense of circular polarization.

Lusignan[1] derived the following expression for the relative phase shift in radians between the perpendicular linear modes (into which circular polarization can be divided)

$$\phi_p = -D\left(\frac{\omega}{c}\right)\left(\frac{\omega_0^2}{\omega^2}\right)(\tfrac{1}{2}\beta^2 \cos^2 \theta)$$

where

D = the distance

ω = the wave angular frequency

ω_0 = the angular plasma angular frequency and is proportional to the square root of electron density

c = the velocity of light

β = the electron velocity radial from the Sun divided by the velocity of light. It is assumed that $\beta \ll c$

Θ = the angle between the electron velocity vector and the wave front.

Assuming that all electrons are streaming radially from the Sun at the same velocity as the protons, then we can use the 500 km/sec value obtained by *Mariner II*.[5] We can use a value of 8 electrons/cm³ at a distance of 1 AU and assume an inverse square law for the electron spatial distribution. Since both the angle θ and electron density change, it will be necessary to integrate the phase change along the ray path

$$\phi_p = \frac{\beta^2}{2\omega_c}\int \omega_0^2 \cos^2 \theta dD$$

and

$\omega_0^2 = 3.19 \times 10^9 N$, where N is electrons/cm³

$$\phi_p = \frac{3.19 \times 10^9 (1.67 \times 10^{-3})^2}{4\pi \times 2.295 \times 10^9 \times 3 \times 10^{10}}\int N \cos^2 \theta dD$$

$$\phi_p = 1.028 \times 10^{-17}\int N \cos^2 \theta dD$$
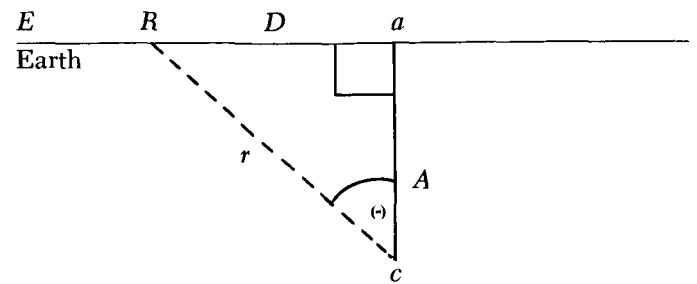
[1]B. B. Lusignan, private communication.
[5]M. Neugebauer and C. W. Snyder, *Mariner II Observations of the Solar Wind, 1. Average Properties*, to be published.

Converting the unit of length to astronomical units (AU) and the angles to degrees

$$\phi_\beta = 8.65 \times 10^{-3}\int N \cos^2 \theta dD$$

$$N = \frac{8}{r^2}$$

where r is the distance for the center of the Sun in AU

The range and angles subtended by *Mariner IV* were computed by D. Tito.[6]

let

a = point of closest approach to the Sun

A = line between center of Sun c and a

p = point along ray path

D = distance between a and p

r = distance between c and p

$\Theta = \angle pca$

then $\qquad r = \dfrac{d}{\cos \theta} \qquad$ and $\qquad D = A \tan \theta$

$$\phi_\beta = 8.74 \times 10^{-3}\int \frac{8}{r^2}\cos^2 \theta dD$$

$$\phi_\beta = 6.92 \times 10^2 \int \frac{\cos^4 \theta}{A^2} dD$$

$$D = A \tan \theta$$

$$dD = \frac{A d\theta}{\cos^2 \theta}$$

$$\phi_\beta = 6.92 \times 10^{-2}\int \frac{\cos^2 \theta}{A} d\theta$$

and for the case of April 1, $A = 0.02$ AU.

[6]D. Tito, "*Mariner IV* Solar Corona Equipment — Trajectory Related Information," 312.4-323, unpublished memo, November 3, 1965.

Let us integrate from the Earth to the spacecraft

$$< Eca = 88.95\,\text{deg} = 1.552\,\text{rad}$$

$$\phi_\beta = 3.46 \int_{1.552}^{-1.552} \cos^2\theta\,d\theta$$

$$= 3.46\,[\tfrac{1}{2}\theta + \tfrac{1}{4}\sin^2\theta]_{1.552}^{-1.552}$$

$$= 5.4\,\text{deg}$$

To correct the phase shift to the ratio of RCP to LCP

$$\left[\frac{1 + \tan\left(\dfrac{\phi}{2}\right) + 45}{1 - \tan\left(\dfrac{\phi}{2}\right) + 45}\right]^2 = \frac{\text{RCP}}{\text{LCP}} = 26.5\,\text{db}$$

which would be well below detectability. It is pointed out by Lusignan that we may assume either that the velocity and number of protons are equal to the velocity and number of electrons, as above, or we may assume, as an upper limit, that electron and proton energies and currents are equal so that the stream effects are proportional to N_β^2; and N is proportional to $1/\beta$, so that the stream effects are proportional to β. If we set proton and electron energies equal, then $\beta = 0.085$, and the previous value of $\beta = 0.00167$ gives a ratio of 50 for a total phase shift of approximately 275 deg, which would be a case where the energy has been completely converted to LCP and has gone slightly more than halfway back to RCP. In this case, RCP and LCP would be approximately the same magnitude.

The solar wind has been assumed to be the sole cause of the depolarization, and the solar corona influence has been found to be negligible, because of the low β values in the corona at four solar radii.

V. Conclusions

The path of *Mariner IV* passed within 0.9 deg of the center of the Sun just after superior conjunction. Figure 73 shows this path, relative to the Sun, in projection upon the celestial sphere. Figure 74 is the elongation angular distance from the Sun of *Mariner IV* as a function of time. It can be seen that the region of the corona examined by this experiment lies roughly between 1 and 2 deg from the center of the Sun.

All of the relevant information contained in each of the spectrograms can be reduced to a single quantity, the bandwidth of the signal. Spectral broadening is thus our primary observable result of passing a monochromatic signal through the solar corona.
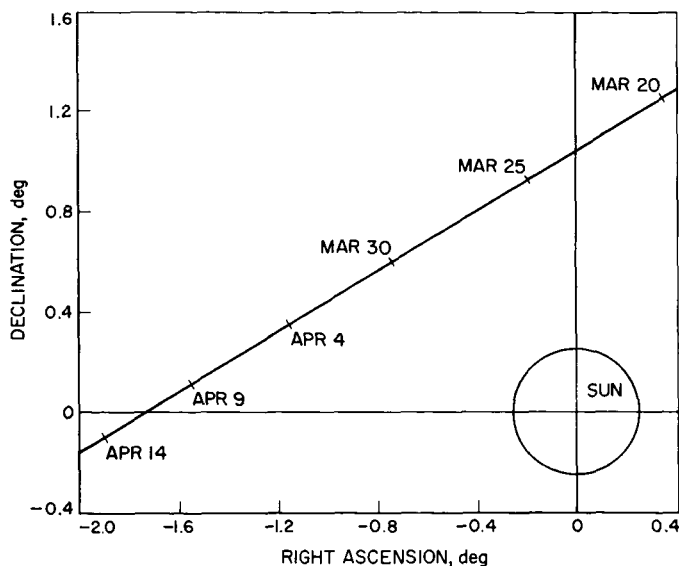

Fig. 73. *Mariner IV solar passage*
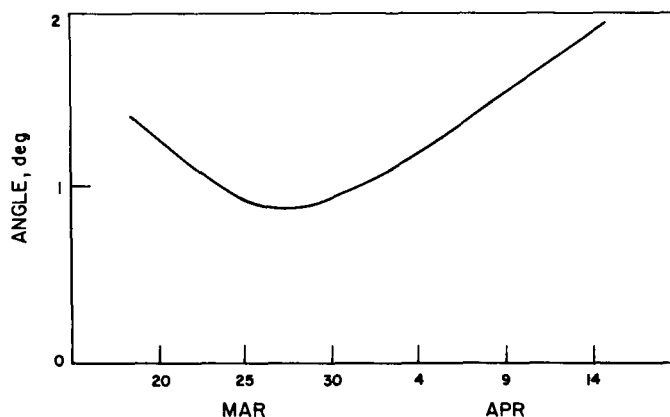
Fig. 74. Sun—Earth—probe angle as a function of time

We have defined bandwidth as the width of an equivalent rectangle, of the same height and area as the measured curves. This is a convenient method of obtaining bandwidth, which avoids the problem of defining a band edge on these noisy spectrograms. The bandwidths so defined have been plotted in Figs. 75 and 76 as a function of angular distance from the Sun. Figure 75 contains the one-way data, Fig. 76, the two-way. These figures are plotted to the same scale and reveal an apparent inconsistency in the data: the two-way bandwidths are more than twice as great as the one-way bandwidths.

This difference might be attributed to the action of the *Mariner IV* transponder. However, for the reasons which follow, this explanation is not satisfactory. Since the

Fig. 75. One-way bandwidth as a function of angular distance from the Sun

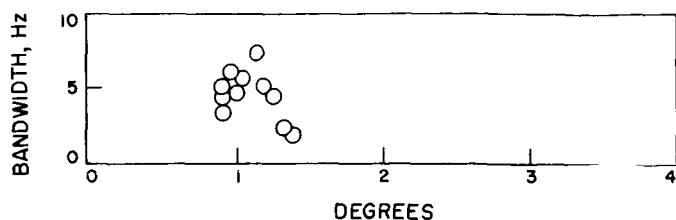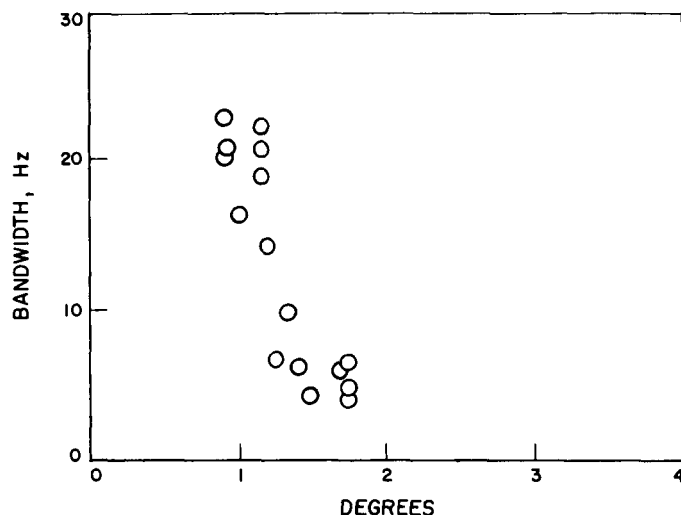**Fig. 76. Two-way bandwidth as a function of angular distance from the Sun**

bandwidth of the transponder phase-locked loop was >200 Hz, much wider than the one-way spectra, the loop would track the phase variations easily. Thus, the transponder would faithfully return the same phase modulation it received.

Of course, the one-way signals may experience more modulation than just phase fluctuations. In the limit of traversing a very turbulent medium, the signal would resemble narrow-band gaussian noise. Such noise may be thought of as random phase modulation with occasional deep fades. The transponder would then follow the phase variations, and would drift quiescently during the fades.

To verify these possibilities, the *Mariner* transponder was tested with signals having random phase and random amplitude modulation. The test signals were generated with spectra closely resembling those measured from *Mariner IV*. In fact, the received spectra differed in no essential way from the test signals, demonstrating that

Mariner IV did not produce the observed additional spectral broadening.

The geometry of the one-way and two-way situations was quite symmetric. That is, the Sun–*Mariner IV* distance was almost equal to the Sun–Earth distance. One asymmetry must be noted, however, which may help explain the asymmetry in the results. And that is, the transmitting antenna was 85 ft in diameter, producing a beamwidth of 0.35 deg; and the receiving antenna was 210 ft with a beamwidth of 0.14 deg.

Suppose that the observed spectral broadening was caused by either multipath transmission or diffraction through that extent of the corona which was illuminated by the radio waves. Then the up-link broadening would be 2.5 times that of the down-link, and the two-way effect would be 3.5 times the one-way effect.

Figure 77 is a plot of the two-way bandwidths superposed on the × 3.5 one-way bandwidths. As can be seen, the agreement is excellent. Certainly, it is within the noisiness of the data.

Our assumption of the underlying causes of the spectral broadening thus removes the apparent inconsistency of our data. However, this assumption runs into difficulty from another quarter. From the bandwidths observed, it is possible to calculate the velocity of this assumed diffracting medium. These calculations result in velocities perpendicular to the line of sight of only a few hundred
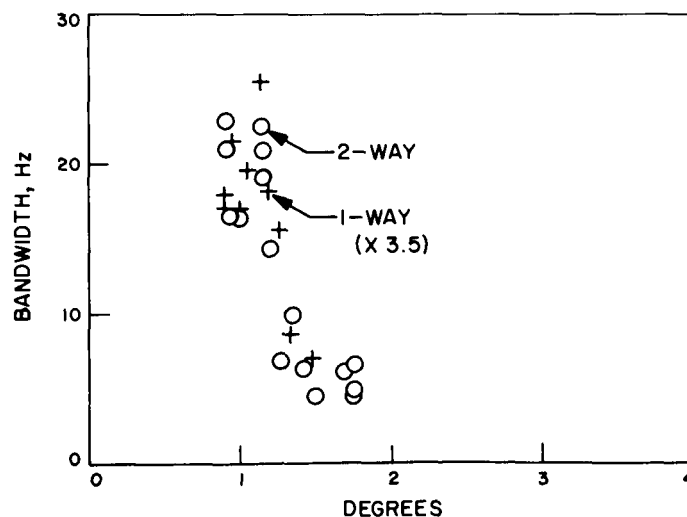

Fig. 77. Two-way bandwidths superimposed on ×3.5 one-way bandwidths

meters per second—much too slow to be accommodated by the existing knowledge of the solar corona.

The spectrograms reproduced in the data section reveal an important fact relative to communications with our deep space probes. It was not possible either to transmit effective commands to, nor receive telemetry from, *Mariner IV* when it was within 2 deg of the Sun. The coherency required by the design of *Mariner IV* was not maintained through the corona. Should a deep space mission ever require communications through the corona, it will be necessary to design a different system. Perhaps frequency-shift-keying could be used, with a frequency spacing greater than the measured spectral broadening. In any event, the data contained in this report will aid in the design of such a system.

References

1. Goldstein, R., *Radar Exploration of Venus: Goldstone Observatory Report for Oct–Dec 1962*, Technical Report 32-396, Jet Propulsion Laboratory, Pasadena.

2. Ludwig, A., "Antennas for Space Communications," *Space Programs Summary 37-34*, Vol. IV, Jet Propulsion Laboratory, Pasadena, April 31, 1965, p. 236.

3. Ludwig, A., "Antennas for Space Communications," *Space Programs Summary 37-36*, Vol. IV, Jet Propulsion Laboratory, Pasadena, December 31, 1965, p. 249.

4. Bathker, D., "Antennas for Space Communications," *Space Programs Summary 37-38*, Vol. IV, Jet Propulsion Laboratory, Pasadena, April 30, 1966, p. 192.

5. Ludwig, A. C., "Efficient Antenna Systems: Calculated Gain of the Advanced Antenna System," *Space Programs Summary 37-42*, Vol. III, Jet Propulsion Laboratory, Pasadena, November 30, 1966, pp. 37–40.

6. "Efficient Antenna Systems: Gain Measurements of the AAS Using the *Surveyor I* Signals," *Space Programs Summary 37-44*, Vol. III, Jet Propulsion Laboratory, Pasadena, March 31, 1967.

7. Ludwig, A., "Antenna Feed Efficiency," *Space Programs Summary 37-26*, Vol. IV, Jet Propulsion Laboratory, Pasadena, April 30, 1964, p. 200.

8. Rusch, W. V. T., *Scattering of a Spherical Wave by an Arbitrary Truncated Surface of Revolution*, Technical Report 32-434, Jet Propulsion Laboratory, Pasadena, May 27, 1963.

9. Bathker, D., "Efficient Antenna Systems: Advanced Antenna System Radiation Patterns Obtained Using the *Surveyor I* Spacecraft," *Space Programs Summary 37-40*, Vol. III, Jet Propulsion Laboratory, Pasadena, July 31, 1966, pp. 75–80.

10. Higa, W., and Wiebe, E., "Experimental Closed Cycle Refrigerator for Masers," *Space Programs Summary 37-39*, Vol. III, Jet Propulsion Laboratory, Pasadena, May 31, 1966, p. 79.

11. Cormack, R. E., "R&D Listening Cone for AAS," *Space Programs Summary 37-35*, Vol. IV, Jet Propulsion Laboratory, Pasadena, October 31, 1965, pp. 268–270.

12. Stelzried, C. T., "S-band WR-430 Waveguide Liquid Nitrogen Cooled Terminations," *Space Programs Summary 37-31*, Vol. IV, Jet Propulsion Laboratory, Pasadena, February 28, 1965, pp. 283, 284.

References (contd)

13. Stelzried, C. T., and Petty, S. M., "Microwave Insertion Loss Test Set," *IEEE Transactions Microwave Theory and Technique,* Vol. MTT-12, No. 4, p. 128, July 1964.

14. Finnie, C. J., Schuster, D., and Otoshi, T. Y., *AC Ratio Transformer Technique for Precision Insertion Loss Measurements,* Technical Report 32-690, Jet Propulsion Laboratory, Pasadena, November 30, 1964.

15. Beatty, R. W., "Insertion Loss Concepts," *IEEE Proceedings,* June 1964, pp. 663–671.

16. Stelzried, C. T., and Otoshi, T. Y., "RF Techniques," *Space Programs Summary 37-39,* Vol. III, Jet Propulsion Laboratory, Pasadena, May 31, 1966, pp. 86–100.

17. Reid, M. S., and Stelzried, C. T., "Error Analysis of CW Signal Power Calibration with Thermal Noise Standards," *Space Programs Summary 37-36,* Vol. IV, December 31, 1965, p. 269.

18. Worthing, A. G., and Geffner, J., *Treatment of Experimental Data,* John Wiley and Sons, Inc., New York, p. 195, December 1960.

19. *Handbook of Geophysics and Space Environments,* S. L. Valley, Ed., McGraw-Hill Book Co., Inc., New York, New York, 1965.

20. "Digital Control Subsystem for Programmed Local Oscillator," *Space Programs Summary No. 37-18,* Vol. III, Jet Propulsion Laboratory, Pasadena, November 1962, pp. 32–38.

21. "Programmed Exciter," *Space Programs Summary No. 37-36,* Vol. III, Jet Propulsion Laboratory, Pasadena, November 1965, pp. 54–63.

22. "Mod V Programmed Oscillator," *Space Programs Summary No. 37-39,* Vol. III, Jet Propulsion Laboratory, Pasadena, May 1966, pp. 71–76.

23. Van Duzer, V. E., "A 0–50 Mc Frequency Synthesizer with Excellent Stability, Fast Switching, and Fine Resolution," *Hewlett-Packard Journal,* Vol. 15, No. 5, May 1964.

24. "Nine-Channel Autocorrelator," *Space Programs Summary No. 37-26,* Vol. III, Jet Propulsion Laboratory, Pasadena, March 31, 1964, p. 33.

25. "Evaluation of Atomic Oscillator Performance," *Space Programs Summary No. 37-17,* Vol. III, October 1, 1962, p. 30.

26. "Evaluation of Stable Oscillator Performance," *Space Programs Summary No. 37-16,* Vol. III, July 31, 1962, pp. 33–35.

27. Lusignan, B. B., "Detection of Solar Particle Streams by High Frequency Radio Waves," *Journal of Geophysical Research,* Vol. 68, No. 20, pp. 5617–5632, October 15, 1963.

28. M. Easterling, and R. Goldstein, *The Effect of the Interplanetary Medium on S-Band Telecommunications,* Technical Report No. 32-825, Jet Propulsion Laboratory, Pasadena, September 1, 1965.